Development of Nanostructured Materials for Drug Delivery and Tissue Engineering

A Dissertation

Presented to

the Faculty of the Department of Biomedical Engineering

University of Houston

In Partial Fulfillment

of the Requirements for the Degree

Doctor of Philosophy

in Biomedical Engineering

by

Iman K. Yazdi

May 2015

Development of Nanostructured Materials for Drug Delivery and Tissue Engineering

Iman K. Yazdi

Approved:

Co-Chairman of the Committee
Metin Akay, Professor and John S Dunn Endowed Chair, Biomedical Engineering

Co-Chairman of the Committee
Mauro Ferrari, Ernest Cockrell, Jr. Presidential Distinguished Chair
President and CEO,
Houston Methodist Research Institute
Professor of Medicine, Weill Cornell Medical College of Cornell University

Committee Members:

Ennio Tasciotti, Co-Chair and Associate Member, Department of NanoMedicine, Houston Methodist Research Institute

Ravi Birla, Associate Professor
Department of Biomedical Engineering

Yasemin Akay, Assistant Professor
Department of Biomedical Engineering

Suresh K. Khator, Associate Dean,
Cullen College of Engineering

Metin Akay, Professor and John S Dunn Endowed Chair, Biomedical Engineering

Acknowledgements

Upon submission of this dissertation, I would like to thank the chairmen of the committee, Dr. Mauro Ferrari and Dr. Metin Akay, for the immense support and guidance they have provided me throughout the course of this journey. I owe my deepest gratitude to my mentor and advisor, Dr. Ennio Tasciotti, for his invaluable support, assistance, and guidance at every step of this research. His immense knowledge and enthusiasm helped me overcome the obstacles in the completion of this work. Also, I would like to thank my other committee members, Dr. Ravi Birla and Dr. Yasemin Akay for their advice and support in the completion of this work.

There are many people that I would like to thank for their contributions to my research and academic career. For their great assistance with my research over the years, I would like to thank the members of the Ferrari and Tasciotti laboratories. Most especially, I would like to recognize the contributions of Dr. Alessandro Parodi, Dr. Matthew Murphy, Dr. Zahangir Khaled, Dr. Jeffrey Van Eps, Dr. Arturas Ziemys, Dr. Dongmei Fan, Dr. Nima Taghipour, and Ms. Sarah Hmaidan. Thank you for all your helpful criticisms, suggestions and enormous support throughout the course of my research. As a team, we have accomplished a great deal in the field of drug delivery for various tissue engineering applications during our time at Houston Methodist Research Institute and I am proud to call myself your colleague.

Additionally, to all the friends that I have met along the way, I would not have been able to complete this journey without, all the fun and laughter that you all have brought into my life. Finally and most importantly, I must thank my family. My wife, Maryam, for her love, understanding, and her continuous support. Mom and Dad, your love and support all these years are what fueled my passion and kept me striving to be the best I could be. Mom, Dad, Maryam,

and Ashkan, this work is dedicated to you. I hope I can continue to make you as proud of me as I am of you.

Development of Nanostructured Materials for Drug Delivery and Tissue Engineering

An Abstract

of a

Dissertation

Presented to

the Faculty of the Department of Biomedical Engineering

University of Houston

In Partial Fulfillment

of the Requirements for the Degree

Doctor of Philosophy

in Biomedical Engineering

by

Iman K. Yazdi

May 2015

Abstract

In the last decades many classes of nanoscale materials have been developed to improve the delivery of therapeutics to tissues and cells. The goal of this work was to rationally design and engineer multifunctional nanomaterials with tunable properties to control the release kinetics of therapeutic payloads. The work described herein focuses on the development of materials with nanoscale features that allow them to be environmentally responsive and to sustain the release for long periods of time in a controlled fashion. These materials enhance the pharmacological property of the therapeutics by prolonging their half-life, improving drug solubility and availability, and reducing cytotoxic side effects. All the delivery platforms presented in this work were based on multistage mesoporous silicon nanocarriers (MPS).

Firstly, we showed that cefazolin loaded MPS exhibited sustained bactericidal properties. Secondly, we described the surface modification of these particles with natural hydrogel coatings to enhance their ability to extend the release of cargo and preserve its stability. Thirdly, we embedded MPS into a polymeric matrix to provide long-term controlled release of growth factors for tissue engineering applications. Fourthly, we combined all these approaches to engineer a hybrid composite nanomaterial loaded with therapeutic molecules delivered via a bioactive angiogenic hydrogel. This system released all molecules in a sustained and controlled fashion while simultaneously promoting wound healing and neovascularization. Finally, we developed and validated an injectable nanostructured delivery system to provide an extended local anesthetic release for the purpose of surgical analgesia using an incisional model of pain in rodents. We demonstrated the controlled release of anesthetics from a multilayered nanohydrogel and showed the homogeneous diffusion of the drugs at the site of injection.

The combination of different nanostructured materials allowed us to build on the individual strengths of each component and resulted in the development of drug delivery system with tunable properties. These nanoscale materials were tested in the context of different clinical

domains: infection control, wound healing, pain management and regenerative medicine. The results presented in my work provide the fundamental proof of principle demonstration of the feasibility of these approaches in view of their translation to the clinic.

Table of Contents

List of Figures

List of Tables

1 Introduction

Nanoscale medicine involves the engineering of multi-functional systems at the cellular and molecular levels to enable fast, reliable and effective interventions for drug delivery, diagnostic, imaging, and tissue engineering. Significant developments in nanoscale medicine address some of the shortcomings of modern medicine such as poor solubility and short half-life associated with potent pharmaceutical agents. Nanoscale platforms can significantly enhance pharmacological outcomes by prolonging half-life, improving drug solubility, reducing potential immunogenicity, and releasing the drug molecules in a sustained or stimuli-triggered fashion [1]. Development of novel classes of nanotherapeutics has resulted in Enhancement in efficacy of previously Food and Drug Administration (FDA) approved drugs. They offer several advantages for the enhancement of the therapeutic efficacy of drugs, including better biocompatibility, tissue adhesion and integration capabilities to mimic the physicochemical properties of original tissues. Consequently, they can lead to significant reduction of the toxic side effects of drugs and overall administration frequency. Indeed, nanotherapeutic agents currently under development and validation can potentially transform the drug discovery and pharmaceutical manufacturing landscape.

Nanotherapeutics can be passively or actively accumulated in specific tissues. Passive accumulation through the enhanced permeability and retention (EPR) effect and active targeting through surface modification of nanotherapeutic with ligands, aptamers, or antibodies has the potential to enhance therapeutic efficacy and reduce side effects from conventional administration [2].

Current delivery platforms are effective at releasing cargo with high local concentrations in a controlled fashion at tissue level even though the scope is limited at the cellular scale. The nanoscale approach allows the delivery to cross cell membranes at the expense of a lower loading capacity [3]. Nanoscale materials have greater surface area-to-volume ratios, which increase their

dissolution rate and enhance their bioavailability, [4] while nanoscale delivery systems take advantage of the fact that nanomaterials can exhibit distinctive physicochemical properties that differ from those in the macroscopic level [4, 5], through rational design, these materials can be engineered to combine desirable functions for various drug delivery applications.

Many properties of nanoscale delivery systems can be customized for improving specific aspects of drug delivery such as solubility, biodistribution, biocompatibility, biodegradability, and drug loading and release. Drug delivery from these systems can be systemic or localized. Several platforms have been developed for various applications with their advantages and disadvantages. For instance, liposomal formulations have a high drug loading capacity but their release kinetics is challenging to control. In contrast, polymeric formulations can be synthesized to generate specific physical properties, but their drug loading efficiency is relatively low [6]. An ideal drug delivery platform can be hybrid delivery systems that incorporate the benefits of various approaches based on the structural, compositional and biological characteristics of different nanomaterials that can be tailored to address the needs of specific applications.

Combination therapy can also be offered through nanoscale platforms to provide synergistic effects and reduce the chances of developing drug resistance, proving its increased effectiveness over single drug therapy. Several nanoscale lipid and polymeric based drug delivery platforms have been developed and applied to facilitate co-delivery of therapeutic cocktails [7]. Nonetheless, due to the distinct pharmacokinetic profiles of individual drug molecules, there is still a high demand for the development of novel delivery platforms with desired functionalities required to combine targeted imaging and therapeutic agents.

“Smart” drug delivery systems are the next generation of nanoscale therapeutics currently under development to enable new therapies that go beyond current clinical outcomes. Integration of responsive nanomaterials into targetable delivery carrier and implantable depots can benefit from activation and feedback control of the cargo release [8]. With major advancements in

engineering “smart” drug delivery systems for screening and targeted delivery will become the main backbone for development of next generation of therapies.

Future research in this arena will assist us to fully investigate the absorption, distribution, metabolism and excretion of nanoscale materials and their pharmacokinetics in drug delivery applications. In addition, advancements in characterization of materials and tissues at the nanoscale will likely stimulate rational design for delivery platforms and innovative developments in co-delivery systems. By combining targeted imaging and therapeutic moieties we can visualize targeted sites and deliver therapeutics simultaneously [9]. Such advances demonstrate great promise in delivering new nano-based technologies for diagnostics and therapeutics for making large impacts on essentially every branch of medicine in near future.

2 Background – Physicochemical properties affect the synthesis, controlled delivery, degradation and pharmacokinetics of nanoporous materials

Controlling size, shape, and uniformity of porous constructs remains a major focus of the development of porous materials. Over the past two decades, we have seen significant developments in the fabrication of new, porous-ordered structures using a wide range of materials, resulting in properties well beyond their traditional use. Porous materials have been considered appealing, due to attractive properties such as pore size length, morphology, and surface chemistry. Furthermore, their utilization within the life sciences and medicine has resulted in significant developments in pharmaceutics and medical diagnosis. This article focuses on emerging classes of porous materials, providing an overview of principle concepts with regard to design and fabrication, surface chemistry, and loading and release kinetics. Furthermore, predictions from a multi-scale mathematical model revealed the role pore length and diameter could have on payload release kinetics.

Introduction

Porous materials, irrespective of their composition, have gained significant attention from the scientific and technological communities. Nature, commonly turned to for inspiration, is filled with many examples of porosity both at the nano- (i.e., mitochondrial cristae) and micro-scale (i.e., lungs and callus bone) [10]. Taking inspiration from these examples, the development of constructs with high surface area, tailorable porosity, thermochemical stability, and surface functionalization are all properties currently being explored [11, 12]. For example, nanomedicine [10], drug delivery [13], and tissue engineering [14, 15] have already seen tremendous success in this regard.

Optimizing the surface area can be critical for biomaterials by providing a higher capacity for the material to interact with ions and molecules, not only at the surface, but also throughout the bulk structure. To achieve this, pore size is commonly modified to provide materials an increase in surface area, thereby allowing better interaction with the microenvironment. Micro- (<2 nm), meso- (2-50 nm), and macro-pores (>50 nm) are all under extensive investigation for their physiochemical properties. In addition, volume, narrow size distribution, stability, and surface functionalization are all considered fundamental characteristics and are being applied to maximize payloads, tailor pharmacokinetic behavior, and target bioavailability in diagnostic and theranostic applications [16].

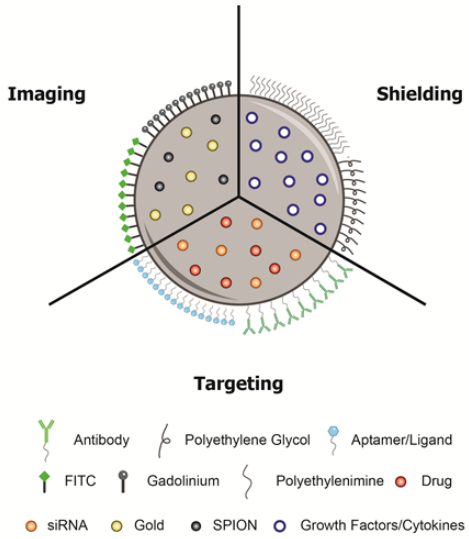

Figure 1. A schematic representation of a multifunctional porous particle showing possible core/shell design, surface modifications, and multiple types of cargos.

The design, synthesis, and chemical modification of mesoporous structures have been investigated extensively over the past two decades, demonstrating the versatility of synthetic approaches and the effectiveness of material design. Furthermore, ordered mesoporous materials have been synthesized using two common techniques (i.e., sol-gel and surfactant chemistry), demonstrating the versatility of a templating approach and the effectiveness of mesopores [10]. Overall, porous materials offer several advantages over organic based materials: compatibility

with hydrophobic/hydrophilic solvents, tunable stability, and ease of synthesis. Further modification of the surface with chemical conjugates paves the way for a plethora of potential applications (Figure 1). With a variety of porous materials currently being investigated, this article aims to discuss porous materials currently being implored in the field of nanomedicine with an emphasis on the multi-scale modeling approach. Herein, we use a multi-scale modeling approach to evaluate the impact a variety of factors may have on the pharmacokinetic properties of these materials.

Mathematical Modeling

Method

We apply a hierarchical multiscale modeling approach to elucidate the impact of interface and pore structure effects on payload diffusion. To overcome the limitations of classical diffusion modeling and prediction, we have recently developed a hierarchical computational approach that bridges nanoscale interface effects with a discretized continuum Finite Element (FE) method [17-20]. This new computational approach relies on a diffusivity scaling function, $S()$, derived from a diffusion coefficient profile at the interface of the nanochannel with the use of Molecular Dynamics (MD) simulations. The function $S()$ rescales an experimental bulk diffusion coefficient, D_B, so that the effective diffusivity depends on the local concentration c and the proximity to surface h:

$$D(c,h)=S(c,h)\cdot D_B(c). \quad (1)$$

This methodology was incorporated into the FE method [21, 22], used to model nanochannels, and it was quantitatively and qualitatively validated against experiments [20]. The following diffusivity scaling function were used: S(0) – no interface effects as in classical Fickian diffusion, S(1) were evaluated for rhodamine 6G , S(2) – as S(1) only size of molecular was

modified to evaluate size effects to diffusion, and S(4) was formulated to mimic 5 nm particle with long range interaction exceeding pore diameter. The basic mass balance equation, which also includes Fick's law

$$J = -D\nabla c \tag{2}$$

is

$$-\frac{\partial c}{\partial t} + \frac{\partial}{\partial x_i}\left(D\frac{\partial c}{\partial x_i}\right) + q = 0, \tag{3}$$

where J is the mass flux, $c(x_i,t)$ is concentration at a spatial point with coordinates x_i and at a time t; D depends in general on x_i and on c, as in case of surface interaction effects described above; $q(x_i,t)$ is a source term, and summation over the repeated index is implied ($i=1,2,3$). By using a standard Galerkin procedure, this non-linear differential equation is transformed into a linear incremental-iterative system of balance equations for a finite element assemblage [23].

Results

The computational model evaluated the kinetics of payload loading and release inside pores with different pore diameter, length, and surface properties, affecting interaction with payload (Figure 2). The dimensions cover representative values of the actual porous materials in order to emphasize the pore size effects on payload transport.

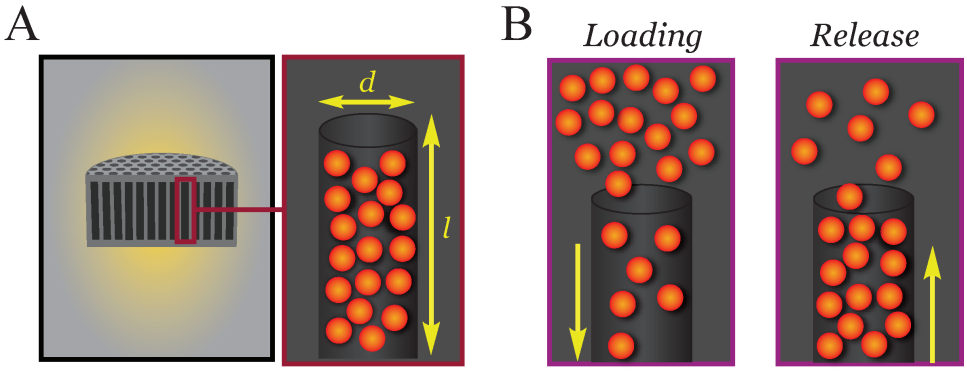

Figure 2. (A) Schematic of porous particle with pore diameter 'd' and pore length 'l'; (B) A diagram depicting the loading and release of the cargo molecule used to develop the diffusion model.

Figure 3A shows that the release rate, as well as the loading rate, decreases when the pore size is smaller. The pore diameter has very strong effects when the pore size approaches the payload size. This can be seen from the curves corresponding to 1 nm molecules in the pore with 2 nm diameter. Release kinetics has shown a stronger sensitivity to the length of pores, as shown in Figure 3B. By changing the pore length from 50 to 1000 nm, the release or loading time of pores changed by about four orders of magnitude. As expected, the increase in pore length increased the time for payload exchange.

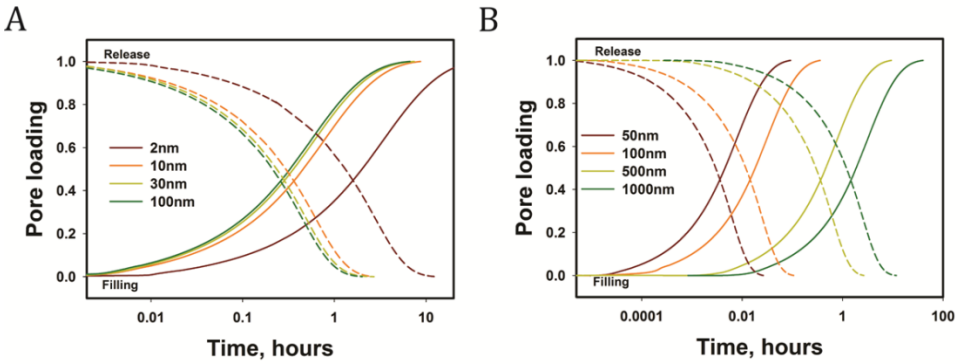

Figure 3. A) The effect of pore size on release and loading kinetics of pores with the 500 nm length for small payload molecules; B) The effect of pore length on release and loading kinetics of pores with the 30 nm diameter.

The half-lives of calculated curves in Figure 3A and 3B are summarized in Figure 4A. The payload exchange kinetics is slowed down by increasing the pore length (since trajectories of diffusing molecules become longer) and decreasing the pore diameter (smaller mass flux through cross-sectional area with overall surface effects more pronounced). Another interesting observation is that the times of full pore loading, in all cases, are larger than the time times of full release, which follows from the half-lives in Figure 4A. This can be explained as follows. In terms of release, we have zero concentration at the common boundary between pore and the surroundings, while in terms of loading, maximum concentration is at the entrance of the pore and concentration increases over the whole pore length. From these conditions, it follows that the concentration gradient is larger in case of release than for loading, which induces the observed transport kinetics. Finally, the interactions of payload with pore surfaces were evaluated using

unique features of our computational model. As it was shown in published data, the surface interactions may reduce diffusivity of molecules at solid interface. This effect was included in our model to represent payload diffusion more realistically as the classical Fickian diffusion alone cannot explain drug transport kinetics in porous materials. Figure 4B depicts four cases of payload diffusion with different scaling functions and the case with no surface effects (Fickian diffusion).

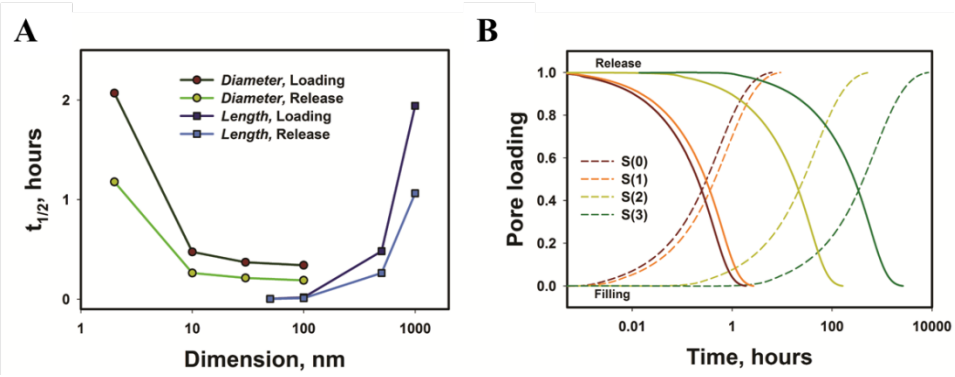

Figure 4. A) The effect of pore size and length to on the half-lives of release and loading kinetics of pores; B) The effect of surface properties inside pores to on loading and release. The surface effects alter diffusivity of payload at pore interface to different extent, depending on the payload characteristics.

As our model intrinsically incorporates diffusion particle dimension, the surface effect was significantly increased for 5 nm particle diffusion, with respect to 1nm particle, in the 30 nm pore. The 1 and 5 nm particles are adequate examples of small molecule drugs and proteins that are most frequently considered for drug delivery. Strong interactions inside pores might have equally strong effect on diffusion as the size itself, suggesting that payload with strong and long-range interactions would have the largest obstructions for mass exchange in pores.

Silicon

Porous silicon (pSi) was accidently discovered by A Uhlir at the historic Bell Labs in the 1950s [24]. However, it was not until work performed by LT Canham demonstrated the emergence of photoluminescent features of pSi arising due to quantum confinement that spurred

scientific interest in the early 1990s [25]. Further investigation revealed the tunable and versatile nature of pSi permitting high surface areas (up to 1,000 m^2/g) [26], low-cost and reproducible fabrication, large pore volumes (> 0.9 cm^3/g) [27] and exhibited enhanced biocompatibility [28-30] and biodegradation [31]. Hence with these unique characteristics, pSi has been applied to several diverse applications such as energy storage [32], microelectronics [33], biosensing [34, 35], tissue engineering [36], brachytherapy [37], and drug and protein delivery [38]. In the subsequent section, we will review and highlight the use of pSi materials and the impact of adjusting its pore size (or porosity) on drug delivery.

Fabrication of pSi

The fabrication of pSi is typically achieved using anodic electrochemical etching in specific mixtures of hydrofluoric acid (HF) and ethanol thus enabling a "top-down" approach [26]. Other fabrication methods to etch pSi include stain etching [39] and photosynthesis [40] but are limited due to poor control of the porosity and may result in incomplete porosification of pSi and are thus less common to the preferred anodization for drug delivery [41]. In addition, recent progress was successful in fabricating pSi in a "bottom-up" process similar to other nanoparticles, such as mesoporous silica [42]. Several parameters including HF concentration, current density, type of wafer, and time contribute to the porosity, pore size, and shape of pSi materials with the general rule that increases in current or HF/ethanol solution generate larger pores or higher porosity [41]. The pore sizes of pSi materials can range from 2 to 100 nm and further pore enlargement could be achieved using both thermal and chemical methods [43]. Furthermore, by adjusting the porosity of pSi one can modulate the photonic properties such that the emergence of distinct "barcodes" can be generated and detected using simple fluorescent methods [35, 44]. The two main pore morphologies fabricated in pSi materials generally consist of two types of cylindrical pores: interconnected/branched and dead ended [45]. The intrinsic flexibility of these fabrication parameters, allowed the manufacturing of pSi is several morphologies, including

membranes [46-48], micro- and nanowires [49, 50], microparticles [51, 52], and nanoparticles [53-55]. In addition to avoid the polydisperse fragments of various shapes and sizes typically achieved for pSi microparticles, Ciro and Godin et al. developed a microfabrication techniques enabling precise control for monodisperse pSi particles at the submicrometer scale for size, shape, and aspect ratio by patterning silicon wafers using photolithography methods and etched through a silicon nitride sacrificial layer shown in Figure 5 [56, 57].

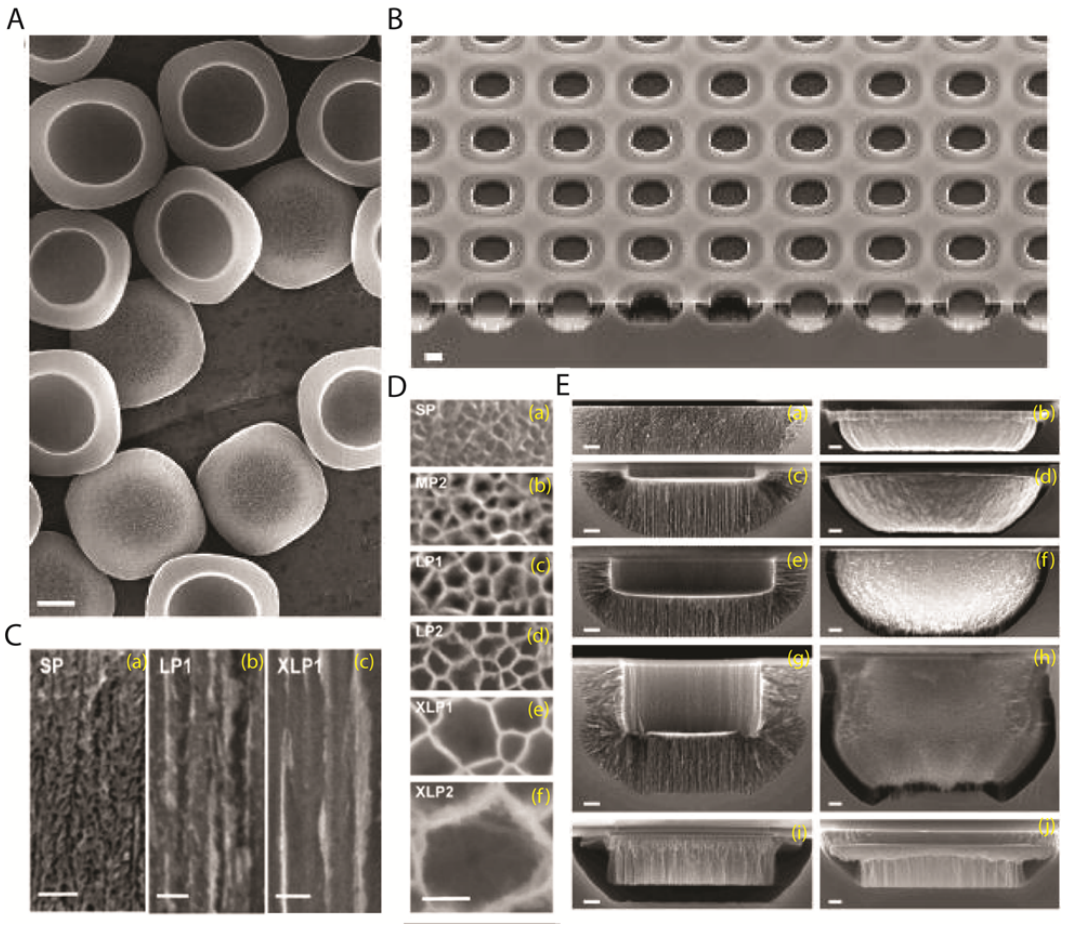

Figure 5. (A) Close-up of a small cluster of CF4 etched discoidal pSi particles; (B) Overview of a large cluster of SF6 etched Bowl shaped pSi; (C) SEM micrographs of the pSi porous structure cross section along the pore axis; (D) SEM micrographs of the central bottom region of the pSi; (E) a discoidal pSi obtained by trench formation by CF4.

Surface modification of pSi

After successful anodization, the surface of pSi materials is hydrogen terminated and is unstable and highly reactive. The surface of pSi can be modified using thermal or aqueous

oxidation, thermal carbonization, and hydrosilyation [45, 58]. These conjugations convert the unstable hydrophobic surface of pSi into a stable hydrophilic surface with a negative charge. In addition, these new surface modifications permits further functionalization enabling the introduction of carboxyl and amine groups [59, 60], PEGylation [61], recognition molecules [59, 62], porphyrins for photodynamic therapy [63], and fluorescent probes [64] allowing for the biodistribution assessment of pSi particles when the photoluminescent fluorescence [54] is not possible.

Loading and release of payloads from pSi

The pore size and surface are the two most important features of pSi that dictate the loading and release kinetics of payloads. Formulation of drugs into pSi enhances their bioavailability and potentially can increase the solubility of poorly soluble drugs without introducing extraneous agents (i.e., DMSO, Cremopher EL). Materials comprised of pSi for drug delivery have been applied to several different administration routes including implantable, injectable, transdermal, oral, intraocular, and brachytherapy [41]. The loading of pSi can be segregated into three major categories: adsorption/immersion, covalent attachment, and physical entrapment [27, 45, 65]. The most common method is the adsorption of payloads by simple immersion using a suitable solvent and has been used to load anti-inflammatory drugs [52], chemotherapeutics [54, 66, 67], proteins [38, 68], antibiotics [69], antivirals [70], small molecules [53], siRNA [71, 72], and nanoparticles [51, 59, 73-76]. The loading and release of drugs and nanoparticles from pSi can be engineered by varying the surface chemistry and pore sizes [45]. A poor choice in the surface chemistry can result in significant reduction in payload activity [77] and a summary of various studies illustrating the importance of surface chemistry is reviewed by Jarvis et al. [45]. Covalent attachment of chemotherapeutics was demonstrated by attaching doxorubicin [67] and daunorubicn [78] via hydrosilyation with undecylenic acid. Both methods

demonstrated sustained and delayed release compared to drug simply adsorbed into the pores. In addition, this method enabled the surface to dictate the drug release such that drug was specifically released as the surface became oxidized (or degraded) resulting in broken covalent linkage between pSi and the drug. The physical trapping of payloads was achieved by taking advantage of volume expansion (i.e., pore shrinkage) via aqueous or thermal oxidation after loading with payload. The Sailor research group demonstrated the entrapment of iron oxide nanoparticles [79] which retained and enhanced their magnetic [80] and heating properties [81]. In addition, expanding on this result Gu et al. demonstrated the simultaneously trapping of iron oxide nanoparticles followed by the adsorption of doxorubicin [82]. Using this approach, the authors demonstrated the ability to take advantage of the magnetic properties of their pSi particles to guide them to a specific location and enable targeted delivery of doxorubicin. In addition, the release of payloads from pSi can be modulated using a 'capping' or 'gate-keeping' approach. For example, pSi can be capped with poly(L-lactide) [83], poly(DL-lactide-co-glycolide) [84], agarose [85], cellular membranes [86], and hydrogels [87] allowing for the release of proteins and chemotherapeutics or act as sensors. Furthermore, these approaches enable a responsive drug delivery platform capable of delivering payloads in response to variations in temperature [88, 89], voltage [90], proteases [91], and pH [92, 93].

Impact of pore size

The pore size is another essential factor that can regulate the degradation and release of pSi materials. By adjusting the pore size (or porosity), pSi can be bioinert, or bioactive and slowly degrade, or biodegradable and dissolve in physiologically simulated environments [26, 31, 41]. The degradation of pSi yields silicic acid as their main byproduct, a molecule that has been shown to be beneficial for bone homeostasis [94] and synthesis of collagen type 1 [95]. In addition, the degradation rates of pSi can be tailored based on variations within the pore size or

porosity demonstrated on both films [96] and microparticles [97]. Selecting the optimal pore size can bestow tunable release kinetics for both free drug [98] and nanoparticles [97]. For example, by using pores that closely matches that of the drug, pSi can use pore confinement and concentrate poorly soluble drugs and retain the drug more than larger pores [99].

Additionally, Limnell et al. demonstrated that the release of ibuprofen could be controlled by modulating both the pore size and the surface of pSi, such that increased drug release was achieved from small pore thermally carbonized while thermally oxidized pSi achieved faster release with larger pores [100]. Also, Sethi et al. demonstrated that the loading of gadolinium-based contrast agents in smaller pores allowed the greatest magnetic relaxivity enhancement due to the increased adsorption of contrast in the pore walls and reduced mobility of water permitted by smaller pores [101]. This effect was further validated *in vivo* following the ocular release of daunorubicin in eyes of rabbit. Hou et al. demonstrated that engineering larger pore sizes in pSi microparticles a 63-fold increase in the release of covalently attached daunorubicin compared to smaller pores, thus showing a direct correlation between pore size and drug levels in the eye [98].

Furthermore this pore confinement was also observed with nanoparticles, such that upon loading within pSi microparticles the nanoparticles enabled the emergence of enhanced magnetic relaxivity [102], cooperative thermal heating [75], and prolong gene silencing [74, 76, 103] and chemotherapy [104] delivery. Martinez et al. demonstrated the impact of pore size on the loading and release of nanoparticles [97]. Here, the researchers demonstrated that the loading of quantum dots into pSi microparticles exhibited a direct correlation towards pore size, such that larger pores allowed higher retention of the nanoparticle payload. Interestingly the release kinetics demonstrated that larger pore pSi particles effectively delayed the release of the nanoparticles, compared to the smaller pores. Using a continuum diffusion model, they verified that the delayed release was attributed to the penetration of the nanoparticles within the pSi matrix further confirming their microscopy results.

In summary, pSi-based materials can be used as a powerful tool to tailor the delivery of therapeutics while triggering minimal immune response and can be tuned to modulate its degradation behavior. The pore size and surface chemistry of pSi enable unique features to engineer distinct pharmacological regimens dictated by the needs of the patient, thus effectively generating a critical material useful in various applications for drug delivery.

Silica

Since the discovery of surfactant-templated synthesis of mesoporous silica nanoparticles (MSN) in 1992 [105], many breakthroughs have been made in the development of various synthesis approaches of MSN with controlled size, morphology, and porosity, as the material of choice among many classes of mesoporous materials for various applications, such as sensors, separation, adsorption, and catalysis [106-108]. Their unique properties for ease of synthesis and surface modification, robust mechanical characteristics, and relatively inert chemical composition made an exponential increase in research on biomedical application of this class of material. The first report using MCM-41 type MSN as drug delivery system was published by Vallet-Regi et al. in 2001 [109]. They have attracted a great attention to render the possibility of designing a new generation of drug/gene delivery cargos with desired physicochemical properties, imaging moieties, and biosensors in biomedical applications [110-112]. In addition, recent findings in this field showed superior biocompatibility properties exhibited by MSN at concentrations adequate for pharmacological applications [113]. They also offer several advantageous physical properties, such as high surface area (>700 m^2/g), pore volume (>1 cm^3/g), structural stability, tunable pore size, and relatively easy surfaces functionalization [112]. These features allow MSN to achieve higher drug loading efficiency with tunable diffusional release of drug molecules from the highly ordered MSN at the targeted area, which lowers the overall dosage and prevents any acute or chronic complications. Moreover, they offer they provide effective protection of pharmaceutical

cargoes from premature release or undesired degradation of construct before reaching the designated target [114]. Additionally synthetic strategies in template fabrication have further enabled the synthesis of MSN with controlled size, shape and surface characteristics with increasing interest in their evaluation in biological systems.

Fabrication of Silica

Mesoporous silica particle (MSP) with controlled size and monodispersity was first synthesized by Stucky, Unger, and Zhao for chromatography applications [106, 107, 115, 116]. Their synthesis approach was based on the well-established Stober reaction for the synthesis of monodisperse non-porous particles. This reaction involved co-hydrolysis and subsequent condensation of tetraethoxysilane (TEOS) and an alkyltrialkoxysilane to obtain porosity in a mixture of three substrate: water, ethanolas a co-solvent to form a homogeneous solution and ammonia as a morphological catalyst [106]. Mesoporous silica particle was later developed by other groups using surfactant-stabilized emulsion chemistry [117], cosurfactant methods [118] or static acidic conditions [116]. In addition, the fine-tuning of reaction conditions such as the relative amounts of reagents, reaction temperature, led to the synthesis of particles with specific size distribution. Additionally, choosing various kinds of surfactants, such as n-alkyltrialkoxysilanes, at different concentrations regulated the pore size and surface area of the mesoporous silica particles [117]. While MSP are potentially useful for many non-biological functions, several protocols have been developed for snythesizing a series of MSP materials to circumvent potential problems with triggering acute immune response,efficient delivery of agents for gene transfection, or intracellular drug molecule.

For one of the well-established synthesis procedures of MCM-41 MSP, TEOS has been used as a silica source, while cetyltrimethylammonium bromide (CTAB), a cationic surfactant used as a structure directing agent, and sodium hydroxidewas were used as a morphological catalyst [119]. The template surfactant was then removed from material either by solvent

extraction (acidic solution) or calcination to generate a uniform pore structure. A typical MSP has an approximate particle diameter around 100 nm, surface areas around 900 m^2/g, pore sizes around 2 nm, pore volume around 0.9 cm^3/g, and a hexagonal porous channel structure (Figure 6).

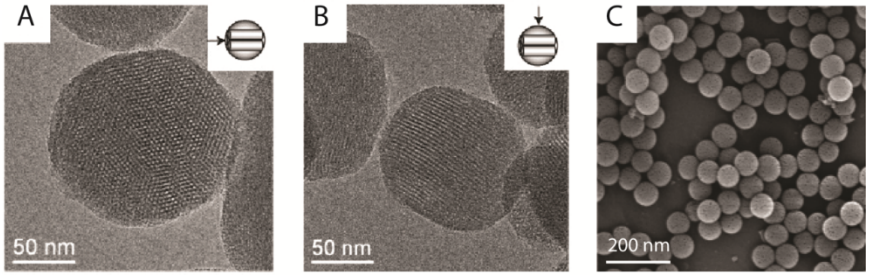

Figure 6. TEM images of monodispersed MPS recording from the direction (A) parallel or (B) perpendicular to the long axis of the pores, (C) SEM image of monodispersed MPS with uniform size distribution

Several groups have developed various methods to synthesize particles with controlled pore size, shape and surface chemistry [120-122]. In addition to previously stated properties, other unique characteristics of MPS such as tunable particle size, stable and rigid framework, and narrow pore size distribution brought enormous attention for use of these materials for various controlled release delivery systems. These applications allow their use in the loading of different drug molecules and evaluation of their release kinetics with high precision. Large pore volume and high surface area allow higher loading potential of drug molecules compared to other classes of nanomaterials.

Particle shape has been shown to have a significant effect on the agglomeration and circulation properties of several classes of non-porous nanomaterials *in vitro* [123-127]. Several methods have been established to tune the particle morphology in order to investigate the impact of different MSP particle sizes and shapes. The first method involved the use of various alkyl chain antimicrobial agents as templates for the synthesis of MSP. Spheres, ellipsoids, and rods were successfully synthesized by using 1-alkyl-3-methylimidazolium with different alkyl chain

lengths. Trewyn et al. demonstrated that the antimicrobial activity of these MSP can be tuned by modifying the morphology of these nanoparticles[128].

Che et al. was the first who observed the helical mesoporous structures in a rod-shaped MSP using an achiral 1-octadecyl-3-methylimidazolium as surfactant template. Moreover, a rod-shaped MSP with a pseudomoire porous was observed and parallel channel pores were twisted into a helical structure along the long axial of the nanorods [129]. The second method was based on a co-condensation reaction using TEOS and different organo-alkoxysilanes. For instance, hexagonal tubular structure can be produced using TEOS and 3-aminopropyltrimethoxy-silane (APTMS) in a co-condensation reaction. The shape of the particle can be easily transformed into other structures by easily replacing the APTMS with other similar organoalkoxysilanes, such as N-(2-aminoethyl)-3-aminopropyltrimethoxysilane (AAPTMS) and 3-[2-(2-aminoethylamino) ethylamino]propyltrimethoxy-silane (AEPTMS) [119]. Finally, we can control particle morphology by changing the ratios of reactants. Huh et al. have shown in detail how to tune MSP morphology and pore properties with multiple organic functional groups [130].

Surface Modifications

Targeting is especially relevant in the context of therapeutic application and surface modification can reduce unspecific interactions with proteins and thus increase circulation time, active cellular uptake and further enhancement of retention time. Methods of surface modification to obtain hybrid composite MSP are usually employed to provide particles with additional functionality and enhanced biocompatibility. Surface modification can bear functional groups to allow the covalent grafting of biomolecules and therapeutic agents for targeting.

One-pot synthesis (co-condensation) reaction, post-synthesis modification (grafting), and imprint coating method are the three general methods of surface modification of MSP [131-133]. Co-condensation using one or more organoalkoxysilanes has been widely used for synthesis of

inorganic–organic hybrid networks. This method is a suitable condition for a wide range of reaction conditions applicable to wide varieties of organoalkoxysilanes, which allows homogeneous surface modification coverage of functional groups across porous material without affecting the structural integrity of the pores. Radu at al performed extensive study on various anionic organoalkoxysilanes modifications including: thiolate-, carboxylate- and sulfonate-containing organoalkoxysilane [134].

In addition, inorganic coatings have been used over polymeric coatings due to the several advantages such as enhanced chemical and mechanical stability over naked particles and lack of swelling or porosity changes in various pHs. They also shield the cargo molecule against denaturalization induced by extreme environmental changes (temperature and pH) [135]. Many of the synthesis approaches in the literature are based on core–shell settings [136, 137]. The silica coating on a magnetic core leads to enhancement of stability and biocompatibility of these constructs in a wide range of applications [138].

Loading & Release

As emphasized previously, any drug/gene delivery system has to fulfill a list of desirable properties in order to achieve the release of the cargo in a suitable concentration at the desired target within desirable time of delivery. MSP-based controlled release systems have been demonstrated to deliver different kinds of guest molecules such as anti-inflammatory, anticancer, antibiotics, peptides, RNA, and DNA using different strategies to modify the control of drug release [135, 139-143].

Conclusion

Porous materials have attracted great attention as potential drug delivery platforms for various biomedical applications. They can be selectively modified at their inner and outer surface

in order to be efficiently loaded with desired cargo molecule. Additionally, their outer surface can be chemically functionalized to act as pore gatekeepers to delay the release. Compared to most other prominent organic drug delivery platforms, nanoporous materials offer several advantages including high loading capacity, high stability, and the ability to protect the payload from degradation. The high degree of tenability in porous materials makes these systems highly attractive candidates for delivery applications. Although much progress has been made, many obstacles still remain unsolved. Today's challenge is the investigation of pharmacokinetics and pharmacodynamics of these materials for in vivo diagnostic and therapeutic applications to bring them to clinical studies. The biological effects of these materials involving cytotoxicity, biodistribution, biocompatibility, and biodegradation at different scales from molecules to tissues and organ levels, are currently under excessive investigation. Moreover, identification of proper surface modification for each class of porous material seems to be crucial in order to decrease rapid clearance, facilitate target specificity and efficient delivery of payload. Finally, recent studies focus on the ultimate combination of diagnostic and therapeutic capabilities of these materials, such that the nanocarrier uses diagnostic information to control its therapeutic effects. These features allow porous materials to exhibit a signal that is affected in a predictable way when exposed to environmental changes, presenting possibilities for the development of advanced multifunctional systems that incorporate sensors for diagnostic or therapeutic functions. The future is bright for multifunctional porous materials in imaging, diagnostics and therapy.

3 Cefazolin loaded mesoporous silicon microparticles show sustained bactericidal effect against Staphylococcus aureus

A manuscript published in *Nanomedicine* 5, 2041731414536573

I. K. Yazdi, M. B. Murphy, C. Loo, X. Liu, M. Ferrari, B. K Weiner, and E. Tasciotti

Cefazolin is an antibiotic frequently used in preoperative prophylaxis of orthopedic surgery and to fight secondary infections postoperatively. Although its systemic delivery in a bulk or bolus dose is usually effective, the local and controlled release can increase its effectiveness by lowering dosages, minimizing total drug exposure, abating the development of antibiotic resistance and avoiding the cytotoxic effect. A delivery system based on mesoporous silicon microparticles (MPS) was developed that is capable of efficiently loading and continuously release of cefazolin over several days. The in vitro release kinetics from MPS with three different nanopore sizes was evaluated and minimal inhibitory concentration of cefazolin necessary to eliminate a culture of *Staphylococcus aureus* was identified to be 250 μg/mL. A milder toxicity towards mesenchymal stem cells (MSC) was observed from MPS over a 7-day period. Medium pore size loaded MPS exhibited long lasting bactericidal properties in a zone inhibition assay while they were able to kill all the bacteria growing in suspension cultures within 24 hours. This study demonstrates that the sustained release of cefazolin from MPS provides immediate and long-term control over bacterial growth both in suspension and adhesion while causing minimal toxicity to a population of MSC. MPS offers significant advantageous properties for drug delivery applications in tissue engineering as it favorably extends drug bioavailability and stability, while reducing concomitant cytotoxicity to the surrounding tissues.

Keywords: antibiotics; controlled release; drug delivery; microparticles; mesoporous silicon

Introduction

Orthopedic surgeries represent a substantial portion of total medical treatments in the United States with over 25.8 million procedures or consultations related to the back or spine, 14.5 million for knee problems, and 9.7 million for shoulder injuries [144]. Even with modern sterilization and aseptic surgical techniques, orthopedic surgery is still associated with infectious complications, especially in the setting of intervention after traumatic injuries. Approximately 1 to 3 out of every100 patients who have surgery develops infection, representing one fourth of all nosocomial infections [145]. Treatment of implant related infections, on the other hand, involves long-term systemic administration of antibiotics and multiple operations to remove hardware and locally decontaminate the surgical field. Serious problems can arise from this approach, including a failure to produce therapeutic tissue concentrations of the antibiotics secondary to poor tissue perfusion, selection of highly resistant bacteria through repeated low dose exposure, and the multiple complications associated with the subsequent operations to repair the problem [146].

According to the guide for elimination of orthopedic surgical site infections published by the Association for Professionals in Infection Control and Epidemiology (APIC), *Staphylococcus aureus (S. aureus)* is considered as one of the major gram-positive microorganisms associated with surgical site infections, possess a high degree of virulence due to its ability to produce toxins and develop resistance to many classes of antibiotics, and accounted for 48.6% [147]. Antimicrobial agents are decided according to the type of microorganism based on the clinical practice guidelines for post-surgical infections. Cefazolin serves as the standard of care and first drug of choice according to current practice in antimicrobial prophylaxis [148]. It has been the most widely used agent with confirmed efficacy against *S. aureus* as well as widely common organisms encountered in surgery such as *Escherichia coli*, various strains of *Streptococci*, *Proteus mirabilis*, and *Klebsiella* species [149].

Ideally, an antibiotic delivery system should provide sustained and controlled release to nearby tissues, eliminating the need for systemic infusions or repeated injections of the drug [150-152]. Localized release allows for total dose reduction and minimizes systemic toxicity and resistance and various biodegradable and bioresorbable carriers of antibiotics for the treatment and prevention of prosthetic infections have been studied [9, 153, 154]. Therefore, many materials have been introduced and chemically modified to maintain extended-release properties in past decade [155]. Simultaneously, with the development of new polymers [156-159] and inorganic porous matrices [160-165], nanotechnology has increasingly influenced the field [166, 167]. One of the widely used techniques to deliver antibiotics locally to a wound site is through the introduction of polymethylmethacrylate (PMMA) beads or poly(lactic-co-glycolic acid) (PLGA) particles loaded with antibiotic. Although effective for treating most infections, these polymeric materials are not always fully bioresorbable and their acidic degradation byproducts locally irritate surrounding tissues, create acute inflammation and may elicit an immune response thus hampering tissue healing [168, 169].

Porous silicon based biomaterials with nanoscale features [170-175] are appealing for this purpose, as their release and degradation kinetics [176] are tunable as a function of porosity and pore size [177-179]. Mesoporous silicon microparticles (MPS) can enhance drug availability and distribution over time similar to PLGA particles as they degrade to control the payload release kinetics with a negligible inflammatory tissue response and no toxic side effects *in vivo* [180-182].

Previously, MPS have been employed for the targeted or controlled delivery of ibuprofen, griseofulvin, ranitidine, furosemide, antipyrine, daunorubicin, Q-dots, ethionamide, peptides, RNA interference and imaging agents [183-190]. In this work, we have shown the release kinetics of cefazolin with three different nanopore sizes of MPS, bactericidal activity of them on *S. aureus,* as one of the most prevalent bacteria strains associated with post-operative infections [191-193] and also cytotoxicity effects of antibiotic loaded MPS towards mesenchymal stem

cells (MSC) to ensure this technology would be conducive for wound repair and tissue regeneration [175, 194].

Materials and Methods

Preparation and characterization of Porous Silicon Microparticles

Microparticles of three different pore sizes were generated and characterized for this study: small (SP), medium (MP) and large (LP) pore MPS with mean pore diameters of 3, 6, and 10 nm, respectively. All microparticles had a mean diameter of 3.2 +/- 0.2 μm. MPS particles were designed and fabricated in the Microelectronics Research Center at The University of Texas at Austin as previously reported [179, 195, 196]. Briefly, Heavily doped p++ type (100) silicon wafers (Silicon Quest Inc, CA) were used as the base for the deposition of a 200 nm layer of silicon nitride using low-pressure chemical vapor deposition followed by standard photolithography with a EVG 620 contact aligner. To produce a highly porous layer, current density of 320 mA/cm^2 was applied for 6 seconds in a 49% mixture of hydrofluoric acid (HF) in ethanol (2:5 (v/v)) [179]. The particle surface was further oxidized by H_2O_2, and then the suspension was heated to 100-110ºC for 4 hours, washed with deionized water, and resuspended in isopropyl alcohol (IPA). The morphology of MPS particles was examined in detail by scanning electron microscopy (SEM) and transmission electron microscopy (TEM).

Microparticles Size and Charge characterization

MPS particle volume, size, count and charge were obtained using a Multisizer™ 4 Coulter Counter (Beckman Coulter, Inc., CA) and Zetasizer Nano ZS (Malvern Instruments Inc., MA). Before the analysis, the samples were dispersed in a balanced electrolyte solution and sonicated for 10 seconds for sufficient dispersion. The zeta potential of the microparticles was analyzed by a Zetasizer nano ZS [197]. For all analysis, 2 μL particle suspension containing at

least 1×10^5 particles to achieve a stable zeta value evaluation were injected into a sample cell countering filed with phosphate buffer (1.4 mL, pH 7.2). The cell was sonicated for 2 min, and then an electrode-probe was placed into the cell. Measurements were conducted at room temperature (23°C) in triplicates runs.

Antibiotic Loading

10^7 MPS/mL were combined with a concentrated antibiotic solution (cefazolin sodium, 5 mg/mL in phosphate buffered saline (PBS), Sigma Aldrich, Saint Louis, MO) at room temperature. The MPS and loading solution were sealed in a centrifuge tube, which was gently stirred during the loading process for 1 hour. After loading, the MPS were separated by centrifugation from the solution, rinsed twice with PBS to wash off any drug substance from their surface and lyophilized overnight. The loading efficiency was determined by High-performance liquid chromatography (HPLC) and confirmed by the cumulative release of cefazolin from the particles.

Analytical method to determine cefazolin concentration

A mobile buffer solution composed of 20% methanol, 10% acetonitrile, and 70% monobasic phosphate buffer was passed through a Agilent Zorbax SB-C18 column (4.6mm ID x 250mm length) [198]. The buffer was passed through the column at a rate of 0.5 mL/min, and the absorbance of cefazolin in solution was measured at a wavelength of 270 nm on a Hitachi L-2455 Diode Array Detector. The retention time for cefazolin was 2.5–3.0 min. Injection volumes were 20 μL for all samples. Standard curves were created with serial dilutions of cefazolin in PBS, so that linear regression could be used to determine sample concentrations based on peak height and retention time area. All HPLC measurements were performed at room temperature.

In vitro drug release

Individual batches of cefazolin-loaded MPS (10^7 particles) were incubated in 1 mL of fresh PBS solution in a humidified 95% air/5% v/v CO_2 incubator at 37 °C with gentle shaking (100 rev/min). The release solution was collected and replaced by fresh PBS at every time points. Drug concentration was determined by measuring the collected solution with HPLC and UV-Vis spectroscopy. Three samples were measured for each time point and the results were reported as average values ± standard deviation (SD). Samples were collected until no additional cefazolin was released (5 days).

Antibacterial Assessment

Minimum Inhibitory Concentration Assay

The toxicity of cefazolin sodium to *S. aureus* ATCC 29213 was investigated by adding 0, 50, 100, 250, and 500 μg/mL to 1 mL of 10^6 CFU/mL bacterial suspension. Cells were counted at 3, 6, 12, 24, 48, and 72 hours, with triplicate samples at each time point using conventional plate count method.

Determination of the zones of inhibitory concentration

1.5 mL from a 10^6 CFU/mL LB broth suspension, were added to the 37°C pre-warmed nutrient agar medium (BD Falcon 100x15 mm style) plates and incubated at 37°C for 24 hours. Cefazolin-loaded MPS (250 μg in 10^7 SP or MP particles in 50 μL PBS) were deposited at four equidistant locations on the agar plates and left at room temperature for 30 min before incubation at 37°C. The diameters of inhibition zones were measured for day 1, 2, 3, 7 and 21 and expressed as mean ± SD. The corresponding positive (with equivalent concentrations of cefazolin to loaded particles in PBS) and negative (using unloaded microparticles without antibiotic) controls were prepared and tested.

Antimicrobial Activity Assay

S. aureus bacteria were suspended in 2.5 mL of sterile rich LB broth medium. The suspension was standardized using spectrophotometry at a wavelength (λ) of 800 nm to match the transmittance of 90, equivalent to 0.5 McFarland scale (1.5×10^8 colony-forming units/mL (CFU/mL)). A 2.0 mL volume of the LB broth medium (37°C) was gently poured into a 6-well cell culture plate and each well was inoculated with 10^3 CFU/mL of *S. aureus* cells. Antibiotic was added to each well either directly or loaded into MPS. The plates were incubated for 72 hours at 37°C and the cells collected and counted at 1, 2, 4, 8, and 24 hours. Three replicates were performed for each time point.

Cefazolin and MPS Toxicity to Rat Mesenchymal Stem Cells

Rat mesenchymal stem cells (MSC) were isolated from the compact bone of young male Sprague Dawley rats. Tibae and femora were cleaned of periosteum and connective tissue, flushed and washed of marrow, crushed with a mortar and pestle, and enzymatically degraded in a solution of collagenase (3 mg/mL) and dispase (4 mg/mL) in PBS. Liberated mononuclear cells were cultured in media containing 20% fetal bovine serum under hypoxic conditions (5% O_2) to promote colony formation [199]. MSC from these primary colonies were passaged up to four times prior to toxicity studies.

The cells were seeded in a 24-well plate at a density of 1000 cells/well and allowed to stabilize for 24 hours prior to treatment. Rat MSC were cultured for a period of 7 days, in the above described experimental conditions as a control, or in complete media supplemented with 0, 50, 100, 250, and 500 µg/mL cefazolin sodium (either direct dose or loaded into 10^7 MPS). Cell proliferation was determined by quantification of double-stranded DNA using the Quant-It PicoGreen assay (Invitrogen). Lactate dehydrogenase (LDH) activity assay (Sigma-Aldrich) was used as a determination of cell membrane damage and toxicity. At time points of 1, 5, and 7 days, the culture medium was collected and assayed for LDH-cytotoxicity, and the adherent cells were

washed twice with PBS, and lysed by addition of 1 mL deionized water and freeze-thaw to -80°C for DNA collection and quantification.

Results and Discussion

Characterization of MPS particles

MPS particles were fabricated through photolithography and electrochemical etching as previously described [179]. The average diameter of all three MPS types used in this study was evaluated through Multisizer Coulter Counter analysis and their relative surface charge was measured by Nano Zetasizer (Table 1) while the uniformity of the structural properties (aspect ratio, shape and pore size) were characterized by SEM (Figure 7).

Table 1. Characterization of different types of MPS: zeta-potential, particle size (diameter), average pore size, total porosity, and pore volume.

MPS Type	Mean Zeta Potential (mV) ± SD	Particle Size (µm)	Avg. Pore Size (nm)	Porosity (%)	Pore Volume (fL)
SP (Small Pore)	-31.15 ± 1.48	3.2 ± 0.2	3.04 ± 1.08	33	6.34
MP (Medium Pore)	-27.64 ± 2.73	3.2 ± 0.2	6.02 ± 1.86	47	5.61
LP (Large Pore)	-24.73 ± 1.62	3.2 ± 0.2	10.08 ± 3.14	51	4.15

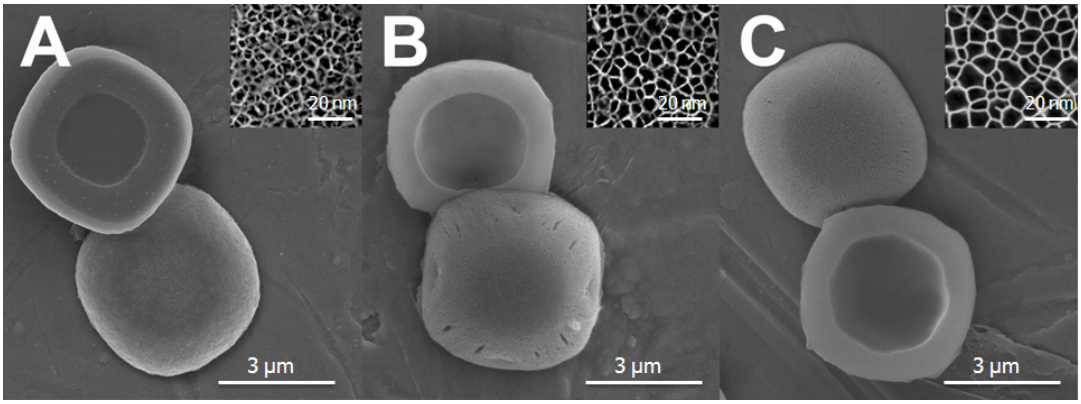

Figure 7. Scanning electron microscopy images of mesoporous silicon microparticles with their relative three different pore sizes

Scanning electron micrographs of all different pore sizes MPS were shown and their pores were presented in more details (Figure 7 A-C). During synthesis and oxidation, the partial surface erosion led to the hydroxylation of MPS creating a net negative charge (Table 1). The

direct correlation between MPS pore size and charge was demonstrated through zeta potential analysis. As the particle pore size increased, the overall porosity increased and surface area of the particles decreased. Consequently, fewer hydroxyl groups were displayed on MPS surface, causing the net total charge to be less negative (Table 1).

In vitro drug release

The porosification of silicon during electrochemical etching created a large surface area per volume ratio, allowing for the adsorption of high amounts of drug molecules during the loading process. A relationship between the pore diameter and the loading and release profiles of MPS was observed. The parallel-etched pores within the SP microparticles allowed increased drug loading capacity due to their higher surface area than the MP or LP particles. However, total porosity dominates total drug loading mass among these three particle types, as LP possessed the highest total porosity than MP or SP, while SP particles are holding the highest surface area among them. The average cefazolin loaded mass per 10^7 MPS is reported as 275, 392 and 452 µg for SP, MP and LP microparticles. The amount of antibiotic loaded directly correlated with porosity, pore size and pore volume as reflected in Figure 8A.

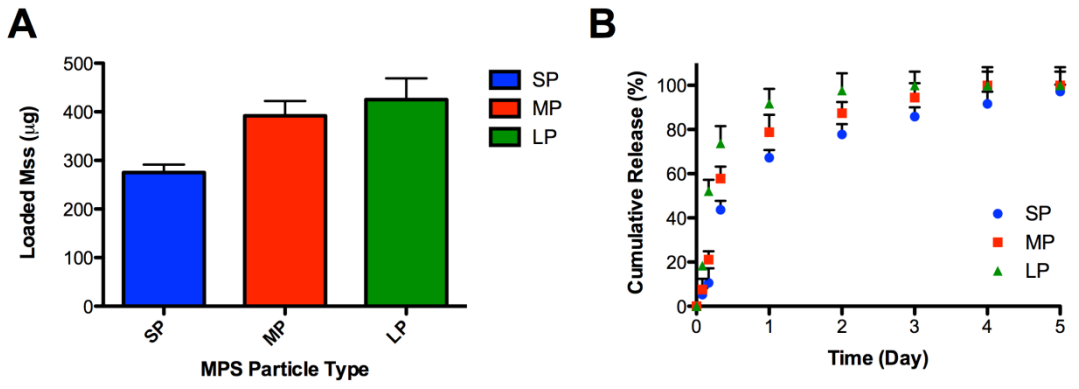

Figure 8. (A) Mass of cefazolin loaded into three MPS particle types (B) The cumulative percentage of released cefazolin as a function of time from MPS particles in vitro over 5 days.

The antibiotic release profiles from cefazolin-loaded MPS particles obtained over 5 days are shown in Figure 8B.MPS particles with larger pores (LP) showed a higher initial burst release

of cefazolin [200]. The release delayed with decreasing pore sizes, potentially due to the limitations in the diffusion of the drug through 3 and 6 nm pores (SP and MP). This effect reinforced the notion of the emerging properties of nanostructured materials on drug release kinetics [201]. Complete release was obtained by day 5, at which time the MPS also completely degraded.

Antibacterial activity

The assessment of antibacterial activity of cefazolin-loaded microparticles was tested against *S. aureus*, which is the most common bacterial pathogen seen in osteomyelitis [202]. After the minimum inhibitory concentrations were determined, the antimicrobial activity of the antibiotic-loaded MPS was evaluated by two different techniques: antimicrobial activity and zones of inhibition assay against *S. aureus*.

Minimum Inhibitory Concentration Assay

The antibacterial activity was significantly effective for the three higher cefazolin concentrations. Cefazolin was 90% bactericidal to *S. aureus* ATCC 29213 at concentrations greater than 100 µg/mL. Concentrations of 250 and 500 µg/mL demonstrated more than 98% bacterial elimination within 48 and 24 hours, respectively (Figure 9).

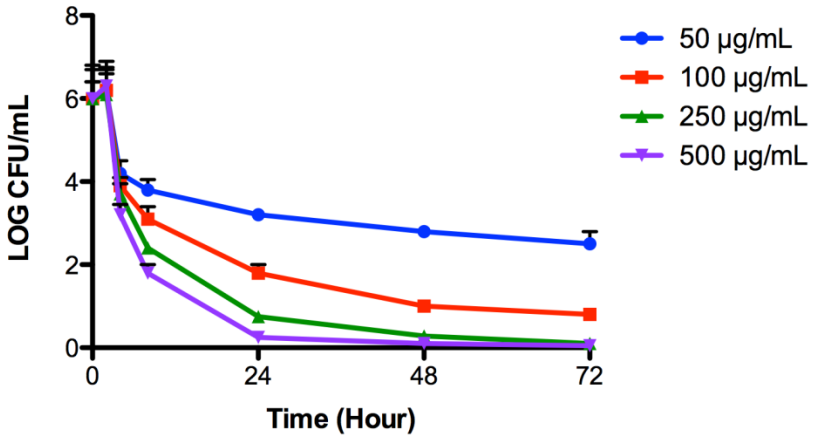

Figure 9. *S. aureus* bacteria growth inhibition against different cefazolin sodium concentrations over 72 hours.

Zones of inhibition Assay

The bioactivity and potency of the released antibiotic was evaluated using Kirby-Bauer methods determined by creating zones of growth inhibition on agar plates [203]. Disposable agar plates inoculated with the tested *S. aureus* ATCC 29213 at a concentration of 10^6 CFU/mL. SP and MP MPS (10^7 microparticles unloaded or loaded with 250 µg of cefazolin) were selected due to their slower release kinetics for this study and applied to distinct locations of each plate. The diameter of the regions devoid of *S. aureus* growth were measured daily for day 1, 2, 3, 7 and 21. The purpose was to determine the bactericidal effects of the gradual release of cefazolin form MPS. Both particle types showed a significant activity against *S. aureus* by release of cefazolin (Figure 10).

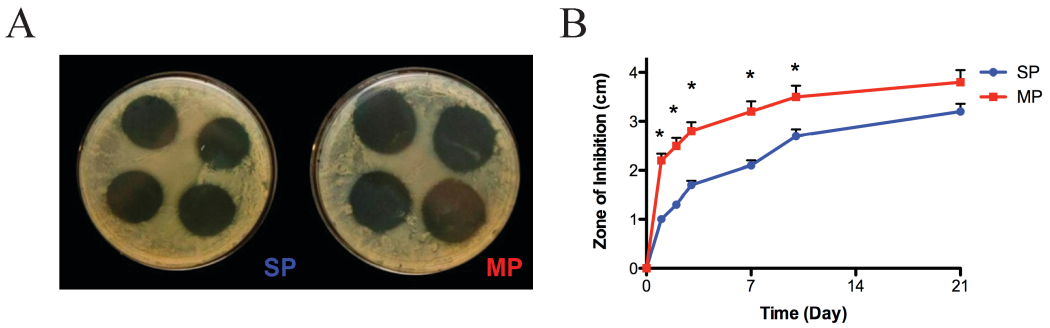

Figure 10. (A) Bacteria inhibition zones surrounding SP and MP cefazolin-loaded MPS particles at day 21. (B) Zone of inhibition (cm) of SP and MP microparticles over 21 days against S. aureus from release of cefazolin which indicates a successful long-term elimination and prevention of *S. aureus* growth.

During the first two days, the average zones of inhibition obtained with cefazolin-loaded MP treated plates, was approximately twice that of SP treated plates. The difference in clear-zone diameter of growth inhibitions of SP and MP were correlated to their release kinetics respectively, which shows that zone of inhibition was increased as the amount of loaded cefazolin was increased in MPS particles. There was no significant difference found in the zone of inhibition between the two particle types once they have completely released their antibiotic payload (from days 10 to 21). This result successfully indicated a long-term elimination and prevention of *S. aureus* growth in the presence of antibiotic-loaded MPS for up to 21 days.

Additionally, unloaded SP and MP MPS control groups did not display any zone of inhibition, meaning the MPS particles themselves or their degradation byproducts were not responsible for the antimicrobial activity observed.

Antimicrobial Activity Assay

MP microparticles were selected on the basis of their high loading efficiency and longest inhibitory properties compared to other types of MPS. *S. aureus* was cultured with empty and drug-loaded (250 µg cefazolin) CFZ MP for 24 hours. Photographic images of the cultures through the first 24 hours are shown in Figure 11A. Plates with cefazolin-loaded MP microspheres exhibit a significant decrease in the bacteria growth, which correlates with the release of cefazolin within the first 24 hours. The wild-type control (WT) exhibited an exponential growth expansion between 4 and 8 hours. The number of bacterial colonies (CFU/mL) over the equivalent time range is reported as log (CFU)/mL in Figure 11B. As determined by the *in vitro* release study, this growth expansion corresponded with the cumulative release of 40-50% of the loaded drug by 8 hours using the MPS particles. The controlled release of cefazolin was capable of preventing colony formation throughout the course of the study. There was no inhibitory effect was detected for unloaded MP microparticles (Ctrl MP), which indicates that the major bactericidal effect was due to the released antibiotics and not from the microparticles degradation byproducts.

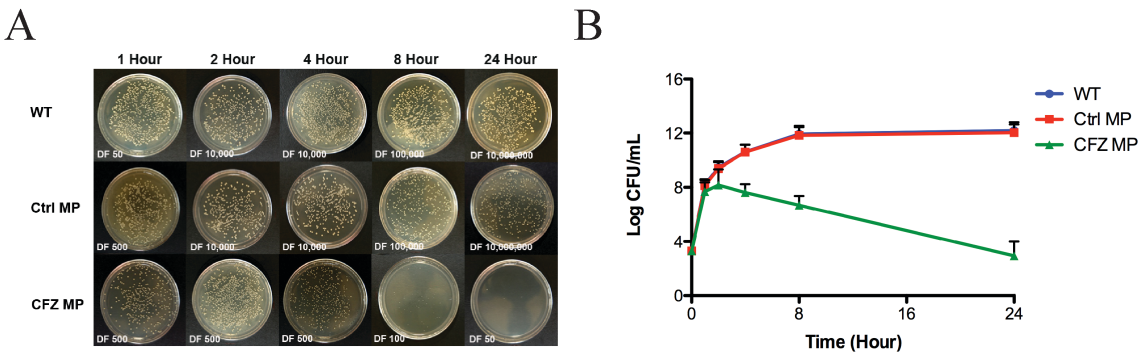

Figure 11. (A) Antimicrobial activity of cefazolin-loaded medium pore MPS particles against S. aureus. (B) Antibiotic loaded MPS prevented *S. aureus* growth over the course of the 24 hours compared to wild type control (WT) and unloaded MPS (Ctrl MP) groups.

Rat MSC cell proliferation and cell membrane integrity were evaluated over 7 days to determine the cytotoxic effect of the MPS particles at various doses of cefazolin. Cell viability at days 1, 5, and 7, normalized against drug-free and MPS-free controls are reported in Figure 12.

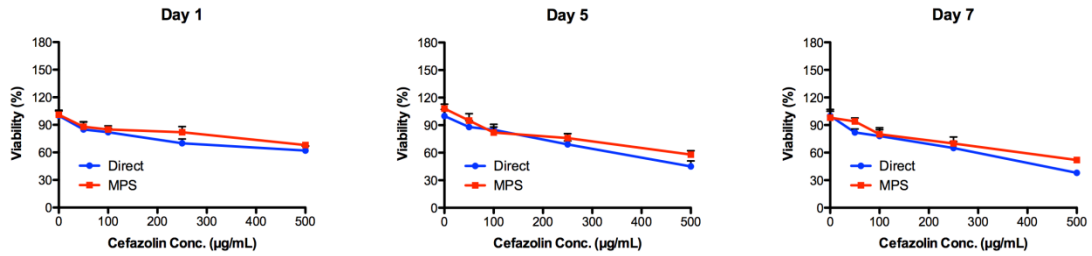

Figure 12. Effects of the presence of different concentrations of cefazolin (direct dose or release dose from MPS) on the growth of Rat MSC. The controlled release of cefazolin from MPS was able to reduce the cytotoxic effects on MSC compared with direct doses of antibiotic.

Direct administration of the antibiotic had a significant effect on cell viability at 250 and 500 µg/mL. However, the controlled release of cefazolin from MPS caused reduction of the toxic effect of direct exposure of cells to the drug (day 5 and 7). This effect was also observed at 100 µg/mL dosages, although the advantages of MPS were not found statistically significant. Most importantly, the release of 250 µg/mL by MPS, a dose previously was found to exhibit over 98% bactericidal efficacy within 48 hours and clearly formation of inhibition zones, was not found to reveal any adverse effects on MSC proliferation and cell membrane integrity, while their direct exposure to a higher concentration of the antibiotic (>250 µg/mL) induced signs of toxicity at all time-points. The growth of cells in the presence of antibiotic-loaded MPS was approximately 2, 13, 26 and 18% greater at day 5, and 15, 7, 13, and 18% greater at day 7, than for cells cultured with the direct dose applied of 50, 100, 250, and 500 µg/mL respectively. Overall the controlled release of cefazolin from MPS was found to reduce the cytotoxic effects on MSC compared with direct doses of antibiotic (Figure 12).

Cell membrane integrity and general cell health was evaluated by LDH release in the culture media at 1, 5 and 7 day after treatment and reported results were normalized to cefazolin-free, MPS-free controls in Figure 13. No significant effects were detected for 50 or 100 µg/mL

dosages for either the direct treatment or MPS treated groups. In agreement with MSC viability, dosages of 250 and 500 µg/mL showed enhancement of the LDH activity for both groups at all-time points. Likewise, similar levels of LDH production from MSC were observed at 100 µg/mL concentration for both groups. The direct administration of cefazolin exhibited slightly higher LDH activity compared to MPS and the difference was statistically significant at days 5 and 7 for 500 µg/mL ($P<0.01$). At the three highest dosages used in the study, the sustained release of cefazolin from MPS significantly lessened these cytotoxic effects on MSC compared to the direct administration of cefazolin.

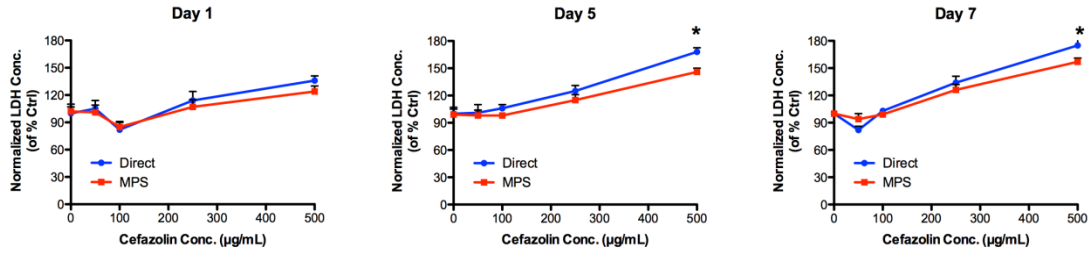

Figure 13. LDH activity in culture media of MSC in the presence of different cefazolin concentrations (direct or released from MPS) at days 1, 5, and 7.

From this investigation, it was found that a local concentration of 250 µg/mL cefazolin was sufficient as an antibacterial prophylactic. Administration of this drug concentration via MPS exhibited no significant effects on MSC cell viability or metabolic integrity compared to controls, while this dosage was found to be toxic to the stromal cells when given as a bulk dose. In contrast to polymeric delivery systems, the MPS particles are fully degradable and biocompatible and do not generate inflammatory byproducts as the polymeric counterparts [204-207]. It is hypothesized that high local concentrations of antibiotic can diffuse through avascular areas of the surgical or implant site that are inaccessible by systemic intravenous methods, which often can only be delivered in concentrations that may result in toxicity or lead to bacterial antibiotic-resistance.

Conclusion

In recent years, the growth of resistant microorganism strains has been accompanied by development of new clinical guidelines and shortage of new formulations. As a result, it is crucial to develop new platforms to maintain the antimicrobial drugs activity while extending their half-lives through new routes of delivery [208]. To overcome these limitations, sophisticated delivery platforms capable of tuning the release of their contents is necessary to fight against drug resistant bacteria strains like Methicillin-resistant *S. aureus* or *Coagulase-negative Staphylococcus* [209].

Past few decades, numerous drug delivery platforms have been developed to enhance the bactericidal properties of antibiotics and meet different clinical needs such as extended shelf-life stability, high biocompatibility, and multifunctional properties [210-213]. In this study, sustained delivery of cefazolin from MPS particles showed to provide adequate bactericidal properties to efficiently inhibit *S. aureus* growth. The pore size and porosity MPS provide tunable drug release characteristics and their surface area can be modified or encapsulated in order to achieve specific desired therapeutic daily dose for various tissue engineering applications [214-217]. This nanotechnology-based delivery system represents an alternative to the current standard of care and addresses the shortcomings of intravenous antibiotic delivery. The MPS antibiotic delivery system may represent a new platform for the prevention of post-operative infections, for the treatment of biofilm formation on orthopedic implants, for the medication, of traumatic musculoskeletal injuries. Due to its decreased toxicity on stem cells, this system represents a promising alternative to direct administration of the drug, with long term advantages on the regeneration of the tissues, the healing of the injury and on the overall wellbeing of the patient.

4 Surface modification of MPS with hydrogels to extend drug release

Drug molecules are often required to be administrated repeatedly to provide a long lasting therapeutic effect. Drug instability is still considered as one of major obstacles for development of controlled drug delivery systems. Here, we describe a surface modification technique of mesoporous silicon microparticles (MPS) with two types of hydrogel (gelatin and agarose) coatings that enhances their ability to load and extend the release of antibiotic molecule and preserving antibiotic molecule stability. We have developed and characterized a hydrogel surface modification of MPS. Stability of the released antibiotic from loaded microparticles was evaluated with high performance liquid chromatography (HPLC) analysis. We showed that the hydrogel coating does not affect the MPS antibiotic release. In addition, hydrogel type and composition affect the release of cargo molecule from the MPS delivery system. For instance, increase in concentration of hydrogel coating slows down the release of the payload. 5% agarose coating reduces the release kinetics of cefazolin by 60% over 7 day study while 5% gelatin coating reduces the release by only 40% over 7 day. Scanning electron micrographs of surface modified MPS indicate that the resulting hydrogel coating was uniform and density increased with respect to hydrogel concentration. Hydrogel matrix filled the pores and covered the particles' surface completely but did not alter appreciably the size and charge of the MPS. This surface modification of MPS adds to its tunability and biodegradability during delivery of therapeutic agent without affecting its integrity.

Introduction

To maintain antimicrobial activity, frequent administration of conventional antibiotic formulations with short half-lives is necessary otherwise antibiotic concentration goes under minimum inhibitory concentration (MIC), which can further develop into antibiotic resistance. By maintaining a constant antibiotic concentration above MIC level for an extended period of time, we can retain maximum therapeutic outcome without any possibility for developing antibiotic resistance [218]. Improved patient compliance is another advantage of antibiotic delivery systems [219]. During the last few decades, drug delivery systems have been developed significantly and gained a significant role in many fields of medicine [1]. The controlled and sustained release of antibiotics can enhance the therapeutic efficacy by maintaining a constant plasma level, reducing MIC and avoiding inconvenience of frequent injections. Structurally unstable antibiotics are rapidly degraded due to their short half-life. Antibiotics such as Cefuroxime, Cefazolin, Metronidazole, and Clindamycin, for example, have half-lives as short as 1 hour [220].

For better bioavailability properties, many materials have been introduced into the matrix and coating extended-release system over the past few years. Excellent biocompatibility and extensive evaluation of these materials provide great potential for development of complex carriers obtained through chemical modification of the existing materials or combinations of different materials in physical mixtures [221]. Meanwhile, with the development of organic and inorganic polymers and inorganic porous materials, nanotechnology is applied increasingly for development of extended delivery of antibiotics [151, 159]. Previously, we showed bactericidal activity of cefazolin-loaded MPS against *Staphylococcus aureus* and we evaluated the release kinetics of cefazolin from three different nanopore sizes of MPS [69]. In this work, we described a novel surface modification technique of MPS with two types of hydrogel (gelatin and agarose) coatings that enhances our ability to load and extend the release of cefazolin and preserving its stability over seven days. Moreover, surface modification with these coatings enhances our ability

to load and extend the release of antibiotic and preserve its stability over extended periods of time.

Materials and Methods

MPS Synthesis and APTES Modification

MPS were designed and fabricated in the Microelectronics Research Center at the University of Texas at Austin by established methods [56]. MPS particles were oxidized by piranha (solution of 2:1 vol. H2SO4 (96%) in H2O2 (30%)) for 2 h at 120°C, then modified with aminopropyltriethoxysilane ((APTES) 2% in IPA) for 2 h at 35°C to provide a controlled positive charge to the particle surface that enhances loading capacity.

Agarose modification of MPS

Agarose coating was performed by suspending MPS particles in warm (40°C) agarose solution (dip-coating) for 15 min, and then the solution was cooled at 4°C for 30 min. Agarose coating solutions were prepared at different concentrations of 5 and 10% w/v with low melt certified agarose (BIORAD), used as received. To remove excess gel, particles were washed with warm PBS (35°C) and cold PBS at room temperature twice.

Gelatin modification of MPS

Gelatin coated MPS particles were also prepared by a dip-coating method. Briefly, two different concentrations of gelatin (5mg/ml and 10 mg/ml) were prepared by dissolving gelatin at 60 °C. Gelatin solution was added to cefazolin-loaded MPS particles. Then, the suspension was sonicated in a water-bath sonicater for 5 sec to achieve homogeneous distribution. The suspension was then placed on a rotator for 20 min at room temperature. The suspension was centrifuged down at 14,000 rpm and the supernatant was removed. The gelatin coated particles was washed by PBS and lyophilized and stored at 4°C.

MPS Characterization

The volume, size, and concentration of MPS particles were characterized by a MultisizerTM 4 Coulter Counter (Beckman Coulter). Their surface-charge before and after APTES modification, agarose and gelatin coatings was measured in a PB buffer at pH 7.4 using a ZetaPALS Zeta Potential Analyzer (Brookhaven Instruments Co.). MPS size and shape were also evaluated at room temperature by scanning electron microscope (SEM) (FEI Quanta 400).

Cefazolin Loading and Release

10^6 MPS/mL were combined with a concentrated antibiotic solution (cefazolin sodium, 5 mg/mL in phosphate buffered saline (PBS), Sigma Aldrich) at room temperature. The MPS and loading solution were sealed and gently stirred during the loading process for 1 hour. Particles were then separated by centrifugation and washed twice with PBS. The loading efficiency was determined by High-performance liquid chromatography (HPLC) as previously described [69]. Individual batches of surfaced coated cefazolin-loaded MPS were incubated in 0.5 mL of fresh PBS solution in a humidified 95% air/5% v/v CO_2 incubator at 37 °C with gentle shaking (100 rev/min). The release solution was collected and replaced by fresh PBS at every time points. Drug concentration was determined by measuring the collected solution with HPLC. Samples were collected until no additional cefazolin was released (7 days).

Results and Discussion

Characterization of MSP

MPS particles used in this study were quasi-hemispherical shape with 3.2 μm diameter and 600 nm thickness engineered for drug delivery applications [51]. Pore size was 10 nm with 51% porosity. APTES modification altered MPS surface charge (zeta potential from −23 mV to +10 mV) and allowed the loading of approximately 400 μg of cefazolin per 10 million MSP particles (Figure 14).

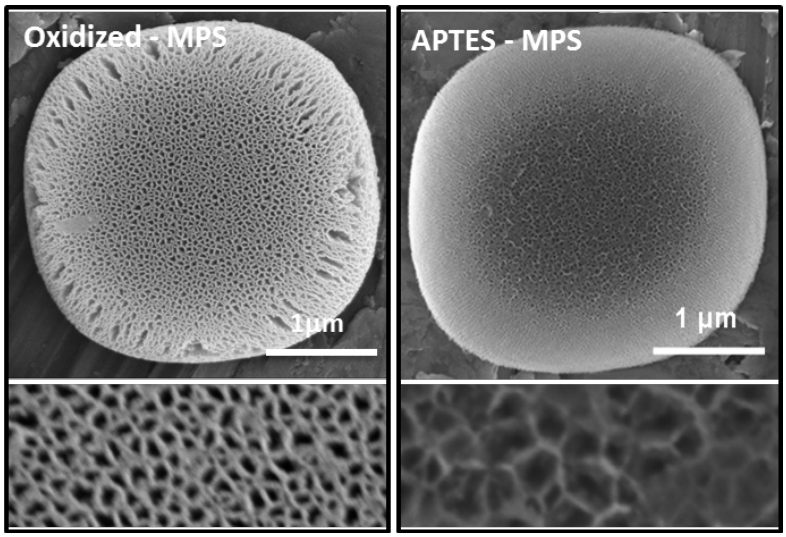

Figure 14. Chemical surface modification of MSP: Oxidized MSP (Left) and APTES modified MSP (Right) observed with SEM.

The hydrogel coatings were developed and optimized to assure a protective function against burst release of cargo from MSP as previously described [85]. SEM images indicated that the resulting agarose (Figure 15) and gelatin (Figure 16) coatings of MSP were uniform and density increased with concentration. Hydrogel coating filled the porous matrix and covered the MSP' surface completely but did not alter appreciably the size and charge of the NSP (zeta potential was +10 for agarose coated and +8 for gelatin coated MSP, respectively). Hydrogel coatings appeared to be uniform and smooth for different concentrations of hydrogel.

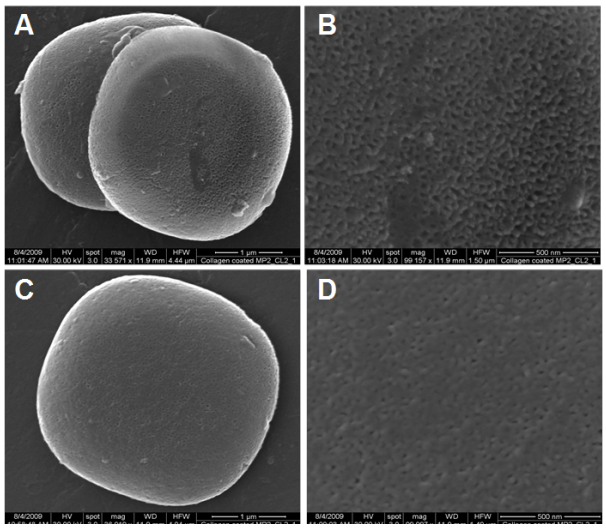

Figure 15. Agarose modification of MSP with 5% (A, B) and 10% (C, D) agarose concentration, respectively. Particles were observed with SEM at low (A, C) and high (E, D) magnification.

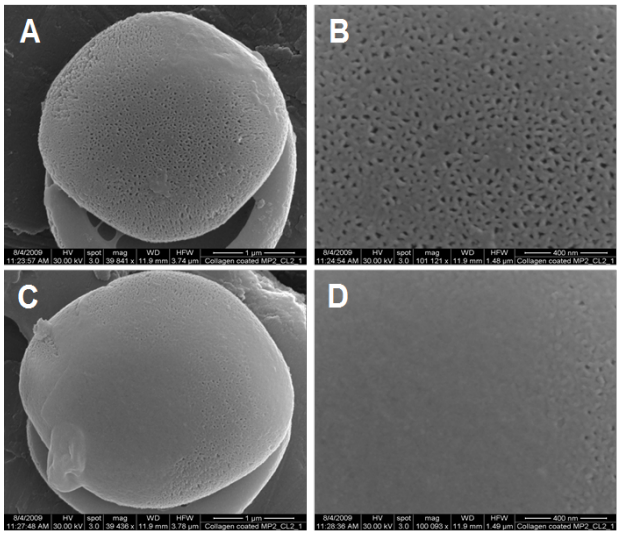

Figure 16. Gelatin modification of MSP with 5 mg/ml (A, B) and 10 (C, D) mg/ml gelatin concentration, respectively. Particles were observed with SEM at low (A, C) and high (E, D) magnification.

Previously we have published extensive characterization of degradation process of unmodified and agarose coated MSP monitored with flow cytometry (FACS), SEM and ICP [31, 85]. As previously reported, degradation rate of exposed MSP was uniform across the entire particle and higher degradation was observed in the outer edge of MSP because of the higher surface area and porosity of its structure.

Quantification of Cefazolin Release

To assess antibiotic release from hydrogel coated MSP, cefazolin sodium was used as model drug molecule. Loading and release of cefazolin from agarose (Ag) MSP and gelatin (Gel) with two concentrations were quantified by HPLC and compared with uncoated MSP. Loading efficiency was about 60-80% for both coatings compared to uncoated MSP (NC) (Figure 17A, B); hence, the hydrogel coating affect the antibiotic loading by 20-30% and increase in concentration of coating slows down the release of cefazolin for both hydrogel types respectively (Figure 17C, D).

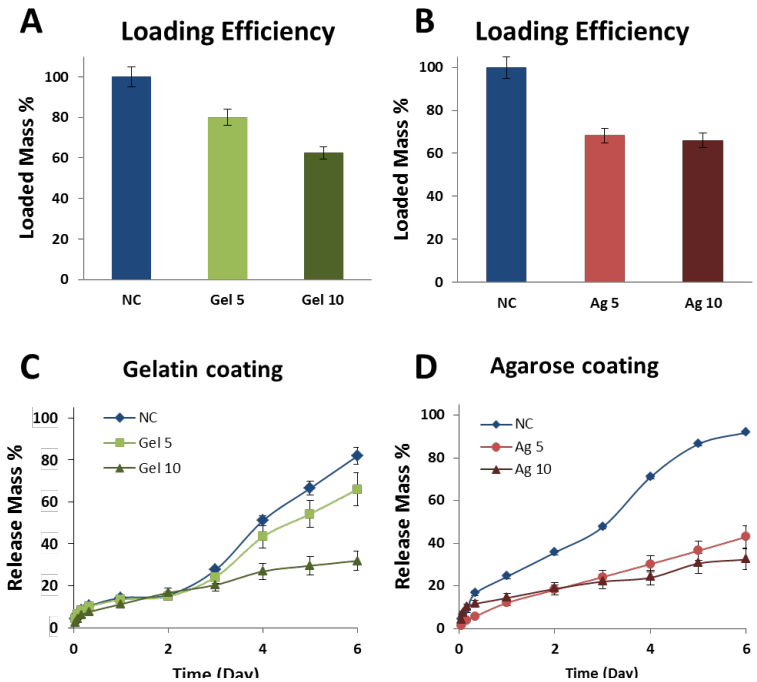

Figure 17. Cefazolin loading and release of hydrogel coated MSP: (A, B) Amount of cefazolin loaded in to NC, Gel and Ag coated MSP; (C, D) Release of cefazolin from hydrogel coated MSP over 6 days.

Conclusion

In this work we successfully demonstrated surface modification of MSP with two types of hydrogel, designed and fabricated for delivery of antibiotics, to improve and extend the release kinetics. We verified that the agarose coating protects the payload using SEM, while it does not affect its cargo integrity and its release by HPLC. We also showed that increase in hydrogel coating influences the loading efficiency slightly and also it slows down the release of cargo molecule in comparison with uncoated MSP. Thus, the hydrogel coating of MSP can potentially improve and extend the use of MSP as versatile delivery system for various therapeutic applications. Additionally, it may act effectively in combination with other surface modification for controlled release systems to preserve the payload and increase its stability during the course of long-term release.

5 Embedding of MPS into polymeric matrix to extend drug release

A manuscript to be submitted for publication

The development of a delivery system able to provide for the long-term controlled delivery of bone morphogenetic protein-2 (BMP2) can improve the clinical outcome of bone grafting and minimize the side effects of current delivery methods. In this study, we investigated the use of poly(lactic-co-glycolic acid)/porous silicon (PLGA/pSi) microparticles fabricated by a solid-in-oil-in-water (S/O/W) method. The release profiles of BMP-2, loaded in the pSi within the PLGA matrix, indicate that both PLGA and pSi contribute to sustained release of active BMP-2 for more than 6 weeks as evaluated by ELISA assays. Cell proliferation (MTT) and alkaline phosphatase (ALP) activity of rat compact bone derived mesenchimal stem cells (MSC) showed biocompatibility of these microparticles and confirmed that the bioactivity of BMP-2 was maintained throughout the release study and stimulated osteogenic differentiation. In conclusion, this study proves that biocompatible, biodegradable, and osteogenic properties of PLGA/pSi microparticles as an ideal candidate for delivery of biomolecules for orthopedic tissue engineering applications.

Introduction

Several current delivery systems designed to provide controlled release of biomolecules have been limited by: (a) a burst release phenomena which leads to similar supraphysiologic dosing, inefficiently sustained dosing, and uncontrolled delivery as that seen with delivery systems currently used clincially; (b) the inability to preserve the quaternary structure of drugs following release from the delivery system; and (c) delivery system (polymer) degradation

byproducts that have a secondary negative impact on the structure of the drugs released. Therefore, a new carrier system capable of sustained, regulated, local release of small but effective doses that does not itself impact upon the functionality of bone morphogenetic protein-2 (BMP2) is needed to allow the avoidance of the biological complications associated with burst supraphysiologic dosing.

Protein delivery using biodegradable copolymer, PLGA, has been widely investigated [222]. PLGA is biocompatible, biodegradable, and approved material under therapeutic devices by the Food and Drug Administration (FDA) [223]. The main advantages of using PLGA over other classes of materials for drug delivery system are that it can be tailored by changing the lactic acid and glycolic acid ratio or molecular weight to control the degradation rate, which plays an important role in successful delivery of drugs in a controlled manner. PLGA has been formulated in form of nano- and micro-particles to provide sustained release of hydrophilic drugs, proteins, and small molecules to the targeting site [224-226]. However, there are still some unresolved issues remain such as uniformity of sustained release of proteins from PLGA microparticles without a significant initial burst [227], acidic degradation by-products [228], or compatibility with water-soluble molecules [229].

pSi is a biodegradable material [230] and its degradation product of silicon is orthosilicic acid, which is not cytotoxic *in vitro* [174]. In regards to interaction of pSi particles with biological systems in diverse contexts evidences a high degree of biocompatibility as a cell culture substrate, they promotes growth without significant cytotoxic effects [231-234]; as a scaffold in tissue engineering applications [235-237]; as therapeutic delivery system without toxic effects [238-240]. A wide variety of therapeutic and imaging molecules have been successfully loaded and released from these particles [68, 69, 186, 241-243]. Their size, shape, and porosity of these particles can be engineered to alter their biodistribution *in vivo* [244] and their surface can be chemically modified to control their cellular uptake [245].

The addition of pSi to PLGA microparticles offers a solution to previously mentioned problems. High surface porosity with interconnected pores allow large storage of therapeutic molecules while PLGA coating offers a tunable layer to seal these pores and slow down the pSi degradation and control the release kinetics. In addition, pSi degradation neutralizes the pH of the PLGA degradation. When the soluble biomolecules are efficiently loaded into the pores of the pSi particles before PLGA encapsulation, their structural integrity and function can be preserved [84]. By integrating the drug preserving and encapsulating capabilities of pSi with the further controlled relaese capabilities achieved by polymer encapsulation of PLGA, a new dual controlled system for growth factor release has been developed. The aim of the current study was to validate a sustained release system composed of PLGA encapsulation of BMP-2 loaded nanoporous silicon particles *in vitro*.

Materials and Methods

Cell isolation and culture

Bone marrow stromal cells (BMSCs) were isolated from the tibiae and femora of male Sprague Dawley rats. Cells were cultured in α-minimum essential medium (αMEM) (Invitrogen) supplemented with 20% (v/v) defined fetal calf serum (Invitrogen), 1%, L-glutamine (Invitrogen), 1% sodium pyruvate (Invitrogen), 100 U/mL penicillin and 100 μg/mL streptomycin (Invitrogen) as the standard growth media. Osteogenic growth media included 10mM β-glycerophosphate, 0.1 mM ascorbate-2-phosphate, and 100 nM dexamethasone. Cells were maintained at 37°C in a humidified 5% CO_2 atmosphere. Cell culture media was changed every 3 days.

Loading of BMP-2 into nanoporous silicon particles (pSi)

200 μL of BMP-2 growth factor solution (Sigma-Aldrich) was added into 8×10^7 oxidized pSi in an Eppendorf tube. The suspension was mixed throughout by vortex mixing and

sonication. The tube was gently rotated on a rotator at room temperature for 2 hours to allow the adsorption of BMP-2 into the pSi particles. The BMP-2 loaded particles were then spun down by centrifugation (Sorvall Legend X1R Centrifuge, Thermo Scientific) (4,500 rpm for 5 min), lyophilized overnight, and stored at -80°C for future use. The concentrations of the BMP-2 loading solution and the supernatant were measured by Elisa assay to determine the amount of BMP-2 loaded into the pSi particles.

Preparation of PLGA coated pSi particles

The PLGA/pSi microparticles were fabricated by a modified S/O/W emulsion method as in our previous studies [84]. Briefly, PLGA (Sigma Aldrich) was dissolved in dichloromethane (DCM) (Fisher Scientific, UK) to form PLGA/DCM organic phase solution (10% and 20% w/v). 8×10^7 BMP-2 loaded particles were suspended into 1 ml of PLGA/DCM solutions (10% and 20%w/v respectively) by vortex mixing and sonication for 2 min. The organic phase containing the pSi particles was transferred into 3 ml of PVA (2.5% w/v) solution (Figure 18A) and emulsified for 1 min by vortex mixing (Figure 18B). The primary emulsion was then gradually dispersed into 50 ml of PVA solution (0.5% w/v). The resulting suspension was stirred continually for 2 h under a biochemical hood, and the DCM evaporated rapidly during the stirring process (Figure 18C). PLGA/pSi microparticles were washed with deionized water 3 times and lyophilized overnight (Figure 18D). The freeze-dried BMP-2 loaded PLGA/pSi microparticles were then stored at -80ºC.

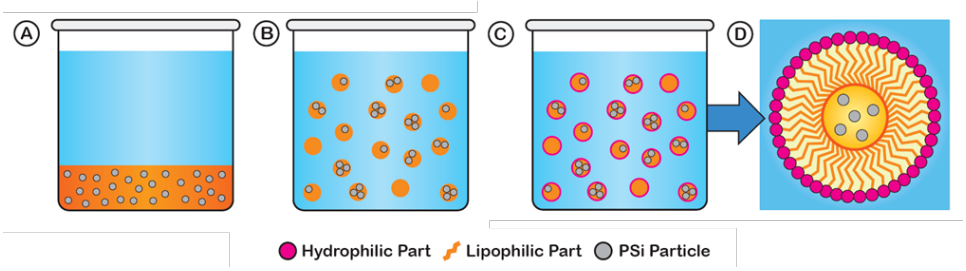

Figure 18. The schematic diagram of PLGA/pSi particles fabrication through the S/O/W emulsion method

Characterization of PLGA/pSi microparticles

The morphology of the microparticles was characterized by scanning electron microscope (SEM) (Nova NanoSEM 230, FEI) and confocal microscope (Nikon A1 laser confocal microscope). The samples were sputter coated with 8 nm of platinum (Pt) (Cressington Sputter coater 208 HR System, Ted Pella, Inc) and examined by SEM under a voltage of 3 kV, spot size 3.0, and a working distance of 5 mm.

In vitro growth factor (BMP-2) release

The BMP-2 loaded PLGA/pSi microparticles (10% and 20%w/v) containing 8×10^7 of pSi particles were dispersed into 0.5 ml of 1% BSA solution at 37ºC. The BMP-2 loaded PLGA microparticles (10% and 20% w/v) were used as control. At predetermined time intervals, the suspension was spun down at 4500 rpm for 5 min and 0.5 ml of each supernatant was collected, and replaced with 0.5 ml of fresh 1% BSA solution. The amount of BMP-2 released from BMP-2 loaded PLGA/pSi microparticles was detected using an enzyme-linked immunosorbent assay kit (BMP-2 ELISA, R&D Systems).

Cell proliferation

Cell cytotoxicity of the PLGA/pSi microparticles was performed by MTT assay [246]. 2,500 BMSCs were seeded and cultured in a 24-cell culture well plate in the presence of the PLGA and PLGA/pSi microparticles (BMSCs: Particles 1:5). Cells only were used as control. MTT (3-(4,5-Dimethylthiazol-2-yl)-2,5-diphenyltetrazolium bromide) assay was performed on day 1, 4, and 7. Cell culture media was removed from cell culture wells and 500 µl of MTT working solution (0.5 mg/ml) were added into the wells. The cells were incubated in the MTT working solution at 37°C for 4h. The solution was removed from the cell culture wells and replaced with 500 µl of dimethyl sulfoxide (DMSO) (Sigma Aldrich). The cells were incubated with DMSO at

room temperature for 30 min. The solutions were transferred to a 96 well plate and the absorbance of the colored solutions was quantified by a spectrophotometer (Synergy H4 Hybrid Reader, BioTek) at 570 nm. DMSO was used as blank. Cells only and PLGA particle wells were used as controls.

Bioactivity of controlled release of BMP-2 on osteogenic differentiation

Osteogenic differentiation was measured by ALP activity, a biomarker of osteoblastic differentiation. The assay was carried out according to a previously published spectrophotometric procedure using ALP reagent (Vector Laboratories, Inc. Burlingame, CA). The BMSCs were plated into a 24 well cell culture plate at a density of 2,500 cells per well with the PLGA/pSi microparticles (10 % and 20 % w/v) loaded with BMP-2 were used as experiential groups. Cells only, cells cultured with BMP-2, PLGA microparticles (10 % and 20 % w/v) loaded with BMP-2, andempty PLGA/pSi microparticles without BMP-2 (10 % and 20 % w/v) were used as controls. Cell culture media was changed every 3 days.

Cells were cultured in α-minimum essential medium (αMEM) (Invitrogen) supplemented with 10% (v/v) fetal calf serum (Invitrogen), 100 U/mL penicillin and 100 μg/mL streptomycin (Invitrogen) as the standard growth media. Culture conditions were 37 °C in a humidified 5% CO2 atmosphere. The osteogenic growth media included 10mM β-glycerophosphate, 0.1 mM ascorbate-2-phosphate and 100 nM dexamethasone. Cell culture media was replenished twice weekly. Cells were cultured in standard media until 60% confluence and then switched to osteogenic media.

ALP assays were performed at week 1, 2, and 3. The medium was aspirated and 1 ml of PBS was added into each well to wash the cells. Cells were washed 3 times with PBS, and fixed in 10 % buffered formalin for 15 min. Cells were then washed twice in DI water and covered in ALP stain made fresh. ALP staining stock solution was made by adding two drops of reagent 1, 2

drops of reagent 2, and 2 drops of reagent 3 from ALP substrate kit III (Vector Laboratories Inc.) into 5 ml of 100 mMtris-HCl (pH=8.2) solution. The experiments were performed in triplicate.

Von Kossa staining

Cell cultures were stained for calcium-triphosphate mineral deposition by Von Kossa staining. Cells were washed twice in DI water and soaked in in 1% aqueous silver nitrate ($AgNO_3$) and placed under Ultraviolet (UV) light for 60 min and then rinsed with DI water .To remove unreacted silver, 5% sodium thiosulfate was added for 5 minutes, removed and cells rinsed in DI water. Following this cell nuclei were counterstained with Nuclear Fast Red (Sigma Aldrich) for 5 min, rinsed in DI water, and serially dehydrated prior to characterization.

Results

PLGA/pSi microparticles characterization

The PLGA/pSi microparticles were characterized by SEM coupled with EDX and confocal microscopy. SEM images show that the spherical-shaped PLGA/pSi microparticles with smooth surfaces had a distribution from a few microns to approximately 50 μm before sieving (Figure 19A). After sieving, the microparticles were separated into 2 parts: > 20 μm (Figure 19B) and < 20 μm (Figure 19C) due to the pore size of the sieve (20 μm). EDX spectrum shows the presence of Si peak (Figure 19D), which indicates the presence of pSi particles inside of PLGA microparticles.

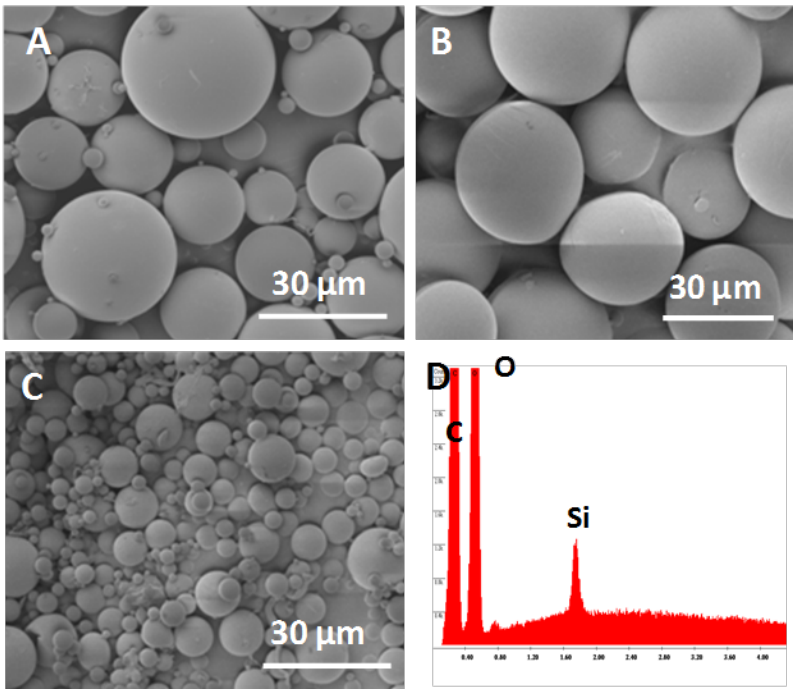

Figure 19. SEM images of the PLGA/pSi particles. SEM image of nonsieved PLGA/pSi microspheres before sieving (A), more uniform sieved PLGA/pSi particles (<20 µm) (B), sieved PLGA/pSi microspheres (> 20 µm) (C), EDX spectrum of PLGA/pSi particles showing the presence of Si peak (D).

pSi particle BMP-2 loading and in vitro release

BMP-2 is a 29 kD protein with an isolelectric point of 8.21 [247]. The BMP-2 loaded PLGA/pSi microparticles (10 % and 20 % w/v) were used for *in vitro* sustained release studies. The loading efficiency of BMP-2 into pSi particles is shown in Figure 20A. Consistent with mass transport theory, the greater amount of particles added to the solution of BMP-2, the greater amount of loading was achieved and thus a higher loading efficiency. The *in vitro* release profiles of BMP-2 from different types of microparticles were monitored for 40 days (Figure 20B). The control samples - PLGA microparticles (10 % and 20 % w/v) showed a massive initial burst release (Figure 20C), followed by achievement of equilibrium in less than 10 days. In contrast, due to the presence of pSi microparticles, 10 % w/v PLGA/pSi microparticles demonstrated a reduced burst release and more sustained release profile with a release equilibrium near 24 days. BMP-2 release from 20 % w/v PLGA/pSi microparticles showed a more linear-like release with a negligible burst release. In this case BMP-2 was steady for 41 days until equilibrium was reached.

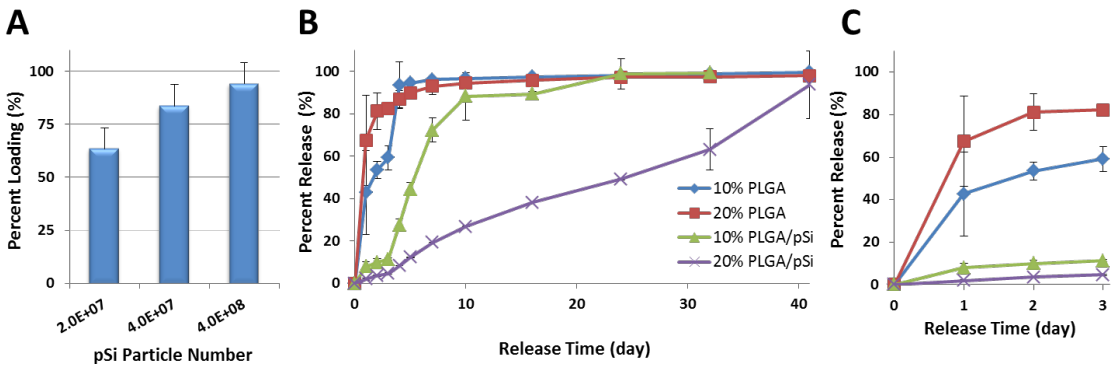

Figure 20. The in vitro loading and release profiles of BMP-2 using PLGA and PLGA/pSi particles. (A) The loading profiles of BMP-2 into pSi particles (B) Cumulative release profile of BMP-2 from different formulations over 41 days, (C) in the first three days.

Cell proliferation

Cell proliferation in the presence of the PLGA and PLGA/pSi microparticles was analyzed using MTT assay. MTT assay is a colorimetric assay that allows yellow MTT to be reduced to purple formazan in living cells. DMSO was added to dissolve the insoluble purple formazan product into a colored solution. Figure 21 shows the results of MTT assay for BMSCs cultured with PLGA and PLGA/pSi microparticles over 7 days.

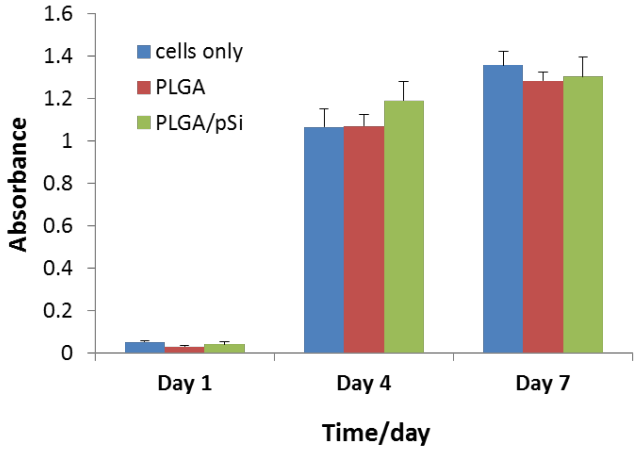

Figure 21. MTT assay for BMSCs cultured with PLGA and PLGA/pSi particles over 7 days.

Proliferation among cells only (control), cells with PLGA microparticles, and cells with the PLGA/pSi microparticles shared the similar trend and there was no significant difference of the proliferation among of the three groups. Cells in each group achieved a comparably high

number and reached equilibrium over 7-day culture. Cells can proliferate normally in the presence of the PLGA/pSimicroparticles without suffering any toxic compounds released from the composite microparticles, which indicates that these materials were nontoxic to cells and compatible with surrounding environment.

Cell differentiation – alkaline phosphatase activity

Assessment of bioactivity of osteogenic differentiation of cells cultured in the presence of the materials is a crucial criteria to evaluate drug loaded carriers for orthopedic. ALP is a biomarker of the ECM produced during BMSC differentiation. As shown in Figure 22, at week 1 cells with BMP-2 loaded PLGA and the PLGA/pSi microparticles showed higher ALP activities compared to cells only, cells with BMP-2, and cells with the empty PLGA or the PLGA/pSi microparticles. This could be due to burst release effect of BMP-2 from both types of the microparticles. At week 2, cells in the presence of BMP-2 loaded the PLGA/pSi particles demonstrated the highest ALP activities and cells with BMP-2 only also showed relatively high ALP activities compared to other control and experimental groups due to the constant release or provision of BMP-2 to the cells. The ALP activities decreased to a fairly low level for all controls and experimental groups after 3 weeks.

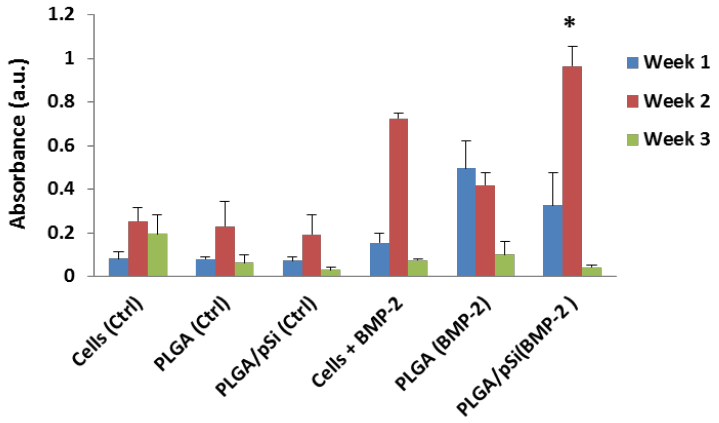

Figure 22. ALP activities of BMSCs only, BMSCs culture with BMP-2 or particles with or without BMP-2 in the osteogenic media over 3 weeks (mean±SD, n=3).

During osteoblastic differentiation and cartilage calcification, ALP is expressed early in developmental program; however, later in the development, when other genes (e.g., osteocalsin) are upregulated, ALP activity declines. It is clear that ALP functions in the initial phase of osteogenic differentiation and calcification.

ALP staining and Von Kossa staining

ALP staining confirms the presence of ALP, a biomarker produced by osteoblasts during cell differentiation. As shown in Figure 23, at the first week most of the cell culture wells started to show ALP activities (light blue area) such as cells only, cells only + BMP-2, 20% PLGA microparticles + BMP-2, 20% PLGA/pSi microparticles + BMP-2. However, ALP activities in the other two wells---20% PLGA microparticles and 20% PLGA/pSi microparticles---were barely observed due to the absence of BMP-2. At week 2, the blue areas became darker and spread to more areas in the cell culture wells. ALP activities in all of the culture wells became very intense, indicating increased ALP activity. At this time point, dark brown areas appeared in 20% PLGA microparticles + BMP-2 and 20% PLGA/pSi microparticles + BMP-2 consistent with increased mineralization. Von Kossa and ALP stains were performed simultaneously and therefore appear in the same wells. At week 3, the blue color became lighter with decreased areas, which indicated the decrease of ALP activities over time. The ALP staining images confirmed with the ALP assay

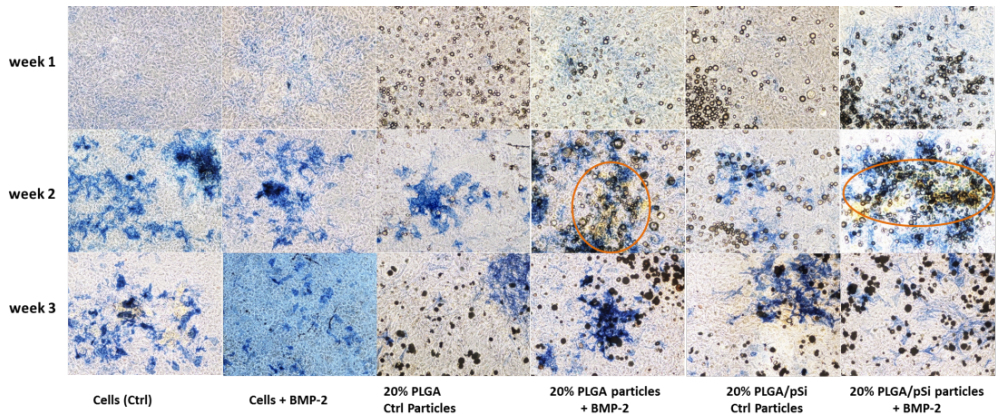

Figure 23. ALP staining of BMSCs (Ctrl) and BMSCs with different control and experimental groups.

results on how the ALP activities changed over the 3-week culture.

Von Kossa method has been used to stain bone nodule and mineral formation and identify cell calcification. As shown in Figure 24, calcification – brown or dark brown regions--- were observed in cells (Ctrl), cells with BMP-2, cells with BMP-2 loaded PLGA and PLGA/pSi microparticles as pointed by the arrows. However, there was no calcification observed with microparticles not loaded with BMP-2 (Ctrl empty PLGA and PLGA/pSi microparticles) at week 1. With the decrease of ALP activities, more obvious calcification was detected for most of the groups, however, still no calcification was observed from the wells with microparticles lacking of BMP-2 (Ctrl empty PLGA and PLGA/pSi microparticles) at week 2. By week 3, much more intense calcification was detected in all cell culture wells with all control and experimental materials and calcification had accumulated to a considerably high level.

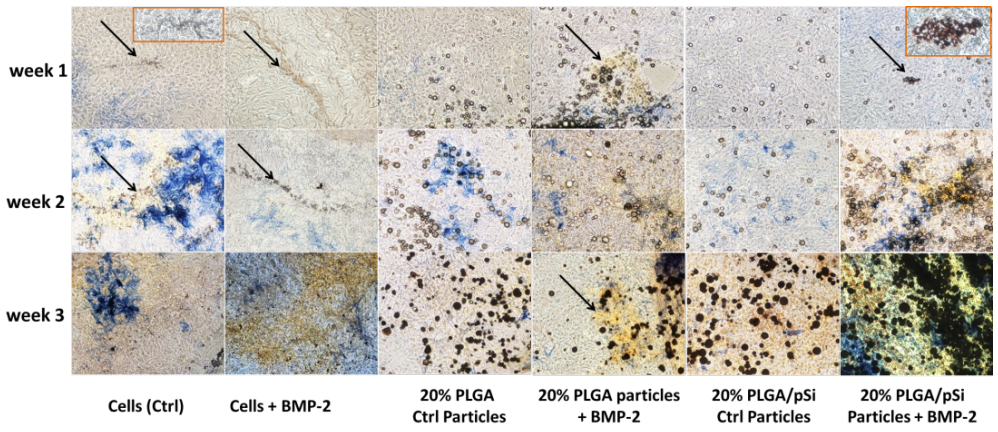

Figure 24. Von Kossa staining of BMSCs and BMSCs with different control and experimental groups over three weeks.

Conclusion

We have developed and investigated a novel protein delivery system – PLGA/pSi microparticles – as an alternative to traditional PLGA microparticles for controlled release of proteins. BMP-2 was successfully encapsulated into these particles and their performance was tested *in vitro*. The experimental results indicate that the PLGA/pSi

microparticles have the ability to release BMP-2 over 4 weeks; The BMP-2 released from PLGA/pSi microparticles can increase ALP activities at the beginning of cellular calcification and mineralization and stimulate the formation of bone mineral. This biocompatible, biodegradable, and osteogenic PLGA/pSi microparticle delivery system could be an ideal candidate for sustain delivery of proteins for orthopedic tissue engineering applications.

6 Multifucntional nanocomposite hydrogel

A multifunctional nanostructured platform for localized sustained release of analgesics and antibiotics

A manuscript published in *European Journal of Pain Supplements* 5, no. S2 (2011): 423-432.

I. K. Yazdi, M. B. Murphy, S. M. Khaled, D. Fan, M. Sprintz, R. M. Buchanan, C. A. Smid, B. K. Weiner, M. Ferrari, and E. Tasciotti

The current delivery methods for pain medication, local anesthetics, antibiotics, and steroids present several limitations mainly due to their route of administration, which results in suboptimal pain management, potential systemic toxicity, and subtherapeutic levels which increases the risk of microorganisms developing antibiotic resistance. Our group developed a hybrid material consisting of nanoporous silicon (pSi) and poly(lactic-co-glycolic acid) (PLGA) nanoparticles, loaded with antibiotics and pain relief medications, respectively. The medications were delivered via a bioactive angiogenic gel of platelet-rich plasma (PRP). This system releases both molecules in a sustained and controlled fashion while simultaneously promoting wound healing and vascularization of the surgical site. The resulting advantages include improved medication efficacy at a lower total drug concentration, decreased risk of systemic toxicity, and for antibiotics, decreased risk of developing resistance.

The versatile nature of our platform allows for a variety of different drugs, molecules, biological factors to be loaded and released by the gel. Moreover, by tuning the chemical and physical properties of each component, it is possible to tailor the release rate of each biomolecule to its desired therapeutic level. Therapeutic and antimicrobial agents were released at potent daily dosages for up to seven days by combination of PLGA and pSi particles free or embedded within the PRP gel. When implanted *in vivo*, the composite gel was vascularized and infiltrated with endogenous cells by two weeks while exhibiting no symptoms of inflammation or immune

response. This novel technology has the potential to dramatically affect the post-operative management of patients with an immediate improvement in post-op pain management, decreased PACU and hospital length of stays, with subsequently decreased hospital and surgical costs. Furthermore, this unique and effective drug delivery platform technology may eliminate the need for subsequent treatments, repeat dosing, and dramatically improve patient convenience and patient compliance.

Introduction

Surgical site infections (SSI) are the most common type of nosocomial infection acquired by surgical patients [248-250]. Postoperative surgical site infections remain a major source of illness and a less frequent cause of death in the surgical patient [251]. These infections number approximately 500,000 per year, among an estimated 27 million surgical procedures, and account for approximately one quarter of the estimated 2 million nosocomial infections in the United States each year [252, 253]. Infections result in postoperative morbidity and mortality, increased length of patient stays in the hospital and subsequent unanticipated re-admissions, and ultimately higher costs to society. In 1999, The Hospital Infection Control Practices Advisory Committee of the Centers for Disease Control (CDC) issued its guideline for prevention of surgical site infection, which outlined procedures and protocols designed to decrease the incidence of post-operative surgical site infections. Since that time other consensus guidelines have been developed, which support the following needs: (i) antimicrobial agents with targeted spectra of activity against organisms likely to be encountered in the particular surgical field; (ii) appropriate timing of antimicrobial administration prior to surgical incision; (iii) bactericidal blood and tissue concentrations until incision closure; and (iv) a duration of up to 24 h following surgery [254, 255]. Despite the presence of such guidelines and the evidence supporting their benefits, several studies have shown that compliance with these practices is not optimal [256-258]. There still

exists a great need to improve compliance with antimicrobial administration both pre- and post-surgical to minimize the risk of SSI's and the subsequent morbidity and mortality they confer. Beyond infection, pain associated with surgery also remains a sustained postoperative complication. Uncontrolled acute postoperative pain may lead to chronic pain and inflammation, nerve damage, and physiological vulnerability [259]. Ineffective or suboptimal pain management occurs for many reasons, including limitations related to the drug used or to the method of drug administration. In oral administration, only a small fraction of active drug reaches the target area because of enterohepatic circulation. The "first-pass" effect refers to the liver detoxifying an orally ingested drug prior to it reaching systemic circulation. In addition, to maintain therapeutic drug levels in plasma, it is sometimes necessary to administer high doses of drugs which peaks may cause systemic toxicity, and troughs, which in terms of antibiotics, may result in the development of resistance [260].

Nanoparticles (NP) have had a vast impact in the fields of drug delivery and diagnostics due to the stability of the nanoparticles, tunable degradation time, controllable release rate by the nanoparticles, the decreased drug dose to lessen side effects, the prolonged circulation time in the blood vessels, and the functionalized surface of nanoparticles to target the diseased areas. Various clinically-relevant drugs such as antibiotics, opiates, local anesthetics, and steroids, can be delivered more safely and effectively at lower dosages by poly(lactic-co-glycolic acid) (PLGA) and silica NP due to the above advantages. Dexamethasone has been successfully delivered from PLGA microparticles to suppress the acute and chronic inflammatory reactions to implants. The release has lasted for over 1-month period. However, due to the larger size (or rather the smaller surface area to volume ratio) of the microparticles (MP), their degradation time is considerably slower than an equivalent mass of PLGA NP [261, 262]. The *in vitro* and *in vivo* release of bupivacaine has been previously studied using PLGA and polyanhydride microparticles [263-265]. Bupivicaine was released in a controllable manner by altering the drug-polymer ratio.

PLGA Nanoparticles have been employed for the release of dexamethasone, but the burst release profile of the drug required a dense alginate hydrogel coating [266]. Cefazolin sodium release from porous silicon and silica (pSi) MP has been studied by our group with sustained release of antibiotics for up to 7 days [69].

Platelet-rich plasma (PRP) is a platelet concentrate from whole blood which provides copious amounts of 7 fundamental growth factors secreted to initiate wound healing. These growth factors include the isomers of platelet-derived growth factor (PDGF-aa, PDGF-bb, and PDGF-ab), transforming growth factors-β (TGF−βl and TGF−β2), fibroblast growth factors (FGF-1 and FGF-2), epithelial growth factor, and vascular endothelial growth factor (VEGF) [199, 267]. These growth factors initiate the healing cascade while promoting angiogenesis via recruitment of blood vessels and stem cells from neighboring tissues [268]. As a carrier vehicle for drug-loaded nanoparticles, PRP may deliver unique or tailored cocktail growth factors in a bi- or multi-phasic manner. The thrombin-initiated gelation of PRP stimulates the release of factors from the platelets and provides a matrix or scaffold for cellular and protein attachment and the deposition of extracellular matrix proteins to generate new tissues. Moreover, the use of PRP as a carrier matrix for NP provides an additional coating layer to retain the NP at the wound site, delay particle degradation, and slow drug release as a permeable membrane or hydrogel. Previously, we have explored PRP as a stem cell and MP carrier gel that promotes cell proliferation without interfering with differentiation for orthopedic applications [269]. We have implemented a multidisciplinary approach towards simultaneous controlled release of analgesic and antibiotic drugs within a PRP-based carrier matrix that encourages rapid tissue repair and angiogenesis. Within the gel are pSi NP and MP loaded with cefazolin sodium, a common antibiotic used in orthopedic surgery, and PLGA NP loaded with bupivacaine and dexamethasone. This system is easily prepared, injectable, and entirely resorbable. We have preliminarily explored its uses for wound closure, soft tissue healing, and fracture repair (Figure 25).

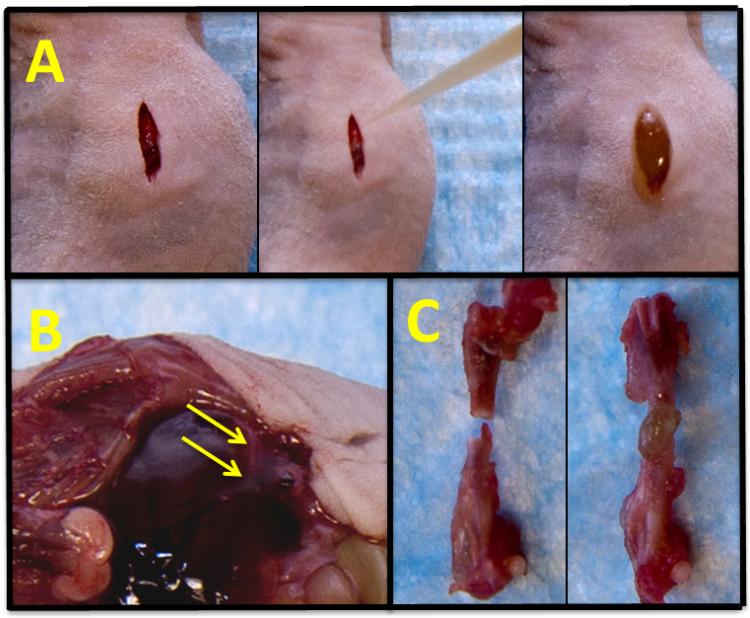

Figure 25. Composite PRP/PLGA/pSi gels applied to dermal wounds seal the injury in less than 2 min (A). A laceration of a hepatic lobe is closed despite its wet environment (B). Non-weight bearing skeletal fractures may be glued with the gel for accelerated healing and biofilm prevention (C).

In this study, we describe the synthesis of the materials and measured the loading and release of these drugs from the free particles in solution as well as from particles impregnated within the gel (Figure 26). We also explored the biodegradation and biocompatibility of the individual and composite materials over 7 days. Finally, we implanted the composite gel into a

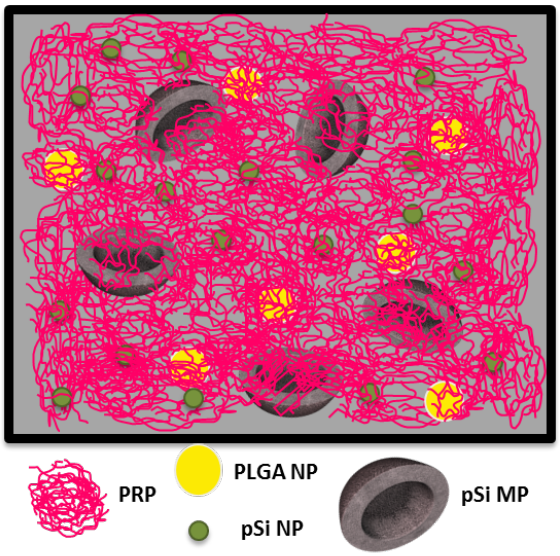

Figure 26. PRP-based Gel for Accelerated Wound Healing

subcutaneous pocket of a rat to evaluate its *in vivo* biocompatibility and the host response. The combination of these materials could be an ideal drug delivery system to release the analgesics and antibiotics in a controllable manner within the therapeutic window to seal wounds and stop bleeding, lessen pain, and improve patient healing and recovery.

Methods

PLGA nanosphere synthesis, analgesic loading, and characterization

The nanoparticles, loaded or unloaded with dexamethasone and bupivacaine, were prepared by a water-in-oil-in-water (w/o/w) emulsion–solvent evaporation method [270]. A solution of 50 mg PLGA (either 50:50 or 85:15 by lactic acid to glycolic acid content) dissolved in 1 mL of methylene chloride was mixed with 5 mg of dexamethasone in 1 mL phosphate buffered saline (PBS), or with 2 mL of bupivacaine solution (2.5 mg/mL) with vortex mixing. The mixture was then poured into 4 mL of 5% polyvinyl alcohol (PVA) aqueous solution. This mixture was homogenized for one minute by vortex and then sonicated using a microtip probe sonicator at 55W of energy output (XL 2002 Sonicator, Misonix, Farmingdale, NY) for 5 minutes to produce the oil-in-water emulsion. The emulsion was then poured into 5 mL of 0.1 % PVA solution and stirred by a mechanical stirrer at 2000 rpm. The nanoparticles were recovered by centrifugation (5000 rpm for 10 minutes). The amount of non-entrapped dexamethasone and bupivacaine in the supernatants was determined by HPLC, as described later. The nanoparticles were washed once with water in order to remove the adsorbed dexamethasone and bupivicaine. The washing solutions were eliminated by a further centrifugation as described above. The purified nanoparticles were freeze-dried. The freeze-dried nanoparticles with or without drugs were characterized by scanning electron microscopy (SEM) (Nova NanoSEM 230, FEI, Hillsboro, OR). The samples were placed on double-sided carbon conductive tapes on SEM stabs

and then were loaded into a sputter coater and coated with 12 nm thick Pt before SEM analysis. The samples were analyzed by SEM under 3 kV and with a working distance of 5 mm.

Silica nanoparticle and silicon microparticle synthesis and cefazolin loading

Mesoporous silica NP with an average size of 250 nm was produced by a modified Stöber process using the sol-gel technique [112]. Tetraethyl orthosilicate (TEOS), the silica precursor, was subjected to base-catalyzed hydrolysis and polycondensation in the presence of NH_4OH solution and the cationic surfactant cetyl trimethylammonium bromide (CTAB) at room temperature. 141.75 mg of CTAB was dissolved in 250 mL of distilled water prior to the addition of 3 mL NH_4OH. TEOS (0.6 mL) was introduced to the mixture with vigorous stirring for 4 hours at room temperature. The silica NP were separated by centrifuging at 8000g for 5 minutes. In order to remove the surfactants, the particles were redispersed in 1:1 acetic acid/dichloromethane solution and washed three times through centrifugation and redispersion. In order to produce fluorescence-labeled silica NP, the particles were synthesized by introducing 5 mg fluorescein isothiocyanate (FITC) homogeneously mixed into 100 μL of APTES in the solution of CTAB in NH_4OH prior to the mixing of TEOS.

Porous Si MP were designed and fabricated in the Microelectronics Research Center at The University of Texas at Austin. Sizes of MP were with mean 3.2 ± 0.2 μm diameters and 3 to 5 nm pore sizes. Heavily doped P++ type (100) silicon wafers (Silicon Quest International, San Jose, CA) were used as the silicon source and a 100 nm layer of silicon nitride was deposited and standard photolithography was used to pattern the MP over the wafer using a contact aligner and photoresist. Then, two-step electrochemical etching was applied and a high porosity release layer was formed by changing the current density. The morphology of the MP was examined by SEM.

The silica NP and silicon MP were placed were lyophilized for approximately 10 min to rid nanopores of any trapped air to reduce surface tension. The 5 mg/mL concentration of cefazolin sodium solution (Sigma Aldrich, Saint Louis, MO) was used for loading. The samples were incubated for 2 hours at room temperature with mild agitation using Thermomixer (Fisher Scientific, Pittsburgh, PA) to allow sufficient time for the drug to fully penetrate into the pores. The drug-loaded samples were centrifuged and supernatants were saved to quantify loading efficiency. Next, the samples (n=6) were individually placed into 0.4 μm translucent membrane transwells (Greiner Bio-One, Monroe, NC) using 24-wells plate and incubated in a humidified 95% air/5% v/v CO_2 incubator at 37 °C in 1 mL of fresh PBS. 100 μL of the solution was removed at each time point through one week, centrifuged (4000 rpm; 5 min) and 100 μL of fresh PBS was added instead. The retained drug amount was determined using spectrophotometry at 270 nm and calculated using standard concentrations.

Platelet-rich plasma injectable particle carrier

PRP was derived from human adult blood buffy coat units from the Houston Gulf Coast Blood Bank (Houston, TX). Blood samples were handled according to Institutional Review Board approved protocols. Platelet, red blood cell (RBC), and white blood cell (WBC) counts were measured on a Sysmex hematology analyzer (model KX-21N, Mundelein, IL) before and after RBC removal and platelet concentration. The blood was centrifuged at 300g for 15 minutes without brake to separate RBC from the PRP. The injectable carrier gel was synthesized as two constituent solutions by adding 6 mg/mL fibrinogen (bovine fibrinogen, Sigma Aldrich, Saint Louis, MO) to either PRP (gel characterization, biodegradation, biocompatibility, and *in vivo* studies) or PBS (release studies) while preparing a second solution of 100 units/mL thrombin (bovine thrombin, BioPharm Laboratories, Bluffdale, UT) in PBS. Antibiotics (1% penicillin/streptomycin) were added for gels used in the biocompatibility studies. The gels were

formed by combining the solutions at a ratio of 80% fibrinogen to 20% thrombin, mixing by repeated pipetting, and setting for up to 5 minutes at 37°C.

To confirm the homogenous distribution of particles within the gel, fluorescent particles were mixed into the fibrinogen phase prior to gel formation. About 15 mg of DyLight 680 conjugated PLGA NP and 5 mg of FITC modified silica NPs were dispersed in 40 μL of fibrinogen solution using vortex mixer and sonication bath. The mixer was then transferred to a glass slide before introducing 10 μL of thrombin into it for crosslinking. The curing gel was covered by a cover slip right after mixing thrombin and was kept at 37°C for one hour prior to the confocal microscopy analysis and SEM. For SEM characterization, the gel was placed in a desiccator overnight in order to dry the sample.

Bupivacaine, dexamethasone, and cefazolin release in vitro

Samples from multiple batches of bupivacaine or dexamethasone-loaded PLGA particles were placed in 1.5 mL Eppendorf tubes (free particles) or 12 well plates (particles embedded in gels) at 4 mg PLGA in PBS per release sample. For composite gel release, particles were mixed with 80 μL fibrinogen (6 mg/mL in PBS) and 20 μL thrombin (100 units/mL in PBS) and allowed to gel for 5 minutes at 37°C in the bottom of the well. Each tube or well received 1 mL PBS, which was completely exchanged with fresh PBS at each time point. Time points included 6, 12, and 24 hours, 2, 4, and 7 days. Bupivacaine and dexamethasone concentrations were measured by UV absorbance at 220 and 242 nm, respectively. These wavelengths were determined to yield peak absorption for the drugs in the concentration range from 100 ng/mL to 100 μg/mL. Concentrations were calculated according to a standard curve of drug dilutions at the given absorbance wavelengths.

Material biodegradation

Free PLGA and pSi NP, as well as particles loaded into a PRP gel, were studied for signs of biodegradation during an initial 7 day period. 25 mg PLGA NP, 10 mg pSi NP, or both within 1 mL PRP matrix, were placed into wells of a 12 well cell culture plate and incubated at 37°C in PBS with daily media exchange. After 7 days, the samples dried in a desiccators overnight and prepared for SEM imaging.

Material biocompatibility

To examine the potential toxicity of these materials and their degradation byproducts, 20,000 bone marrow stromal cells (MSC) were seeded per well in 12 well cell culture plates. Bone marrow cells were isolated from the femora and tibiae of male Sprague Dawley rats (euthanized by CO_2 inhalation) by removal of the bone ends and flushing the marrow with PBS containing 2% fetal bovine serum (FBS) and antibiotics. All animals were treated in accordance to the protocols approved by the Institutional Animal Care and Use Committee (IUCAC). Cells were cultured at 37°C in standard media (α-MEM, 20% FBS, 1% penicillin/streptomycin, 1% glutamate, and 1% sodium pyruvate, Gibco/Invitrogen, Carlsbad, CA) for up to two passages before use. Free PLGA particles, free pSi particles, and a combination gel of PLGA and silica within PRP were placed in transwell inserts with membrane porosity of 400 nm. 4 mg of each particle sample were applied per well. The combination gel was formed by the addition of 40 μL thrombin (100 units/mL) to 160 μL fibrinogen (6 mg/mL) containing the PLGA and pSi particles. The solution was pipetted continuously for 30 seconds to homogenously mix the components until a clot had formed. Cells cultured with an empty transwell insert were used as a positive control. Viable cells were counted at time points of 1, 4, and 7 days by rinsing the wells with PBS, addition of 1 mL deionized water, a freeze-thaw cycle to -80°C, and quantification of double-stranded DNA by Quant-It PicoGreen kit (Invitrogen, Carlsbad, CA) measured at 480/520 nm on a fluorescence plate reader.

In vivo response to injectable drug delivery materials

Composite gels were prefabricated as described above as implants to test the *in vivo* response to the materials. All materials were sterilized by ethylene oxide and handled within a sterile cell culture biohood until the time of surgery. For each scaffold, 50 mg PLGA NP and 10 mg pSi NP were combined with 400 μL PRP (containing 3 mg/mL fibrinogen) and 100 μL thrombin (50 units/mL) and allowed to gel in a sterilized Teflon mold (2.5 mm x 10 mm diameter) at 37°C overnight. The gels were inserted into subcutaneous pockets on the dorsal flanks of male Lewis rats. Briefly, animals were anesthetized with isofluorane (2% in O_2), a small region of the back was shaved and sterilized with iodine, and a local analgesic was administered (200 μL Marcaine). A 1 cm incision was made and four subcutaneous pockets were opened with forceps. Each animal received four implants and were sacrificed at 2 weeks by CO_2 inhalation (2 total animals, n=8). Again, all surgery and animal experiments followed protocols approved by the IACUC. Implants were retrieved for photographic imaging and histological evaluation. Scaffolds were embedded in OCT Compound cryo-medium (Tissue-Tek, Torrence, CA) and quickly frozen to -80°C. 5 μm sections were prepared using a Leica CM1950 Cryostat (Leica Microsystems, Richmond, IL). Each section was fixed in 10% formalin and stained with hematoxylin and eosin.

Results

PLGA nanosphere characterization

All particles generated in this method were spherical with a smooth continuous surface. The diameters of the PLGA NP were analyzed from the SEM images (Figure 27A) with the size distributions performed on the basis of 100+ NP using the ImageJ software (National Institutes of Health, Bethesda, MD). The normal distribution is shown in Figure 27B, indicating an average diameter value of 713 ± 140 nm. The solubility of the drugs to be loaded has a small effect on particle size, as the less soluble dexamethasone produced slightly larger particles than empty or bupivacaine-loaded batches.

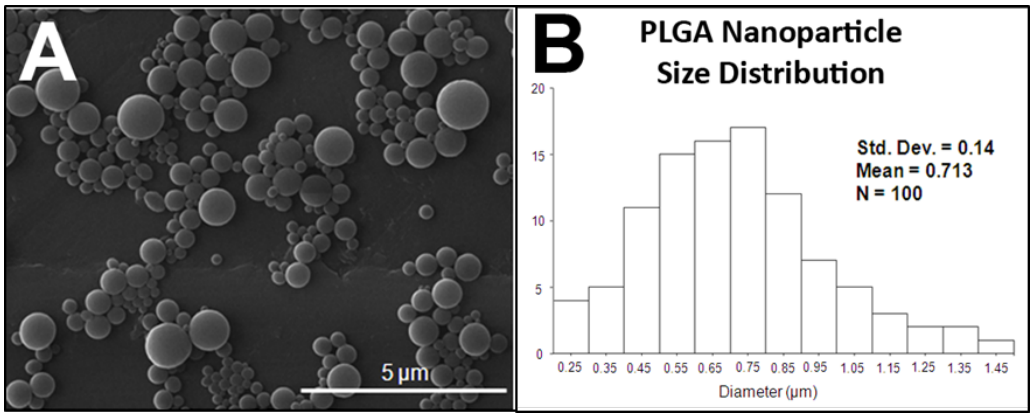

Figure 27. Scanning electron microscopy images of PLGA NP (A). Particle size distribution indicated an average NP diameter of 713 nm with a standard deviation of 140 nm (B).

Cefazolin loading efficiency in pSi NP and MP

The supernatant samples of cefazolin-loaded pSi particles were serially diluted and measured in triplicate using spectroscopy. The method was validated by determination of linearity and precision among all samples. The linearity was evaluated by linear regression analysis, which was calculated by the least squares regression method. 100 µL cefazolin reference solutions in concentrations of 500, 250, 100, 50, 25, 10, 5, and 1 µg/mL were subjected for this quantification. Precision of the determined concentration was expressed by repeatability of serial

dilution. The loading mass of cefazolin into silica NP and silicon MP are reported in the Table 2. The loading efficiency was affected by porosity and particles sizes. The mass of drug loaded per mg pSi was 27% more using MP than NP. The greater encapsulation efficiency is believed to be due to the higher porosity and available surface area to volume ratio of the MP.

Table 2. Cefazolin sodium loading per 1 mg of silicon MP or silica NP.

Particle Type	Loading Mass (µg)	Mean Particle Diameter
Silicon MP	61.66 ± 2.64	3.2 µm
Silica NP	48.42 ± 1.58	250 nm

Platelet-rich plasma injectable particle carrier

SEM and confocal microscopic images of the composite PRP gel with PLGA and pSi NP are shown in Figure 28. Both forms of microscopy indicate that pSi NP tend to aggregate into clusters of approximately 5 µm. However, both types of particles are uniformly and homogenously distributed throughout the depth of the gel. The confocal image exhibits the coexistence of PLGA NP (blue) and silica NP clusters (green) in the PRP matrix. The surface of the gel was smooth (with the exception of surface-embedded NP) and non-porous.

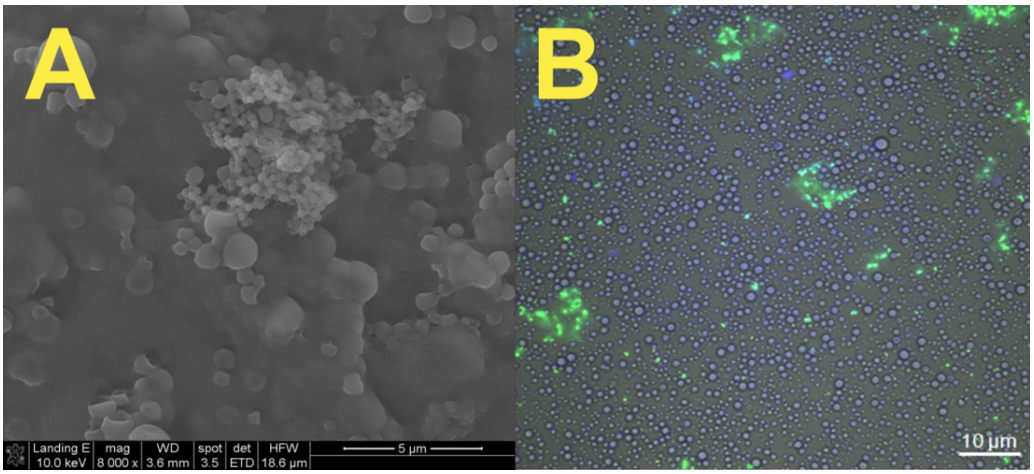

Figure 28. Scanning electron micrograph of PRP/PLGA/pSi gel surface (A). Confocal microscopy of the composite gel (B).

Bupivacaine, dexamethasone, and cefazolin release in vitro

The *in vitro* release of bupivacaine and dexamethasone from PLGA nanoparticles and cefazolin from porous silicon microparticles and porous silica nanoparticles was measured over 7 days both as free particles in solution and particles incorporated into a fibrin gel (Figure 29A-C). A dramatic burst release was demonstrated by PLGA NP for both analgesic drugs, with faster release by 50:50 PLGA than 85:15. The incorporation of the particles within the gel resulted in a nearly linear release profile over the 7 day study. While the free particles emancipate 60-85% of their payload in the first 24 hours, the composite gels release the molecules more uniformly through the first week. The gel complexes with 50:50 and 85:15 PLGA NP release, respectively, 32% and 23% on Day 1, 20% and 12% on Day 2, and 23% and 20% on average for Days 3 and 4. For antibiotic release (Figure 29C), the gel successfully retarded the drug's release compared to free pSi MP, while the release profiles of free and gel-embedded NP were statistically indifferent.

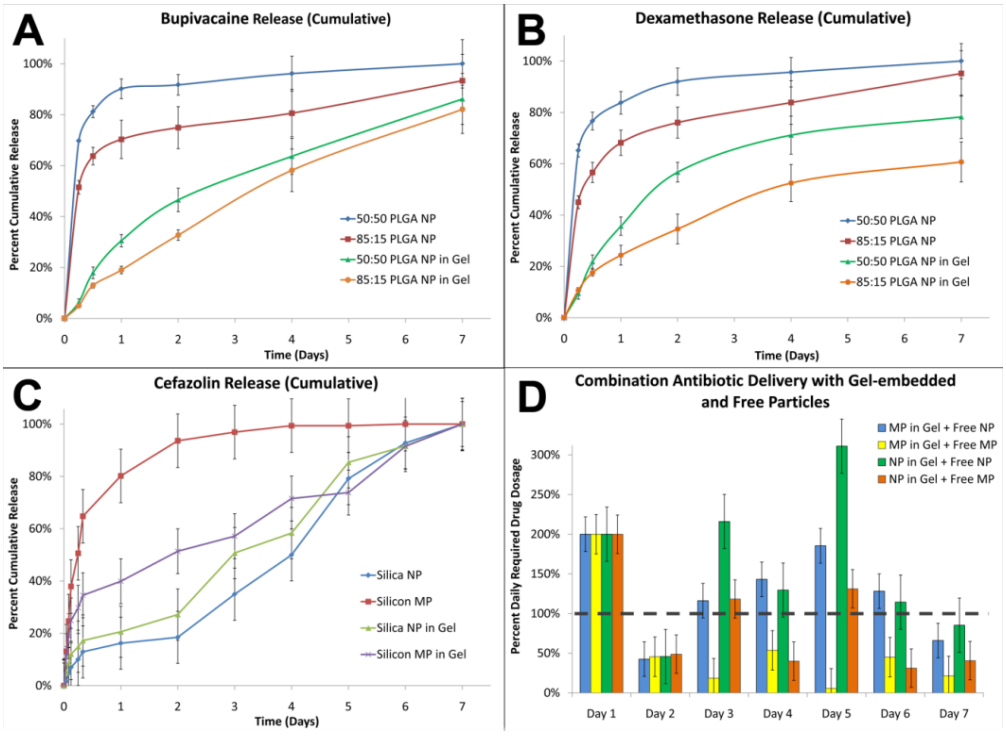

Figure 29. The standard release curves of bupivacaine (A) and dexamethasone (B) from PLGA NP, and the release of cefazolin sodium from pSi MP and NP (C) as a percentage of cumulative total release over 7 days in vitro. The blend of free NP with gel-embedded MP (blue) or NP (green) releases of potent levels of the drug for up to 7 days (D).

In Figure 29D, a daily release dosage is reported for combinations of free NP and MP with gel-embedded NP and MP, scaled with the Day 1 release as a 100% effective dose for each type of particle. This indicates the benefit of multiple delivery vehicles whose combined daily release subsequent to 24 hours can achieve levels equivalent to the 100% Day 1 burst dose. Limited release during Day 2 was apparent for all combinations, although free NP with gel-embedded MP (blue) or with gel-embedded NP (green) were capable of releasing an effective dosage on Days 3-7.

Material biodegradation

After 7 days *in vitro*, samples of free PLGA or pSi NP, or both particles embedded within PRP gels, were analyzed by SEM. The images of the particles and gels are illustrated below in Figure 30. The PLGA NP experienced significant degradation, particularly on the surface of the particles (Figure 30B). The pSi NP were not detectable as free particles by SEM after 7 days, however, they were noticeably absent from the composite gel (Figure 30D) The pores left behind within the gel are generated by the silica resorption. Along the outer edge of the gel, cracks appear by the one week time point indicating the initial breakdown of the fibrin network and increasing the surface area of exposed, drug-loaded NP (Figure 30E).

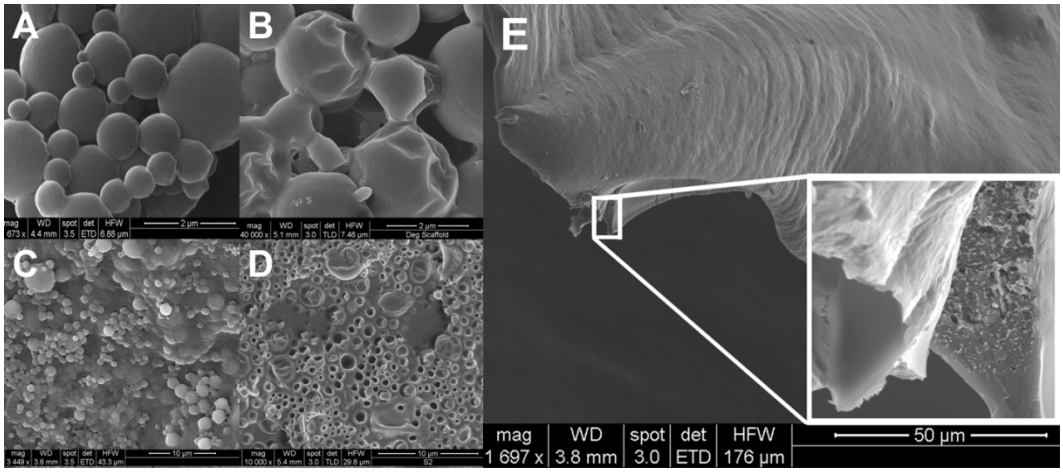

Figure 30. PLGA 50:50 NP after synthesis (A) and after 7 days in vitro (B); the composite gel features PLGA and pSi particles exposed throughout its surface (C), while the PLGA particles undergo significant degradation and most of pSi NP are completely eroded (D).

Material biocompatibility

After an initial seeding of 20,000 marrow stromal cells per well, cell counts were performed at 1, 4, and 7 days. The resulting average cell counts per well are reported in Figure 31. After 24 hours, there is no statistical difference between any of the experimental and control groups. By 4 days, a minor decrease in cell number is observed in the two groups receiving nanoparticles, while the total composite gels featuring PRP exhibit increased cell counts. After one week, the PLGA nanoparticles group possessed significantly less viable cells than the cells-only control or total composite. However, the total gel (PLGA and pSi particles with PRP) caused significantly greater cell growth than all other groups, including the MSC control.

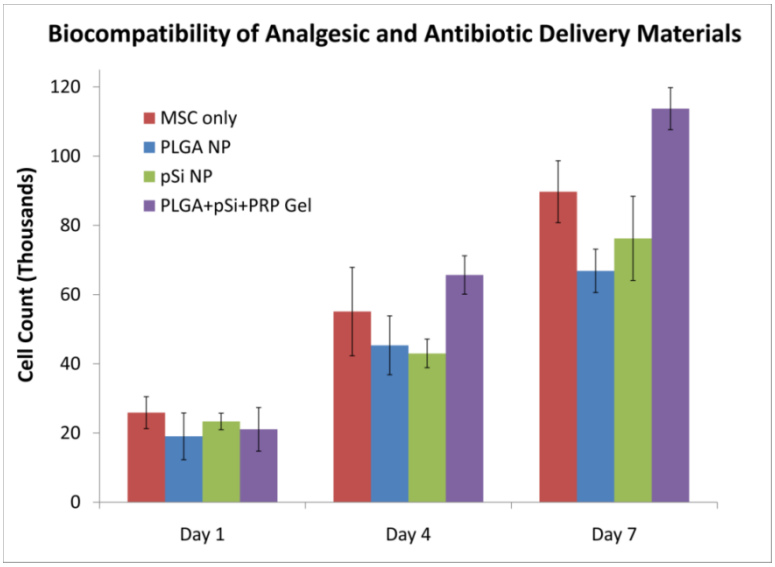

Figure 31. The biocompatibility of analgesic (PLGA NP) and antibiotic (pSi NP) delivery materials was assayed by marrow stromal cell (MSC) growth in the presence of the particles or particle-PRP composite gels at 1, 4, and 7 days in vitro.

In vivo response to injectable drug delivery materials

After 2 weeks *in vivo*, composite PRP/PLGA/pSi implants were removed and histologically evaluated. After removing the dermis and connective tissue, vascularization was apparent to the naked eye for all scaffolds (Figure 32A). The surrounding tissue was examined for signs of inflammation or infection, and the local skin, muscle, and lymphoid tissue appeared normal compared to tissues approximately 4 cm above and below the site of implantation. After

the implants were removed, they had not significantly changed in geometric dimension and demonstrated good mechanical integrity (Figure 32B). Histology stains confirmed that blood vessels were prevalent throughout the scaffolds, with cross-sections of vessels clearly lined with an integrated network of endothelial cells (Figure 32C).

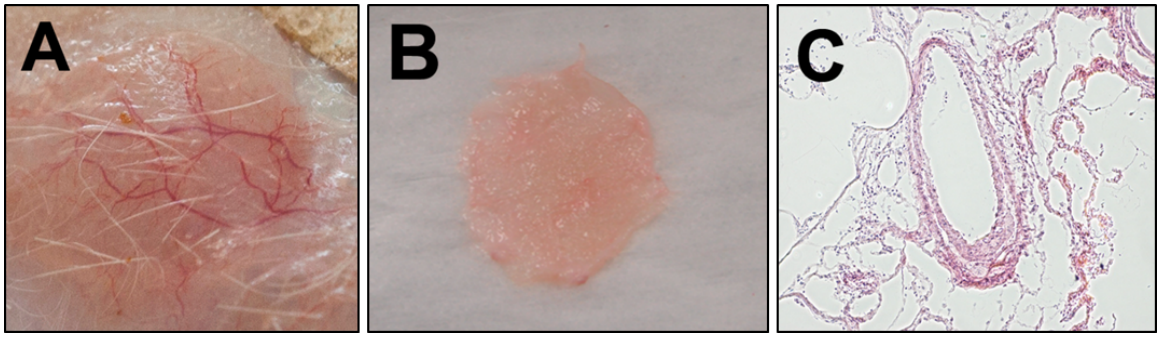

Figure 32. PRP/PLGA/pSi gels exhibited neovascularization after two weeks of subcutaneous implantation (A). The composite gels maintained their original geometry without substantial degradation (B). H&E staining of histological sections indicates the formation of mature blood (C).

Discussion

Assembly and application of PRP/PLGA/pSi gels

This drug delivery platform is biologically-inspired and versatile for multiple applications (e.g., pain relief, biofilm prevention, cell therapies, tissue regeneration). By adjusting the concentration of thrombin and/or fibrinogen, or by the supplement of calcium, the gel setting time and mesh size may be finely altered. Using the described protocols, the gels set in less than 5 minutes at room temperature and in under 2 minutes at 37°C. As shown in Figure 25D, surfaces of soft tissues wetted by blood were also sealed. The platform is designed as an "off-the-shelf" technology for clinicians to select the type (based on material, size, etc.) and mass of particles to be combined with the patient's autologous PRP. The PLGA and pSi NP do not interfere with gel formation or tissue adhesion. As demonstrated in Figure 27 and 29C, mixing of the PRP prior to injection insures a homogenous distribution of particles throughout the gel. This even distribution guarantees a uniform release of factors as the materials naturally resorb.

Analgesic and antibiotic release from free particles and composite gels

This study shows the control available over release rate kinetics of small drugs such as bupivacaine, dexamethasone, and cefazolin. Selection of different PLGA monomer ratios (50:50 versus 85:15) and molecular weights significantly impacts the burst release intrinsic to PLGA MP and NP delivery systems. The PRP or fibrin gels provide an additional diffusional barrier to the biomolecules, prolonging the release of drugs into a uniform and nearly linear pattern. This sustained release platform of PLGA NP (particularly 85:15 PLGA) embedded within the gel continuously delivers analgesics at consistent dosages as may be deemed necessary. This phenomenon was observed previously in the release of dexamethasone from PLGA NP embedded within an alginate hydrogel [266]. The drug dosages or ratios were based upon a median physiologically relevant dose of the drugs to be applied in approximately 50 mg PLGA (analgesics) or 10 mg pSi (antibiotics) NP per 1 mL of PRP. However, the amount of NP per mL PRP is variable, as is the total volume of PRP to be applied dependent on the patient. Alteration of the number of total particles used should result in a linear change to the release dosage at any given time point, although changes to the loading dose per PLGA/pSi would affect the release kinetics. It is proposed that physicians may select various dosages of free and gel-embedded NP formulations to specifically tailor the pharmacokinetic treatment of patients based on the ailment and drug of choice.

A similar trend was observed in the release of antibiotics from free and embedded pSi MP. The gel caused a delayed release of cefazolin, with significantly less drug released through the first 5 days. The free MP demonstrated the traditional burst release with 64% and 80% of total release achieved at 8 and 24 hours, respectively. However, the pSi NP exhibited a prolonged release, with daily drug liberation so low that the gel was ineffective in its retention. Another possible explanation of the similar free and gel-embedded NP particle release profiles is the aggregation of NP observed, especially near the surfaces of the gel. Future studies to optimize the

dispersion of these nanomaterials could yield even more control in the delivery of biomolecules from composite gel systems. Independent and precise delivery of individual drugs may be achieved by combining free NP (PLGA or pSi) with the PRP/PLGA/pSi gel. The combinations of free NP with MP-embedded gels (Figure 29D, blue) or free NP with NP-embedded gels (green) are able to provide daily potent dosages of the drug through 7 days near the theoretical 100% Day 1 dose. As previously alluded to for PLGA NP combination delivery therapies, a system featuring both free and gel-encapsulated pSi NP provides clinicians with the versatility to deliver different drugs simultaneously at specifically prescribed daily dosages.

Biodegradation and biocompatibility of injectable drug delivery materials

Biodegradation studies on the individual and composite materials revealed mild degradation of PLGA, nearly complete resorption of pSi, and little change in the PRP gel matrix through 7 days (Figure 30). This is imperative for post-operative applications to maintain a seal over the healing wound while delivering the therapeutic payload over the critical first days or weeks. The steady degradation of PLGA allows for continuous removal of its acidic byproducts. Also, the resorption of both particle types generates a system of pores for tissue and vascular integration that may accelerate the wound repair compared to currently used fibrin glues or sealants. Although the PRP matrix did not significantly degrade over the course of the 7 day *in vitro* study, it is certain that the network will be degraded, remodeled, and replaced in the presence of cells and digestive enzymes. The system and its degradation byproducts displayed no significant signs of cell toxicity, with only minor decreases in cell counts at later time points for cells exposed to high dosages of free particles. Composite gels with PRP increased cell proliferation at both 4 and 7 days, due in part to the release of proliferative mitogens from platelets as previously observed [199]. The PRP gel provides stimulatory growth factors while

shielding the cells from particle byproducts by slowing the resorption of those particles embedded within the matrix. This validates the use of PRP as an injectable carrier for the drug-loaded NP.

In vivo response to injectable drug delivery materials

In a preliminary study to investigate the *in vivo* biocompatibility of the injectable drug delivery system, we found that materials (namely PRP) promoted rapid vascularization with integrated blood vessels in as little as 2 weeks. This neovascularization is essential for formation of healthy new tissues by providing them with transport of nutrients and waste. The vessels were well-established in both their diameter and structure, which was confirmed histologically. Furthermore, endogenous cells were recruited into the construct and began depositing matrix throughout the PRP network. The overall construct was relatively unchanged in geometry, although the PLGA and pSi particles were significantly degraded and the matrix was being remodeled with collagen. There were also no indications of an inflammatory response to the materials. This system, when applied to a hard or soft tissue wound, will stimulate the accelerated migration of cells and blood vessels for faster healing while discharging factors and biomolecules to fight bacterial contamination and analgesics to soothe recovering patient.

Conclusion

This study demonstrated the ability to control the delivery of multiple drugs with different burst or linear release profiles by use of PLGA and pSi NP and MP in conjunction with a PRP-based gel. The materials showed signs of degradation after a week *in vitro*, while neither they nor their byproducts had any deleterious effect on cells *in vitro* or local tissue *in vivo*. The multifunctional system presented herein demonstrates a novel combination of biomaterials with effective results for immediate translation to human patient care. From the perspective of regenerative medicine or tissue engineering, this platform is applicable as a coating material for

polymer, metal, or ceramic implants. While PRP promotes cell growth, migration, and angiogenesis, NP can transmit a variety of drugs for optimal and expedited tissue regeneration. For the treatment of cancer, the composite gel may incorporate particles for the delivery of chemotherapeutic agents and be applied to the site of tumor resection. The PRP/PLGA/pSi nanostructured system represents a powerful tool in the fields of wound healing, pain relief, biofilm management, drug delivery, and regenerative medicine. Upcoming work will apply this technology to relevant animal models towards the goal of clinical translation in the near future [271, 272].

Nanomedicine offers the potential to dramatically improve the efficacy of antibiotic administration in the perioperative period, by eliminating human error in dose timing, and improving overall compliance via sustained drug release. Additional benefits include improved antimicrobial efficacy by maintaining a constant, sustained drug concentrations in the therapeutic range and eliminating the peaks and troughs associated with intravenous drug administration. Continuous drug release will also decrease side effects and toxicity for the same reason. Additionally, sustained and controlled release of antibiotics decreases multiple dosing schedules, which will decrease risk of medication dosing errors and lessen the labor burden of the healthcare support staff. The benefits of nanomedicine are vast and the impact, profound. In prevention of surgical site infections alone, nanomedicine has the potential to improve outcomes, decrease morbidity and mortality, and decrease the overall burden on our healthcare system. Nanomedicine will improve the quality of life not only for the patient who benefits directly, but also for society at large.

7 Prolonged analgesia via an injectable lidocaine nanohydrogel delivery system in rat surgical incisional pain model

A manuscript to be submitted for publication

Abstract

Successful treatment of acute and chronic pain represents both one of the primary requirements and greatest challenges for today's clinicians. Such pain remains simultaneously the chief limiting factor for patients' resumption of normal activities of daily living and return to work, and the main cause of current dependence upon opioid narcotics for analgesic relief. Sadly, current analgesic adjuncts are limited, leaving great opportunity for improvement through the use of advanced materials such as nanotechnology platforms. We developed one such platform that demonstrates extended, controlled release of lidocaine hydrochloride from a multilayered, nanohydrogel for at least seven days. Beyond *in vitro* loading and release, we clearly defined and illustrated the homogeneous *in vivo* tissue dispersion of our novel platform. Using an incisional model of pain in rodents, we then compared its analgesic efficacy to daily systemic non-steroidal anti-inflammatory (NSAID) or opioid injection. Administered alone at the time of surgery, our experimental hydrogel provided equivalent or superior analgesia to daily NSAID injections; and when combined with daily NSAIDs as part of a multimodal treatment regimen, it outperformed daily opioid narcotic injection over a treatment period of seven days. Pain was assessed by a combination of mechanical stimulus testing and a novel scoring system called the Functional Recovery Index (FRI). These results establish such nanotechnology platforms as potential future analgesic clinical agents capable of diminishing the need for opioid narcotics and their concomitant side effects, meanwhile restoring earlier functional return.

Introduction

The human ability to perceive pain serves a protective role, sending the necessary impulses to the central nervous system to identify and avoid the painful impetus, thus promoting individual and overall species survival - perhaps best evidenced by diseases of impaired nociception like diabetic neuropathy or leprosy, with increased morbidity and mortality in the affected populations [273-277]. Despite its utility in self-preservation, the shadow of pain and its inadequate treatment looms large over today's society, carrying with it significant psychosocial, economic, and both local and distant inadvertent tissue consequences. Unmitigated pain is well documented as the primary fear of patients undergoing acute medical care involving a procedure, and chronic pain patients often display specific pain-related avoidance behaviors [278-283]. Insufficient treatment of acute post-surgical pain is a risk factor for the development of chronic pain syndrome(s), and the related psychosomatic effects and/or diminished quality of life [284-290]. However, pain management remains conspicuously inadequate in daily medical practice [291-296]. Patient fear is substantiated not only by individual psychosomatic effects, but also by the known correlation of uncontrolled pain with adverse local and systemic post-procedural consequences. For example, the unopposed autonomic response generated by inadequate analgesia increases the surgical stress response and accompanying adrenergic tone, thus decreasing local tissue perfusion and oxygen tension and increasing the risk for wound infection from diminished oxidative bacterial killing [297-299]. Meanwhile, factors such as impaired mobility and inspiratory capacity secondary to pain entail increased incidence of pulmonary and thromboembolic complications respectively [300-305]. The resultant economic impact of inadequately treated pain is understandably colossal and yet, incompletely characterized due to the vague, but far-reaching nature of its effect.

In their 2011 report, the Institute of Medicine estimates that pain management costs the US alone over $635 billion annually [306]. The sharp rise in surgical operations performed in the

ambulatory setting to nearly 70% has occurred with a similar evolution in perioperative surgical analgesia, but questionable lasting postoperative efficacy [307-311]. Pain is cited by several studies as the chief complaint upon hospital readmission after surgical procedures and subsequent discharge [312-314]. Despite recent development of numerous biomedical engineering feats adjoined to clinical treatment, the field of pain management lags behind significantly as it remains largely reliant on short iterations of the opium poppy, used since the ancient Greek days of Telemachus [315-319]. Sadly, no one suffers more from this creative stagnation than our patients. Lingering reliance upon opioid narcotics for effective analgesia does not come without ample cost, as it is clearly linked to increased adverse drug effects (respiratory depression, GI dysmotility, etc.) and total in-hospital expenditures, and has emerged as a premier drug of abuse [320-329]. The subjectivity of the human pain experience and its inherent interpersonal variability make providing sufficient analgesia a harrowing task, especially considering the paucity of newly developed analgesic modalities in the past several decades.

The advent of multimodal analgesic regimens verifies the potential for opioid-sparing alternatives, and will likely soon represent the new standard of clinical care [330-335]. Local anesthetics have great potential to contribute to such regimens, but are limited by their short therapeutic duration and toxic potential. Continuous infusion of local anesthetics has been linked to diminished narcotic need and fewer adverse postoperative outcomes, but carry risk of injury with implantation or subsequent catheter-derived infection [336-340]. These shortcomings have fueled a search for long-acting anesthetic formulations for controlled, extended local drug elution. Encapsulation within a biodegradable carrier agent could provide the proper drug release profile to achieve safe, long-term analgesia. The only preparation currently clinically available is a simple liposomal one that has provided proof of concept with its ability to diminish postoperative pain and opioid use, but only for up to 72 hours [341-343]. Given that patients report moderate to severe pain and functional impairment for more than twice that time, improvements are greatly

needed. Alternatives under investigational development include hydrophobic polymer-based formulations like PLGA micropaticles, injectable and solid polymers or their combination applied in various forms from transdermal patches to injectable formulations, but none has been successfully translated to the clinic [344-346].

The aim of this study was to validate our ability to provide an improved, nanostructured, polymeric platform capable of extended local anesthetic release for the purpose of surgical analgesia for potential clinical translation. We hypothesized that an injectable, lidocaine-loaded porous silica nanoparticle (MSP)/polymeric analgesic hydrogel could provide equivalent or superior reduction in postsurgical mechanical hyperalgesia than standard analgesic modalities (NSAIDs or opioids) in a rodent incisional pain model either alone or as part of a multimodal analgesia regimen (Figure 33). Mechanical hyperalgesia can be defined as the sensation of pain to what is normally a non-nociceptive touch stimulus or, as Zahn defines it, "decreased pain threshold to suprathreshold stimuli" [347, 348]. Further, we hypothesized that this enhanced local effect would allow hastened functional recovery in rats treated with our experimental hydrogel. Hydrogel characteristics of specific interest and importance included: controlled drug release for a minimum of seven days, correlate in vivo degradation/release, local tissue compatibility, and in vivo analgesic efficacy.

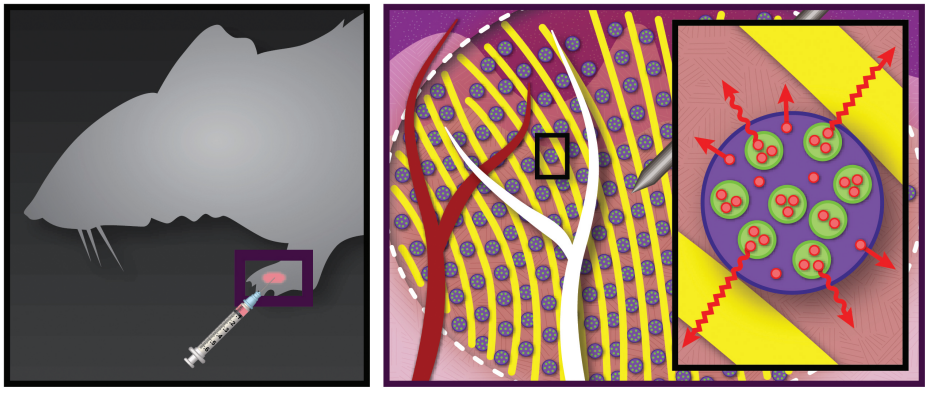

Figure 33. Schematic showing the injectable lidocaine nanohydrogel delivery system that demonstrates extended, controlled release from a multilayers in the hindpaw of rat surgical incisional pain model

Materials and Methods

Study Design

In short, the work described herein was undertaken to establish a sound base of research supporting novel, opioid-sparing analgesic moieties capable of more prolonged and significant analgesia than what is currently clinically available. We sought specifically to prove or disprove the following hypotheses: it is possible to develop a nanostructured anesthetic platform capable of controlled, extended release for at least 3-7 days and, when applied in a surgical model of incisional pain, an equivalent or superior decrease in mechanical allodynia as compared to current treatment standards would be seen. Our reasons for choosing a time period of 3-7 days are twofold: the best clinically available analog to our nanostructured hydrogel - Exparel® (Pacira Pharmaceuticals Inc., San Diego, CA) - has proven effective at providing opioid-sparing analgesia only up to three postoperative days, meanwhile postsurgical patients often report pain-related symptoms that limit quality of life (QOL) and return to work for a full week postoperatively [341-343, 349, 350]. If our novel analgesic platform could exceed these metrics, then its correlative translational potential is great.

Prospectively, quantifiable differences of an analgesic effect amongst study groups served as our primary endpoint. Survival was not an endpoint. After initiation of the study and data analysis, a notable difference in behavioral and activity parameters amongst treatment groups was witnessed, thus a secondary endpoint comparing temporal return of normal function emerged. A power analysis calculator was used to calculate an anticipated sample size, assuming an alpha = 0.05, difference (D) = 10, and a desired power of 0.8, to create anticipate sample sizes of 12/group. However, in light of several historical controls in the literature achieving statistical significance using 6 animals/group a preemptively unknown true D value, and the need for a USDA pain category E negative control group, we elected to begin with 6 animals/group. Like

the historical controls, we achieved statistical significance ($p<0.05$) using this sample size and thus, did not unnecessarily/unethically subject more animals to the study.

To determine analgesic efficacy of our nanohydrogel *in vivo,* 38 adult male Lewis rats (Charles River Labs, Houston, TX) with an average weight of 358g were randomly assigned to one of six study groups (N=6/group) relative to postoperative analgesia administered: sham (S), no postoperative analgesia (-C), experimental nanostructured hydrogel alone (E1), daily subcutaneous non-steroidal anti-inflammatory drug (NSAID) injection (+C1), experimental nanohydrogel + daily subcutaneous NSAID injection (E2), or daily subcutaneous opioid injection (+C2) (Figure 34). Specific comparative interest was given to the following groups: E1 versus -C and +C1, and E2 +C2, with all groups referenced to sham (S). All animal work was performed under approval and supervision of the Institutional Animal Care and Use Committee (IACUC) at HMRI and all investigators complied with the National Research Council's Guide for the Care and Use of Laboratory Animals.

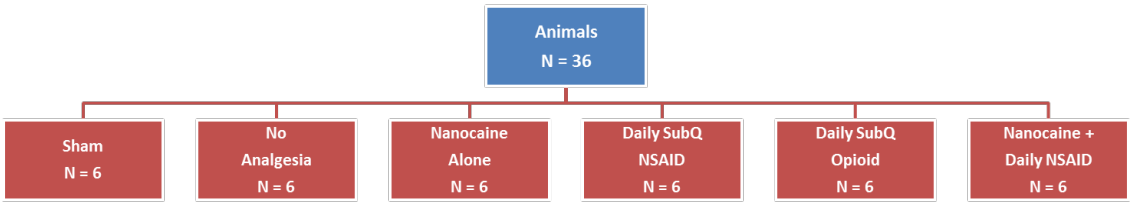

Figure 34. *In vivo* study design for injectable lidocaine nanohydrogel delivery system in rodent surgical incisional pain model

Rats received water and chow ad libitum and were housed in pairs at Houston Methodist Research Institute (HMRI) until the study period began, at which time they were caged singly. After the required 48 hours of acclimation time, two different study personnel handled each rat outside of their cage twice daily for two days to adapt to human interaction prior to operation and formal testing, and animals were allowed to ambulate atop the mesh-bottom testing platform for five minutes to acclimate to testing conditions. Sham rats did not undergo an operation, but instead received twenty minutes of inhalational anesthesia and sterile hindpaw preparation only.

In light of the significance of the first week in human patients' functional recovery and reported pain levels, rats were followed for seven days postoperatively to correlate findings. Incision sites were investigated daily for integrity and animals suffering wound dehiscence were excluded and humanely euthanized. Barring exclusion for complications, data collection was prospectively designed to stop at the end of seven postoperative days. Testing was performed at the same time daily for consistency (less than 24 hours from previous analgesic administration whenever applicable), and entailed: recording animal weight, National Institute of Neurologic Disease and Stroke (NINDS) behavioral scoring, generating a modified Cumulative Pain Score (CPS), and mechanical stimulus testing using von Frey filaments. Study personnel remained effectively blinded while testing by keeping each rat's identifying cage card covered by a blank card until all testing was complete. Only after all subjects finished daily testing were data linked to animal identification. Following a day of testing, staff randomized placement of animal cages on a multicage rack and further, veterinary care staff subsequently rearranged them again daily after testing, thus resetting randomized conditions for the next staff evaluator. Post-hoc data analysis was performed non-blinded.

Nanohydrogel Synthesis

Material

Poly (DL-lactic-co-glycolic acid) (PLGA; 85:15; containing 85% d-lactic units, 85% d-lactic units and 15% glycolic units) (Lactel Absorbable Polymers), lidocaine hydrochloride monohydrate (Sigma–Aldrich), polyvinyl alcohol (PVA) (M.W. 20,000-30,000) (Acros Organics) and Pluronic® F-127(Sigma–Aldrich) were used. Silica nanoparticles (MSP) were synthesized as previously described [351].

Preparation

Lidocaine-loaded PLGA-MSP composite microparticles were prepared by a water-in-oil-in-water (W/O/W) solvent extraction/evaporation technique: 0.5 mg of lyophilized silica were

resuspended in 1 mL of distilled water (pH 7) and dispersed using water bath sonication. 5 mg of lidocaine hydrochloride was introduced into the silica solution and incubated for 2 hours at 37 C under mild agitation. The particles were centrifuged down at 22.1 x1000 g and lyophilized for 3 hours. 1.2 mL of PLGA- Dichloromethane (DCM) solution (60 mg of PLGA in 1.2 mL DCM solution) was transferred to an Eppendorf tube containing 10 mg of lyophilized silica nanoparticles. The mixture was vortexed and briefly sonicated. The final polymer-silica suspension was transferred in to 4 mL of 5% PVA solution in a homogenizer tube and homogenized (2000 rpm; 5 minutes). Then homogenized suspension was transferred into 5 mL of 0.1% PVA solution and stirred with mechanical stirrer for overnight. The reaction content was centrifuged down at 5000 rpm and washed twice with Millipore water and lyophilized. Final nanohydrogel formulation was prepared by mixing 5 mg of loaded PLGA-MSP composite microparticles with 100 μL of Pluronic® F-127 solution in PB 7 buffer (15% m/v) and stored at 4°C prior to use.

Characterization

The morphology of the PLGA-MSP microparticles was characterized by optical microscope (Nikon Eclipse TS 100), fluorescent microscope (Nikon Eclipse Ti), confocal laser microscope (Nikon A1 Confocal Imaging System), and scanning electron microscope (SEM) (FEI Nova NanoSEM 230). Particle size distributions and mean diameters of the complete batch were determined using a Multisizer 4 Coulter® Particle Counter (Beckman Coulter) with an aperture (20 μm). Fourier transformed infrared (FT-IR) spectroscopy was performed by creating a pellet of 5% sample and 95% KBr (Sigma–Aldrich) by volume and analyzing absorbance of the pellet on a Nicolet 6700 FT-IR Spectrometer (ThermoFisher Scientific Inc, Walthman, MA). The crystal-crystal-transition temperature (Tt) and its enthalpy (ΔH) were measured by differential scanning calorimetry (DSC) under N2 at a heating rate of 10 °C/min using a PerkinElmer Pyris.

Lidocaine release & hydrogel degradation in vitro

Lidocaine-loaded microparticles (approximately 5 mg) and Lidocaine-loaded nano-hydrogel (5mg PLGA-MSP in 100 μL of Pluronic F-127 solution) were placed within 250 μL phosphate buffer pH 7.4 in an Eppendorf tube and incubated under mild agitation at 37 °C. At pre-determined time intervals, 200 μL of solutions were withdrawn (replaced with fresh medium) and analyzed by High Performance Liquid Chromatography (HPLC) [352]. Degradation of nanohydrogels was examined with respect to weight loss under aqueous conditions. Weight loss of initially weighed hydrogels (W0) was monitored as a function of incubation time in PBS at 37 °C. At specified time intervals, hydrogels were removed from the PBS and weighed (W_t). The weight loss ratio was defined as $100\%\times(W_0–W_t)/W_0$. The weight remaining ratio was defined as $1–100\%\times(W_0–W_t)/W_0$. Surface morphology of nanohydrogels was characterized by utilizing SEM after gelation. The hydrogels were freeze-dried and then platinum coated using a Cressington Sputter-coater 208HR (Cressington, Watford UK). The surface and cross-sectional morphologies were viewed using a SEM (JEOL, Peabody, MA) operated at 10kV accelerating.

Hydrogel dispersion & biodegradation in vivo

It is known that small molecules and their requisite carriers often behave differently when studied *in vitro* versus *in vivo*. To answer whether a similar pattern of nanohydrogel breakdown and release occurs *in vivo*, fluorescently labeled nanohydrogel was implanted and visualized over time using confocal microscopy. To study the dispersion of PLGA-MSP nano formulated gel components and a drug molecule release from them, Alexa fluor 561, a drug molecule model, has been loaded inside the FITC (Fluorescein isothiocyanate) labeled Si, and then encapsulated within Alexa flour 640 labeled PLGA micro-particles. Lastly, all materials were homogenized inside the Pluronic F-127 thermo-responsive hydrogel. All materials were implanted into the rat incisional pain model. Animals were sacrificed at time point days 0, 2, 5, and 7. Soft tissues around incision area were harvested with 0.5 cm margin and embedded within Tissue-Tek OCT

*(*optimum cutting temperature*)* compound in Tissue-Tek standard cryomold. The embedded tissues were transferred into a -80 freezer, and then sections with 20 um thickness were prepared using Microm^{TM} HM 525 Cryostat.

Images were acquired from 2 um Z stacks using confocal laser point scanning systems with NIS-Elements software and motorized XY stage (Proscan III). Stitching was used to reconstruct a large image from 16 (4x4) block images for each z stack. All settings including laser power, gain, offset, and pinhole were maintained the same throughout each acquisitions. All images were analyzed with NIS-Elements AR 4.12.01 64-bit software. Z stack with highest fluorescent intensity for all channels were used for analysis. Thresholds for all channels were defined in a manner to eliminate all auto-fluorescence and the same thresholds were applied for all image analysis. The relative fluorescent intensity was measured for the selected Z stacks and 5 circular ROI (Region of Interest).

Operative details

Widely accepted as the most validated and tested model of incisional pain, we used the Brennan model of incisional pain [353-357]. For preoperative anesthesia, all rats received Buprenorphine (0.05mg/kg) and Carprofen (5mg/kg) injected subcutaneously. After induction, anesthesia was maintained using a 2.5-3.0% isoflurane/oxygen mixture via nosecone. Before sterile draping, the left hindpaw was sterilized with three alternating scrubs using chlorhexadine gluconate and 70% alcohol, and aseptic technique was maintained throughout the duration of the surgery. In all animals besides sham rats, a 1.0 cm longitudinal incision was made in the hindpaw through the glaborous skin, subcutaneous tissue and plantaris muscle using a #15 scalpel blade, cautiously protecting sensitive periosteal structures from injury (Figure 35A-C). Hemostasis was maintained by direct pressure without the use of electrocautery. For E1 and E2 rats, the surrounding peri-incisional tissues were circumferentially infiltrated with cool (liquid phase) nanohydrogel, which was allowed to gel via thermogenic activation of Pluronic acid by the rat's

body temperature (Figure 35D, E). Finally, incisions were closed with two horizontal mattress sutures using 5-0 Prolene® suture (Ethicon Inc., Raleigh, NC) and neomycin/polymyxin b ointment was applied to the incision (Figure 35F-H).

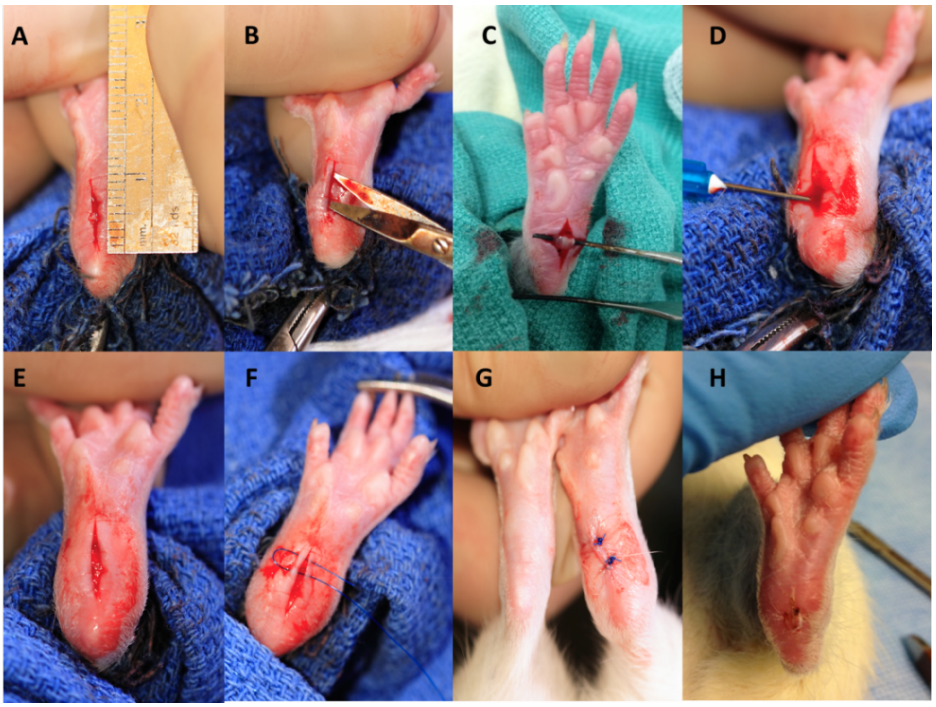

Figure 35. The surgical procedure for development of the Brennan model incisional pain in rat

Creation of the Functional Recovery Index

The importance of an analgesic moiety's capability to restore host functionality in clinical practice is paramount; and the host of different postoperative tests employed in literature for rodent pain studies often muddies the water for data interpretation, making a singular objective representation of this ability quite necessary. Thus, to compare the temporal restorative potential of our nanohydrogel to conventional treatments a comprehensive, novel hybrid scoring system was developed – the Functional Recovery Index (FRI). The FRI was developed as a combination of the following established metrics: a modified Cumulative Pain Score (mCPS) based on weight-bearing capacity, and an observational NINDS behavior scoring system. As outlined in prior studies, the CPS assigns point values 0-2 based on the degree of peri-incisional skin blanching –

and thus weight bearing – present compared to the opposite control hindpaw as viewed from below while the rodent is allowed to stand/ambulate freely (Figure 36) [356-360].

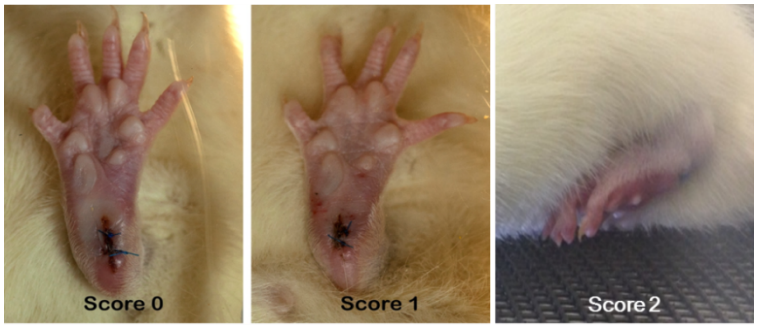

Figure 36 Hindpaw blanching - Cumulative weight bearing index

Although use of a magnifying mirror beneath a mesh-bottom cage has been reported, we chose rather to view rats from an elevated clear chamber, under the belief that it provides more precise observational analysis. In our mCPS, blinded observers scored rats from below a clear plastic chamber at 5-minute intervals for a total of 30 minutes daily (max score = 12/day). Each

Table 3. Blanching functional recovery index

Blanching FRI: Avg 12-Sum	Points
<1.00	0
1.00-1.99	1
2.00-2.99	2
3.00-3.99	3
4.00-4.99	4
5.00-5.99	5
6.00-6.99	6.5
7.00-7.99	8
8.00-8.49	9.5
8.50-8.99	11
9.00-9.49	12.5
9.50-9.99	14
10.00-10.24	16
10.25-10.49	18
10.50-10.74	20
10.75-10.99	22
11.00-11.24	24
11.25-11.49	26
11.50-11.74	28
11.75-12.00	30

rat's scoring sum was subtracted from 12 to generate a daily mCPS score, and each group's overall mean mCPS was determined for days 1-7. Since the mCPS score assesses a singular variable compared to several measured by NINDS assessment, it was weighted less heavily (30 of 100 possible points) for overall FRI scoring. Further, to adequately represent the difference in severity of impairment *in vivo*, FRI scoring was differentially weighted within correlate mCPS scores (0-12) - with smaller integer scoring increases for a mCPS score < 6 and larger increases over shorter intervals as the mCPS score rises from 6-12 (Table 3). As previously applied in literature, the NINDS scoring system assigns point values of 0.0, 0.1 or 0.4 (or whole integers of 0, 1, and 4 respectively) based on the observed presence/absence of abnormalities in: attitude, gait and postures, porphyrin staining, weight and appetite (Table 4) [361-367]. Porphyrin staining in the rat appears as dark red discoloration around the eyes, nose and mouth. It is commonly used as a surrogate marker of stress in rats, as porphyrins are overproduced when rats are acutely ill, poorly fed, or acutely stressed by events such as limb restraint, sleep deprivation, morphine withdrawal or acute pain [368-370].

Table 4. Example of score sheet for assessing rodent postoperatively.

Observation	Individual Score (mark score here)	Score Standards	Details
Attitude		0	Bright and alert.
		0.1	Burrowing or hiding, quiet, but rouses when touched.
		0.4	Burrowing or hiding, quiet, but rouses when touched. No exploration when lid off, burrows, hides, head presses. Might be aggressive when touched.
Porphyrin staining		0	None.
		0.1	Mild around eyes and/or nostrils
		0.4	Obvious on face or paws.
Gait and postures		0	Normal.
		0.1	Mild incoordination when stimulated, hunched posture, mild piloerection.
		0.4	Obvious ataxia or head tilt, hunching, drags one or both limbs, severe piloerection.
Weight		0	Up to 5% weight loss over preoperative weight.
		0.1	5-10% weight loss over preoperative weight.
		0.4	10-20% weight loss over preoperative weight.
Appetite		0	Normal: eats dry food, evidence of urine and feces, food missing from feeder or floor, gelatin gone within 8 hours, evidence that fruit is chewed on.
		0.1	No evidence of eating dry food but likes gelatin and fruit, drinks and appears hydrated (skin does not "tent").
		0.4	No interest in food or treats and or appears dehydrated (poor skin turgor).
Total Score			

We eliminated appetite as a metric of evaluation in our scoring, due to its perceived redundancy with daily weight measurement and the burden that would be required to accurately measure it daily, by changing animal cages daily and manually quantifying urine and feces output. Blinded observers used whole integers of 0, 1, or 4 to score undisturbed animals in their cages with the lid on and off over a 10-minute observational period daily, according to NINDS parameters. Scores for individual behavioral categories were averaged for each group over seven postoperative days.

Table 5. Behavioral functional recovery index average NINDS Scoring chart

Behavioral FRI: Avg NINDS score x 100	Points
300.1-400	0
200.1-300.0	5
100.1-200.0	10
95.1-100.0	22.5
90.1-95.0	25
85.1-90.0	27.5
80.1-85.0	30
75.1-80.0	32.5
70.1-75.0	35
65.1-70.0	37.5
60.1-65.0	40
55.1-60.0	42.5
50.1-55.0	45
45.1-50.0	47.5
40.1-45.0	50
35.1-40.0	52.5
30.1-35.0	55
25.1-30.0	57.5
20.1-25.0	60
15.1-20.0	62.5
10.1-15.0	65
5.1-10.0	67.5
0.0-5.0	70

To compute the NINDS contribution to overall FRI, average NINDS scores were first multiplied by 100 for ease of calculation; then this value (0-400) was used to generate an FRI score (Table 5). Because the NINDS scoring system evaluates several separate gauges of normal versus abnormal function, it was more heavily weighted in overall FRI score calculation (70 of

100 possible points). Also, similar to the mCPS above, FRI scoring was differentially weighted within correlate NINDS scores. Larger decreases in FRI points are seen for scores > 100 and 200 to represent the larger related *in vivo* deviations from what is considered normal behavior.

Mechanical stimulus testing

To determine if our nanohydrogel could diminish peri-incisional mechanical hyperalgesia that is commonly displayed in animals and humans postoperatively, rats underwent mechanical stimulus testing using von Frey filaments (Bioseb, Vitrolles, France). These filaments are made with a wide range of diameters and are finely calibrated to bend only when a corresponding threshold of force is met or exceeded when applying them to a surface [371, 372]. When applied to the rat hindpaw, a characteristic withdrawal response is witnessed if the analogous threshold force is sufficient to cause pain; and this is used to stratify experimental differences in static mechanical hyperalgesia. After a 2-day acclimation and handling period and random animal group assignment, baseline withdrawal thresholds were determined for each animal to account for innate inter-animal variability in pain tolerance and thresholds. Rats were placed atop a mesh-bottom, raised platform enclosed by a clear, polyurethane 3-sided chamber with sufficient room for ambulation and direct visualization of and access to the hindpaw. Filaments ranging from 19.6-588.4mN (2-60 gram-force) were applied sequentially in ascending order to three peri-incisional sites (Figure 37A) by blinded observers until a withdrawal response was generated, and the analogous force was recorded. Sites 1 and 2 are directly peri-incisional, and withdrawal testing here correlates to primary hyperalgia (pain behavior at the site of damaged tissues), while site 3 is more remote and pain behavior here correlates to secondary hyperalgesia (increased sensitivity in undamaged tissues). A withdrawal response was defined as purposeful retraction of the paw from the mesh testing surface or vocalization, with or without subsequent licking of the incisional site. Each of the three testing sites was tested incrementally until a response was

produced before proceeding to the next site. This process was repeated in 5-minute intervals for a total of three withdrawals per site per animal daily (Figure 37B). For each respective group, mean values and standard deviation were generated for both raw withdrawal forces and change (%) from baseline withdrawal force (normalized for each animal) for days 1-7 (Figure 37C).

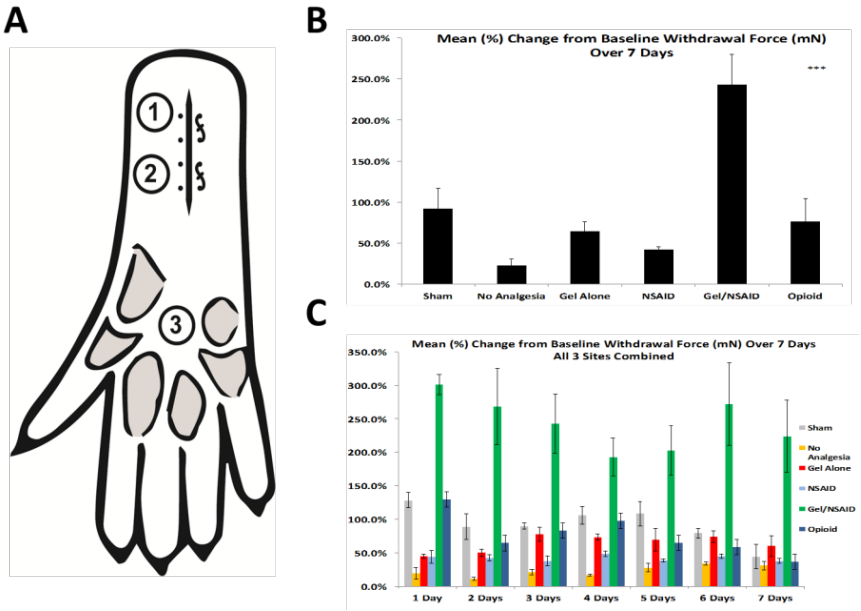

Figure 37. (A) Three peri-incisional sites underwent mechanical stimulus testing; (B) Mean (%) change from baseline withdrawal force over 7 days; (C) Mean (%) change from baseline withdrawal force over 7 days for all three sites combined.

Histology

Animals were humanely euthanized by compressed carbon monoxide inhalation followed by confirmatory thoracotomy, according to NIH guidelines. Laparotomy and median sternotomy incisions were used to access internal organs of interest; and half of each organ (lung, liver, spleen, surgical site) was freshly frozen at -80°C for analysis by ICP-AES, while the other half was fixed in 10% neutral buffered formalin (NBF) for 24-48 hours prior to paraffin embedding and sectioning by standard technique. Paraffin-embedded tissues were serially sectioned axially (internal organs) or coronally (hindpaw) on a microtome at a thickness of 7µm, and counterstained with H&E after deparaffinization and rehydration.

Inductively Coupled Plasma – Atomic Emission Spectroscopy

The portion of the tissues intended for the Si content analysis were weighed, homogenized in ethanol (20%, 5 mL) in 1 N NaOH and left under mild agitation for 2 days at room temperature for extraction of Si. The extracts were centrifuged at 4000x g for 30 min and 1 mL of supernatant was collected and diluted with 3 ml of Millipore water for elemental analysis. Si concentration was detected with a Varian 720-ES inductively coupled plasma optical emission spectrometer (ICP-AES, Varian, USA). Yttrium was used as internal control as previously described [244].

Results

Improved long term, controlled release using combinatorial synthesis

The PLGA-MSP microparticles synthesized for this study ranged in size from ~250 nm to ~4000 nm (Figure 38A). FT-IR spectra of the nanohydrogels obtained before and after encapsulation of lidocaine showed successfully loadings lidocaine, as shown in Figure 38B. DSC measurements of the nanohydrogel with empty and lidocaine loaded particles were performed, and the Tg values of two systems were approximately similar (Figure 38C). Labeled PLGA-MSP particles exhibited a uniformed dispersion throughout the Pluronic hydrogel using fluorescent microscopy, such that the particles can all be considered essentially monodisperse (Figure 38D) as well as the thermoaggregation temperature for nanohydrogel was observed *in vitro* for each tested formulation shown in Figure 38E and upon SEM analysis, PLGA-MSP composite particles showed a very smooth surface (Figure 38F).

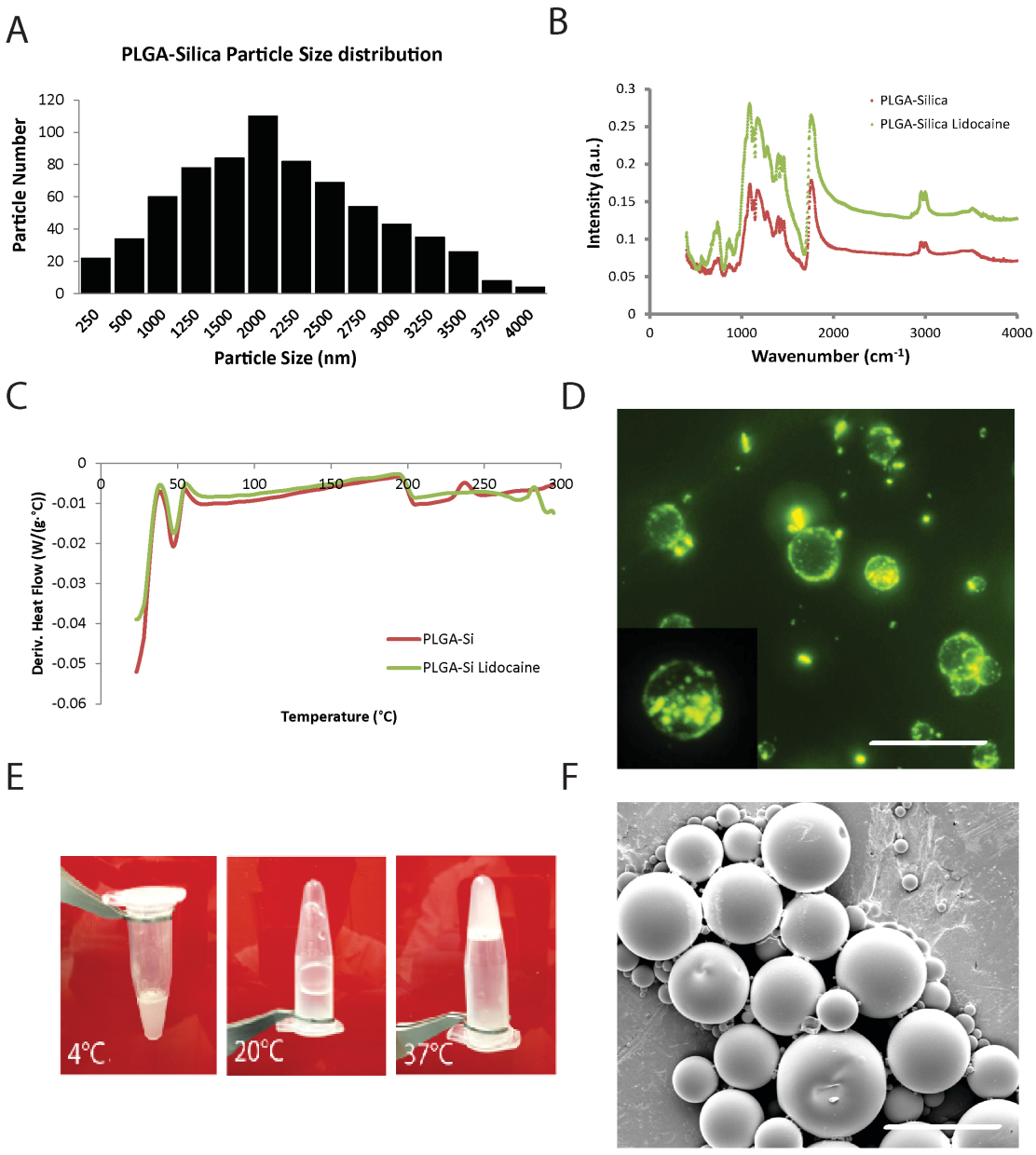

Figure 38. A) Size distribution of PLGA-MSP particles; B) FTIR spectra of free and lidocaine-nanohydrogel; C) DSC curves of free and lidocaine-nanohydrogel; D) Fluorescent micrograogh of PLGA-MSP paricles; E) Evaluation of thermo-responsiveness of nanohydrogel at different temperature; E) Scanning electron micrograph of nanohydrogel microparticles.

Nanohydrogel displays controlled, extended release and degradation over time

Release of lidocaine hydrochloride from the nanohydrogels was detected over 15 days for loaded PLGA-MSP particles imbedded in Pluronic gel *in vitro* (Figure 39) with linear zero order release for first week and slower release for second week time points. In addition, loading efficiency of lidocaine was evaluated using MSP, PLGA and PLGA-MSP particles. PLGA-MSP showed the highest loading efficiency.

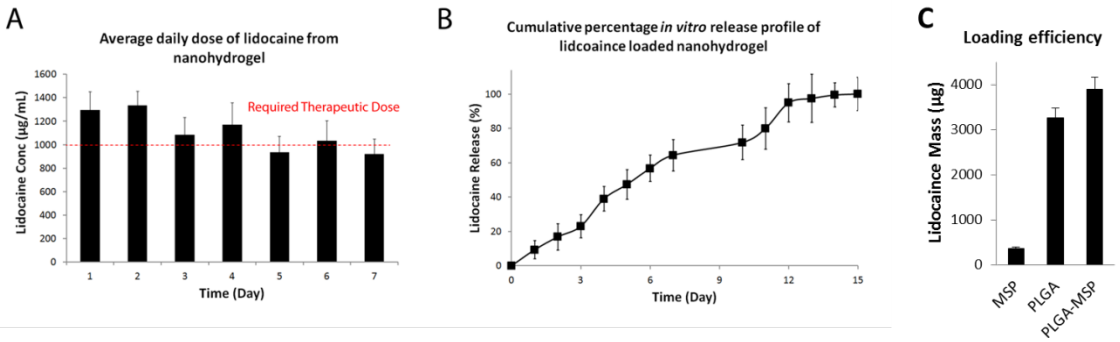

Figure 39. A) Average daily dose from nanohydrogels loaded with the PLGA-MSP; B) Cumulative percent release of lidocaince from nanohydrogel measured by HPLC; C) Loading efficiency of lidocaine at the same concentration using MSP, PLGA, PLGA-MSP (C).

Uniform drug dispersion/degradation from Nanohydrogel in vivo

The identical Brennan incisional model was used to study the local tissue dispersion of our nanohydrogel at time 0 and postoperative days 2, 5, and 7. Each component of the gel was fluorescently labeled with separate fluorophores and the gel was implanted altogether in identical fashion to experimental animals, and then allowed to disperse/degrade over time in vivo prior to harvest and confocal imaging. The quench rate was the slowest for PLGA (Alexa fluor 640) compared to Silica (FITC) and the surrogate drug molecule (Alexa flour 561). The intensity of signal from PLGA decreased gradually days 0-5 (58% on day 5) but was significantly diminished by day 7 (Figure 40). At time 0, 94 % of PLGA was in the center (ROI 1 and 2) and started to disperse in the tissue on day 2 (32% in ROI 3, 4, and 5). The amount of PLGA increased in the

peripheral areas (ROI 3, 4, and 5) on day 5 and reached to the highest level (49%) in the peripheral areas on day 7.

The amount of Silica decreased around 50 % after 2 days and reached to its minimum level on day 5 (5%) and remained the same till day 7. On day 0, 94 % of silica was concentrated in the center (ROI 1 and 2) and decreased to 74% on day 2. On day 5, main part of silica (83%) was in the peripheral areas (ROI 3, 4, and 5). Less than one percent of silica was in the center (ROI 1 and 2) on day 7 and it was dispersed approximately equally between ROI 3, 4, and 5. The amount of Alexa fluor 561 fluorophore decreased in a linear way from day 0 through day 7. The Amount of Alexa flour 561 became 62 % on day 2 and then 13% and 1.8% on days 5 and 7 respectively. 94% of Alexa flour 561 fluorophore was in the center (ROI 1 and 2) on day 0 and started to disperse inside the tissue through 7 days. The amount of fluorophore in the center (ROI 1 and 2) decreased to 76% on day 2 and started to increase in the peripheral areas. On day 5, 54% of fluorophore dispersed between ROI 3, 4, and 5. Only 26 % of fluorophore was in the center (ROI 1 and 2) on day 7 and the rest of the fluorophore was dispersed between ROI 3, 4, and 5.

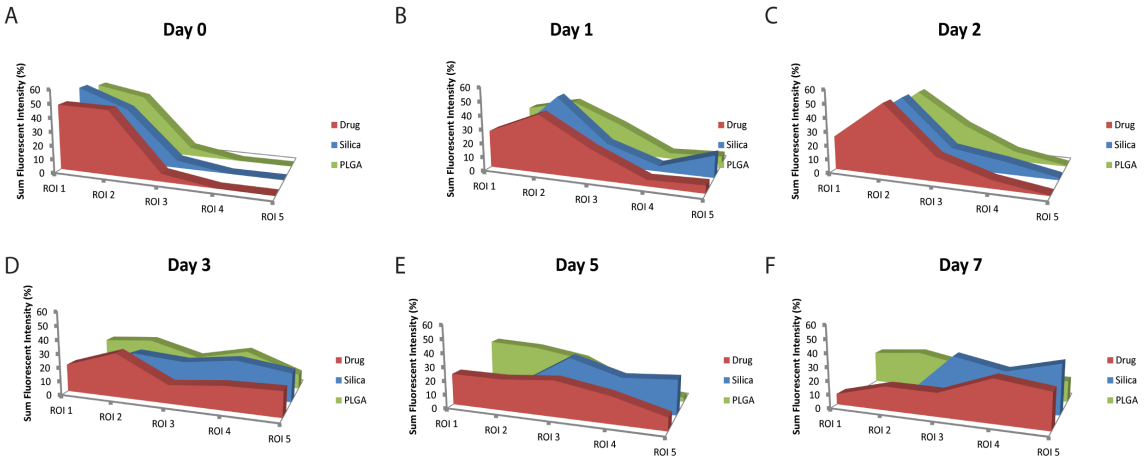

Figure 40. Drug dispersion and degradation of nanohydrogel *in vivo*

Nanohydrogel treatment diminishes mechanical hyperalgesia

Analgesic efficacy was assessed by multiple parameters including those described subsequently, but aesthesiometry testing with von Frey filaments was utilized to mechanically stimulate the peri-incisional hindpaw for comparison of induced mechanical hyperalgesia amongst groups. The analgesic effect of nanohydrogel gel alone (E1) was readily apparent when compared to no analgesia (-C) rats. E1 rats displayed significantly less mechanical hyperalgesia (smaller decrease in force from baseline to elicit withdrawal response) at all 3 peri-incisional sites beginning day 1 and continuing through the duration of the study (Figure 41). The mean withdrawal threshold from all 3 sites combined over 7 days in of the E1 group was 1.84-fold greater (282.5 vs. 153.6mN) than the –C group ($p<0.01$). When compared to NSAID (+C1) rats, this mean of raw threshold force values for E1 subjects is nearly identical (282.5 vs. 280.8mN), suggesting equivalent efficacy to this standard of veterinary care in diminishing postoperative mechanical hyperalgesia.

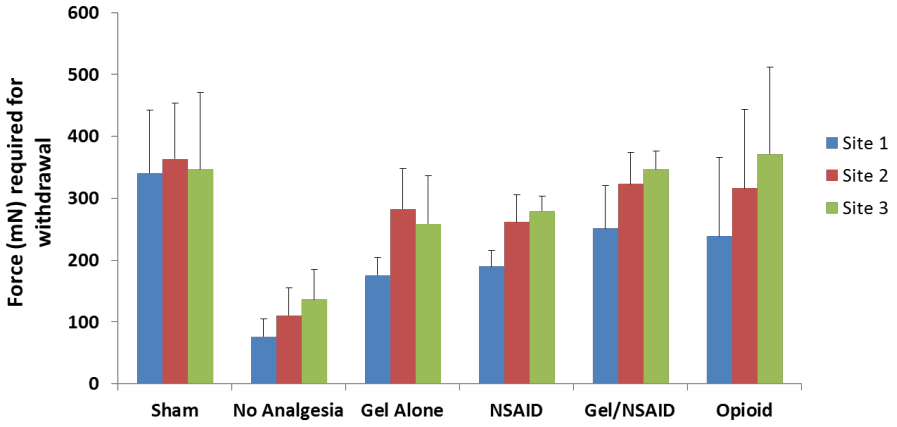

Figure 41. Mean Withdrawal Force (mN) by testing all three sites over 7 days

However, to account for inherent inter-animal variability in mechanical stimulus sensitivity, we normalized these values to each individual animal's preoperative baseline withdrawal threshold force and the differences were even more striking. Represented as percent change from baseline (Figure 42), E1 rats showed significantly smaller changes (hyperalgesia-

related decrease) from baseline than –C rats at all peri-operative sites daily throughout the 7-day study, and a 2.15-fold smaller cumulative decrease (%) when all data is combined and averaged over the study period (35.9% vs. 77.2%, $p<0.01$). Compared to +C1 subjects after normalization, we again witnessed a significant protective effect in E1 rats at all testing sites, particularly during postoperative days 3-7, and a 1.6-fold smaller cumulative decrease (35.9% vs. 57.6%, $p<0.05$). Sham (S) rats performed as expected based upon historical controls, with induced hyperalgesia from repetitive mechanical stimulation appearing on study days 6-7, evidenced by a drop from baseline threshold forces of 20.8% and 56% respectively.

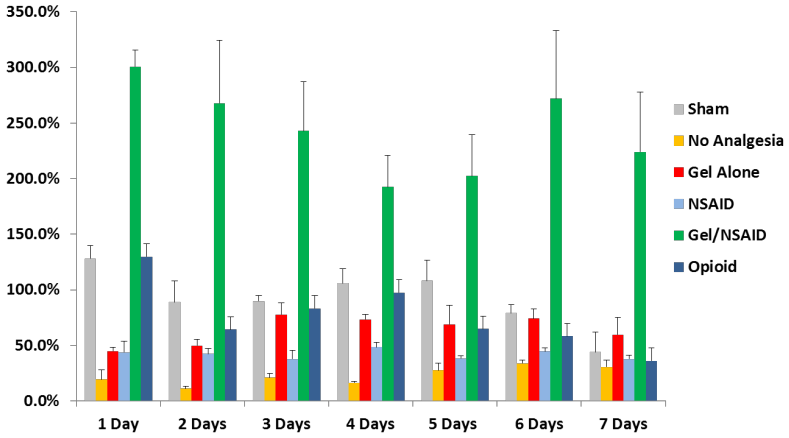

Figure 42. Mean percent change from baseline withdrawal Force (mN) over 7 days for all three sites combined

Interestingly, when nanohydrogel was combined with standard daily subcutaneous NSAID administration as combination therapy (E2), a significant additive analgesic effect was witnessed that far exceeded the performance of all groups, including daily opioid treatment (+C2). Similar to the case above with E1 vs. +C1 rats, the absolute force values for E2 subjects were virtually identical to +C2 when averaged over the 7-day testing period. When normalized to individual rats' baseline threshold forces, a similar trend was seen as above, with E2 rats displaying significantly less change (%) from baseline than +C2 at all 3 testing sites every day of the study.

Nanohydrogel allows earlier functional recovery

A modified Cumulative Pain Score (mCPS) and the National Institute of Neurologic Disease and Stroke (NINDS) behavioral scoring system were jointly used to assess recovery of normal function over time in test animals. They were later combined into a singular, novel scoring system we have developed as a 'snapshot' per se of these differences – the Functional Recovery Index (FRI). As expected in regard to the mCPS, sham rats displayed no abnormalities and maintained an average score of 12 (highest possible score) throughout all days of the study. Group E1 rats performed as well or better than either +C1/2 as compared to –C rats. In the first five postoperative days, E1 rats had significantly higher average mCPS scores than –C rats ($p<0.05$) – equivalent to NSAIDs and opioids (Figure 43). Rats treated with NSAIDs or opioids (+C1/2) had nearly identical mCPS scores. The multimodal E2 group exhibited significantly higher overall scores than either +C1 or +C2 rats ($p<0.05$). Interestingly, beginning as early as postoperative day 1, average mCPS scores of E2 rats were essentially identical to sham rats, suggesting that such multimodal analgesia with nanohydrogel affords tolerance of full weight-bearing within 24 hours of the surgical operation. As expected after such a minor operation and reported in literature, differences amongst groups disappeared beginning on postoperative day 5 as normal function returned. A similar trend was witnessed with NINDS testing over the study course.

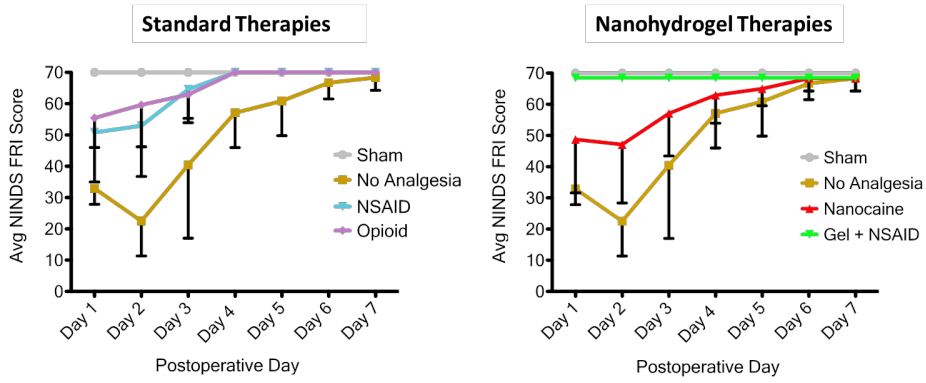

Figure 43. Comparison between standard and nanohydrogel treatments over 7 days.

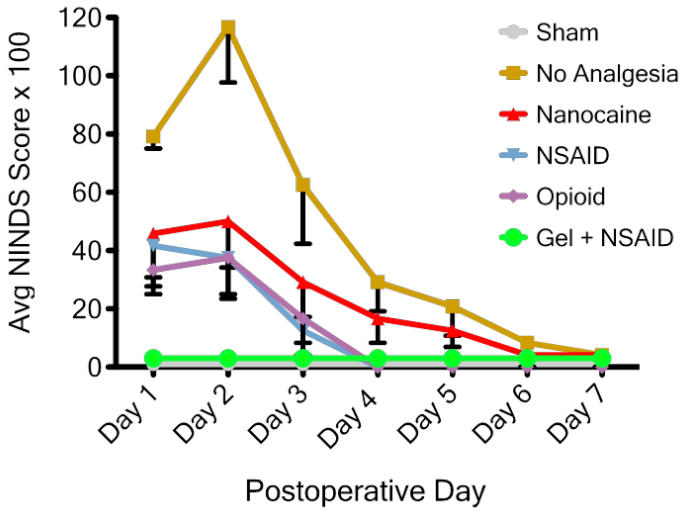

Figure 44. Average NINDS scoring of different groups over 7 days.

Sham set the standard on NINDS evaluation, with no perceived abnormal behavior and perfect scoring. Rats that received no analgesia displayed obvious behavioral abnormalities postoperatively - reflected in significantly higher NINDS behavioral scores than all other test groups including E1, particularly in the first three postoperative days (Figure 44) ($p<0.05$). Rats in groups E1, +C1 and +C2 all displayed moderate behavioral changes on the first postoperative day, followed by mild abnormalities on days 2-3 and essentially normal behavior by day 4. Abnormalities in porphyrin staining and gait were most commonly observed. Notably, the E1 group had multiple rats with abnormal (>5%) postoperative weight loss, compared to only one +C1 rat and none in the +C2 group. This abnormality disappeared in the E2 group, suggesting a possible protective weight loss effect with the addition of NSAIDs. Blinded overall NINDS scoring of E1, +C1 and +C2 groups confirmed their differences to be miniscule and statistically insignificant, indicating an equivalence in effect of nanohydrogel alone compared to NSAIDs or opioids. Finally, group E2 rats again mirrored sham subjects, displaying normal behavior and scores for the entire postoperative study period – again a statistically significant difference from other treatment groups, including nanohydrogel alone (E1) or opioid narcotics (+C2). FRI scoring provides a unified, summed representation of both of these scoring metrics and clearly

conveys the efficacy of nanohydrogel therapy either alone or as multimodal therapy in restoring normal animal function (Figures 43, 44).

Nanohydrogel is biodegraded over time

To prove that silica nanoparticles had not accumulated to toxic levels at the end of the study period, animal organs of interest were harvested for analysis by inductively coupled plasma atomic emission spectra (ICP-AES) and histological evaluation. Extensive work performed by our group as well as elsewhere has shown that when nanoparticles are injected intravascularly, significant accumulation in the lungs and reticuloendothelial system (RES) can be expected and is a function of nanoparticle size, shape, structure, biotranslocation, charge (or other surface modification), and the first-pass clearance effect of these tissues [244, 373-377]. Few studies have investigated the effect of local tissue infiltration with silica nanoparticles, but one such study that utilized them for achilles tendon regeneration in rodents showed an enhanced cellular effect without increased inflammatory cell infiltration as compared to control [378]. Our results mirror this. To verify the silica content, we evaluated harvested tissues samples for their Si content using ICP-AES. ICP-AES data measurements showed greater uptake of MSP by the spleen and liver over 7 days (Figure 45).

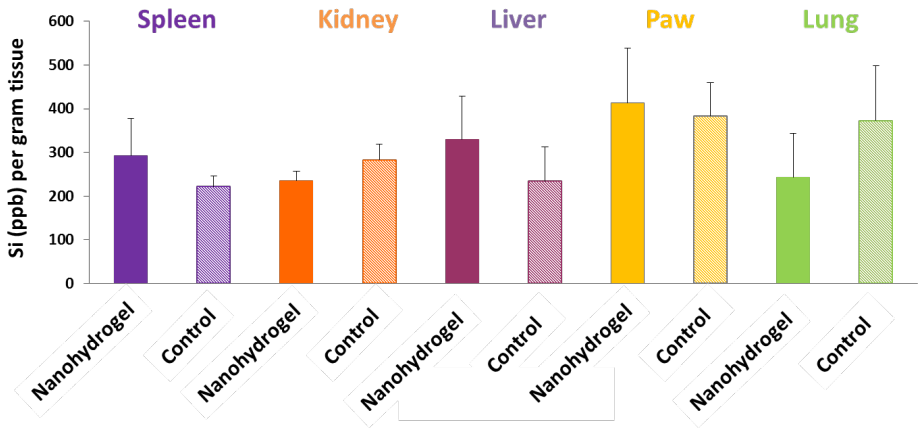

Figure 45. ICP–AES quantitative elemental analysis of Si detected in collected organs.

Our findings were consistent with previously reported biodistribution of MSP [139, 379]. Histological evaluation grossly confirmed the absence of silica accumulation or obvious secondary toxic tissue effects. Mononuclear phagocytic cells play a large role in the first-pass effect, but also in eventual clearing of nanoparticles that are introduced into peripheral tissues. There were no identifiable histologic differences in the lungs, liver, or spleen of experimental rats treated with nanohydrogel as compared to –C or sham rats (Figure 46).

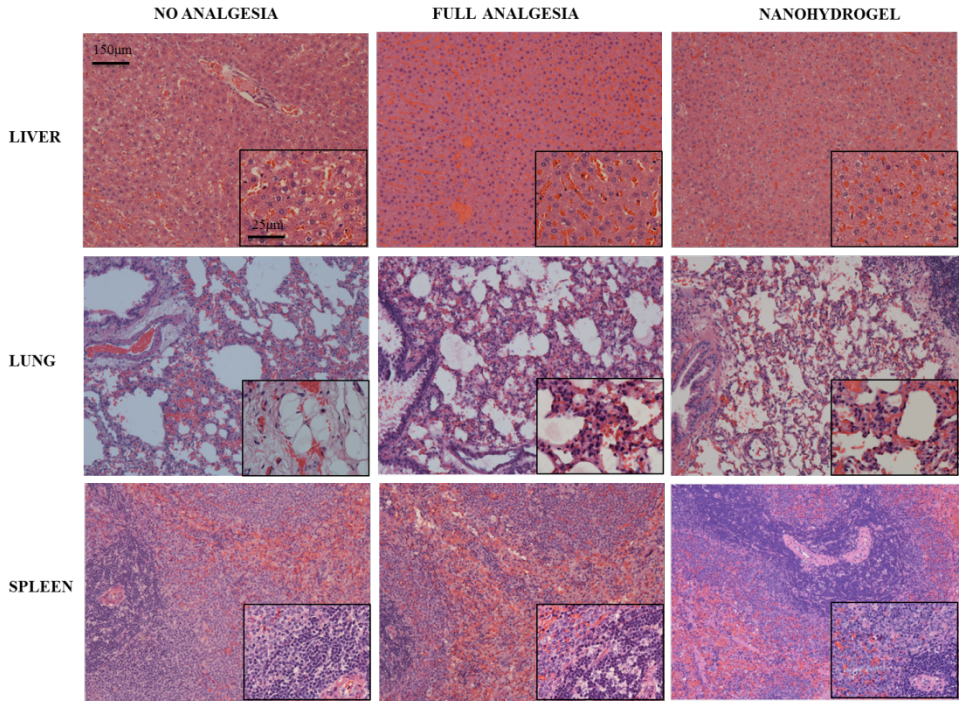

Figure 46. Histological evaluation of liver, lung, and spleen tissues at day 7 stained with H&E.

At the hindpaw surgical site, intact microparticles with enclosed silica nanoparticle 'sediment' could still be identified in hematoxylin and eosin (H&E) stained specimens from E1 rats by magnified light microscopy seven days after hydrogel implantation (Figure 46). As expected after surgical tissue injury, a significant microscopic inflammatory cell infiltrate was seen at the surgical site on H&E stained samples from both –C and E1/2 rats, but the magnitude was similar (Figure 47).

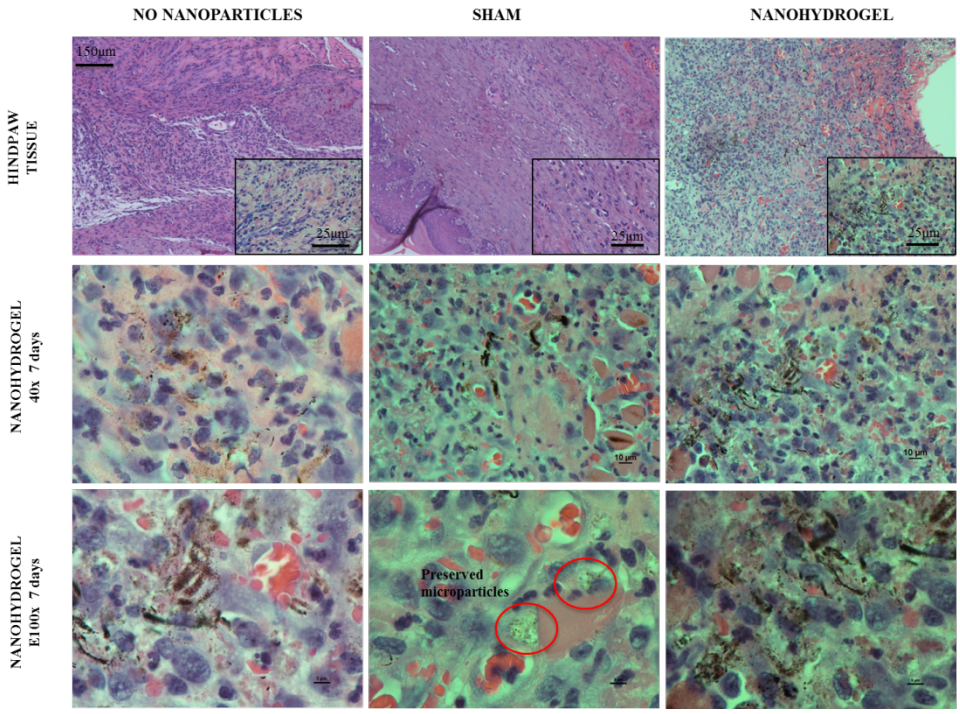

Figure 47. Histological evaluation of hindpaw tissueat day 7 stained with H&E.

Discussion

Nanohydrogels are attractive materials for delivery of different biomolecules given that their structural characteristics such as size, porosity, bulk and surface compositions of the encapsulating polymer can be well-controlled by tuning the synthesis procedure. This is particularly true for the delivery of small molecules such as anesthetics, since the nanohydrogel can be designed to have injectable properties such that it can be used locally at the site of surgery. The change in polymer properties during polymer biodegradation influences the release and degradation rates of incorporated cargo molecules from PLGA-MSP. In addition, thermoresponsive hydrogel facilitates ease of handling during fabrication, formulation, application of nanomaterials and makes such formulations attractive candidates for local drug delivery system. Cargo release from nanohydrogel occurs by two principal mechanisms: (i) drug diffusion from the PLGA-MSP during the initial release phase; and (ii) release of cargo molecule

by the erosion of the hydrogel matrix during the later phase. This effect expedites both higher loading capacity of lidocaine into the nanohydrogel and slower release of lidocaine from the thermoresponsive gel phase via diffusion, prolonging drug availability and thus enhances the overall clinical effectiveness of anesthetic molecule.

Conclusion

Thermoresponsive nanohydrogels are useful as drug vehicles for delivery of local anesthetics. While MSP offer high surface porosity with interconnected pores allow large storage of anesthetic molecules, PLGA encapsulation offers a tunable layer to seal the porous network and control the degradation and release kinetics. In addition, structural integrity and function of anesthetic molecules can be preserved by using PLGA-MSP composite particles. By integrating the drug preserving and encapsulating capabilities of nanoparticles with the further controlled relaese capabilities achieved by encapsulation of PLGA, a new dual controlled system for prolonged local anesthesia has been developed. Moreover, the potential thermo-aggregation of Pluronic hydrogel upon injection facilitates a macroscopic release of cargo molecule for prolonged local anesthesia.

Conclusion

Nanotechnology-based drug delivery is an interdisciplinary field of research that applies the principles of engineering, material and life sciences toward the development of novel classes of therapeutics [201, 380]. The rational design of delivery platforms and the targeted delivery of therapeutics to diseased cells and tissues are among the major benefits of nanoscale approaches in medicine [381-383].

This dissertation explored the development of nanostructured materials for drug delivery and tissue engineering. The main objective behind the design of these platforms was to control the release of molecules in time and space. Poor stability of therapeutic agents against enzymatic degradation, low bioavailability and deficiency of targeted delivery of drugs, are considered major challenges in the development of effective drug delivery approaches for the treatment of conditions with unmet medical needs [384, 385]. Nanostructured drug delivery systems have to potential to deliver small and large molecules including antibiotics, proteins, analgesics, anesthetics, and steroids for a wide range of therapeutic applications.

The physical and chemical characteristics of these materials play a key role in the fine tuning of their pharmacological properties. Unmodified porous silicates provide basic delivery functions due to the natural degradation of these materials in the biological environment of the body. The surface modification and further encapsulation of porous silicates enhance the stability of drugs and biological molecules and extend their sustained release [1]. In addition, by tailoring the size and geometry of these materials it is possible to control their interactions with cells and tissues, in order to obtain successful delivery of signaling molecules to specific areas within the body.

In this work, the surface of porous silicates was chemically modified and coated with natural hydrogels to improve and extend the half-life and release rates of cargo molecules for

various therapeutic applications. Synthetic polymers were used as an encapsulation strategy to increase the storage of larger volumes of therapeutic molecules. By tuning the thickness and density of the polymer layers, it was possible to slow down degradation and extend the release kinetics. Moreover, we demonstrated the ability to control the delivery of multiple drug molecules with different burst or linear release profiles combining nano- and micro-composites embedded within a PRP-based hydrogel. While PRP promoted cell migration, proliferation and angiogenesis, the nanocomposite hydrogel mediated the delivery of a variety of cargos for tissue engineering applications. Finally, we developed a nanostructured, polymeric platform capable of extending the local release of anesthetics to improve surgical analgesia of incisional pain.

The nanostructured materials presented in this dissertation provide new powerful therapeutic tools for the fields of drug delivery, wound healing, pain relief, biofilm management, and regenerative medicine. Upcoming work will focus on the application of these technologies to relevant animal models towards the goal of clinical translation.

References

[1] Shi J, Votruba AR, Farokhzad OC, Langer R. "Nanotechnology in Drug Delivery and Tissue Engineering: From Discovery to Applications," *Nano Letters*. 2010;10:3223-30.

[2] Cheng Z, Al Zaki A, Hui JZ, Muzykantov VR, Tsourkas A. "Multifunctional Nanoparticles: Cost Versus Benefit of Adding Targeting and Imaging Capabilities," *Science*. 2012;338:903-10.

[3] Sahoo SK, Labhasetwar V. "Nanotech Approaches to Drug Delivery and Imaging," *Drug Discovery Today*. 2003;8:1112-20.

[4] Caldorera-Moore M, Guimard N, Shi L, Roy K. "Designer Nanoparticles: Incorporating Size, Shape and Triggered Release into Nanoscale Drug Carriers," *Expert Opinion on Drug Delivery*. 2010;7:479-95.

[5] Pierstorff E, Ho D. "Monitoring, Diagnostic, and Therapeutic Technologies for Nanoscale Medicine," *Journal of Nanoscience and Nanotechnology*. 2007;7:2949-68.

[6] Kumari A, Yadav SK, Yadav SC. "Biodegradable Polymeric Nanoparticles Based Drug Delivery Systems," *Colloids and Surfaces B: Biointerfaces*. 2010;75:1-18.

[7] Bamrungsap S, Zhao Z, Chen T, Wang L, Li C, Fu T, Tan W. "Nanotechnology in Therapeutics: A Focus on Nanoparticles as a Drug Delivery System," *Nanomedicine*. 2012;7:1253-71.

[8] Alvarez-Lorenzo C, Concheiro A. "Smart Drug Delivery Systems: From Fundamentals to the Clinic," *Chem Commun (Camb)*. 2014;50:7743-65.

[9] Goldberg M, Langer R, Jia X. "Nanostructured Materials for Applications in Drug Delivery and Tissue Engineering," *Journal of Biomaterials Science, Polymer Edition*. 2007;18:241-68.

[10] Garcia-Bennett AE. "Synthesis, Toxicology and Potential of Ordered Mesoporous Materials in Nanomedicine," *Nanomedicine*. 2011;6:867-77.

[11] Horcajada P, Chalati T, Serre C, Gillet B, Sebrie C, Baati T, Eubank JF, Heurtaux D, Clayette P, Kreuz C, Chang J-S, Hwang YK, Marsaud V, Bories P-N, Cynober L, Gil S, Ferey G, Couvreur P, Gref R. "Porous Metal-Organic-Framework Nanoscale Carriers as a Potential Platform for Drug Delivery and Imaging," *Nature Materials*. 2010;9:172-8.

[12] Wang S. "Ordered Mesoporous Materials for Drug Delivery," *Microporous and Mesoporous Materials*. 2009;117:1-9.

[13] Vallet-Regí M, Balas F, Arcos D. "Mesoporous Materials for Drug Delivery," *Angewandte Chemie International Edition*. 2007;46:7548-58.

[14] Hollister SJ. "Porous Scaffold Design for Tissue Engineering," *Nature Materials*. 2005;4:518-24.

[15] Jones JR, Lee PD, Hench LL. "Hierarchical Porous Materials for Tissue Engineering," *Philosophical Transactions of the Royal Society A: Mathematical, Physical and Engineering Sciences*. 2006;364:263-81.

[16] Davis ME. "Ordered Porous Materials for Emerging Applications," *Nature*. 2002;417:813-21.

[17] Kojic M, Milosevic M, Kojic N, Ferrari M, Ziemys A. "On Diffusion in Nanospace," *J Serbian Soc Comput Mech*. 2011;5:104-18.

[18] Kojic M, Milosevic M, Kojic N, Kim K, Ferrari M, Ziemys A. "A Multiscale Md–Fe Model of Diffusion in Composite Media with Internal Surface Interaction Based on Numerical Homogenization Procedure," *Computer Methods in Applied Mechanics and Engineering*. 2014;269:123-38.

[19] Ziemys A, Kojic M, Milosevic M, Ferrari M. "Interfacial Effects on Nanoconfined Diffusive Mass Transport Regimes," *Physical Review Letters*. 2012;108:236102.

[20] Ziemys A, Kojic M, Milosevic M, Kojic N, Hussain F, Ferrari M, Grattoni A. "Hierarchical Modeling of Diffusive Transport through Nanochannels by Coupling Molecular Dynamics with Finite Element Method," *Journal of Computational Physics*. 2011;230:5722-31.

[21] Kojić N, Kojić A, Kojić M. "Numerical Determination of the Solvent Diffusion Coefficient in a Concentrated Polymer Solution," *Communications in Numerical Methods in Engineering*. 2006;22:1003-13.

[22] Kojic M, Filipovic N, Stojanovic B, Kojic N. "Computer Modeling in Bioengineering: Theoretical Background, Examples and Software." 2009.

[23] Kojic M, Filipovic N, Stojanovic B, Kojic N. "Computer Modeling in Bioengineering: Theoretical Background, Examples and Software." John Wiley & Sons; 2008.

[24] Uhlir A. "Electrolytic Shaping of Germanium and Silicon," *Bell System Technical Journal*. 1956;35:333-47.

[25] Cullis AG, Canham LT. "Visible Light Emission Due to Quantum Size Effects in Highly Porous Crystalline Silicon," *Nature*. 1991;353:335-8.

[26] Shahbazi MA, Herranz B, Santos HA. "Nanostructured Porous Si-Based Nanoparticles for Targeted Drug Delivery," *Biomatter*. 2012;2:296-312.

[27] Santos HA, Bimbo LM, Lehto VP, Airaksinen AJ, Salonen J, Hirvonen J. "Multifunctional Porous Silicon for Therapeutic Drug Delivery and Imaging," *Current Drug Discovery Technologies*. 2011;8:228-49.

[28] Jaganathan H, Godin B. "Biocompatibility Assessment of Si-Based Nano- and Micro-Particles," *Advanced Drug Delivery Reviews*. 2012;64:1800-19.

[29] Martinez JO, Boada C, Yazdi IK, Evangelopoulos M, Brown BS, Liu X, Ferrari M, Tasciotti E. "Short and Long Term, in Vitro and in Vivo Correlations of Cellular and Tissue Responses to Mesoporous Silicon Nanovectors," *Small*. 2013;9:1722-33.

[30] Martinez JO, Parodi A, Liu X, Kolonin MG, Ferrari M, Tasciotti E. "Evaluation of Cell Function Upon Nanovector Internalization," *Small*. 2013;9:1696-702.

[31] Martinez JO, Evangelopoulos M, Chiappini C, Liu X, Ferrari M, Tasciotti E. "Degradation and Biocompatibility of Multistage Nanovectors in Physiological Systems," *Journal of Biomedical Materials Research Part A*. 2013:n/a-n/a.

[32] Oakes L, Westover A, Mares JW, Chatterjee S, Erwin WR, Bardhan R, Weiss SM, Pint CL. "Surface Engineered Porous Silicon for Stable, High Performance Electrochemical Supercapacitors," *Scientific Reports*. 2013;3:3020.

[33] Hirschman KD, Tsybeskov L, Duttagupta SP, Fauchet PM. "Silicon-Based Visible Light-Emitting Devices Integrated into Microelectronic Circuits," *Nature*. 1996;384:338-41.

[34] Chan S, Fauchet PM, Li Y, Rothberg LJ, Miller BL. "Porous Silicon Microcavities for Biosensing Applications," *Physica Status Solidi (A)*. 2000;182:541-6.

[35] Cunin F, Schmedake TA, Link JR, Li YY, Koh J, Bhatia SN, Sailor MJ. "Biomolecular Screening with Encoded Porous-Silicon Photonic Crystals," *Nature Materials*. 2002;1:39-41.

[36] Coffer JL, Whitehead MA, Nagesha DK, Mukherjee P, Akkaraju G, Totolici M, Saffie RS, Canham LT. "Porous Silicon-Based Scaffolds for Tissue Engineering and Other Biomedical Applications," *Physica Status Solidi (A)*. 2005;202:1451-5.

[37] Goh AS, Chung AY, Lo RH, Lau TN, Yu SW, Chng M, Satchithanantham S, Loong SL, Ng DC, Lim BC, Connor S, Chow PK. "A Novel Approach to Brachytherapy in Hepatocellular

Carcinoma Using a Phosphorous32 (32p) Brachytherapy Delivery Device--a First-in-Man Study," *International Journal of Radiation Oncology Biology Physics.* 2007;67:786-92.

[38] Prestidge CA, Barnes TJ, Mierczynska-Vasilev A, Kempson I, Peddie F, Barnett C. "Peptide and Protein Loading into Porous Silicon Wafer," *Physica Status Solidi (A)*. 2008;205:311-5.

[39] Fathauer RW, George T, Ksendzov A, Vasquez RP. "Visible Luminescence from Silicon Wafers Subjected to Stain Etches," *Applied Physics Letters*. 1992;60:995-7.

[40] Noguchi N, Suemune I. "Selective Formation of Luminescent Porous Silicon by Photosynthesis," *Journal of Applied Physics*. 1994;75:4765-7.

[41] Salonen J, Kaukonen AM, Hirvonen J, Lehto VP. "Mesoporous Silicon in Drug Delivery Applications," *Journal of Pharmaceutical Sciences*. 2008;97:632-53.

[42] Dai F, Zai J, Yi R, Gordin ML, Sohn H, Chen S, Wang D. "Bottom-up Synthesis of High Surface Area Mesoporous Crystalline Silicon and Evaluation of Its Hydrogen Evolution Performance," *Nature Communications*. 2014;5:3605.

[43] Godin B, Tasciotti E, Liu X, Serda RE, Ferrari M. "Multistage Nanovectors: From Concept to Novel Imaging Contrast Agents and Therapeutics," *Accounts of Chemical Research.* 2011;44:979-89.

[44] Chiappini C, Liu X, Fakhoury JR, Ferrari M. "Biodegradable Porous Silicon Barcode Nanowires with Defined Geometry," *Advanced Functional Materials*. 2010;20:2231-9.

[45] Jarvis KL, Barnes TJ, Prestidge CA. "Surface Chemistry of Porous Silicon and Implications for Drug Encapsulation and Delivery Applications," *Advances in Colloid and Interface Science.* 2012;175:25-38.

[46] Hajj-Hassan M, Cheung MC, Chodavarapu VP. "Ultra-Thin Porous Silicon Membranes Fabricated Using Dry Etching," *Micro & Nano Letters, IET*. 2011;6:226-8.

[47] Leoni L, Boiarski A, Desai T. "Characterization of Nanoporous Membranes for Immunoisolation: Diffusion Properties and Tissue Effects," *Biomedical Microdevices*. 2002;4:131-9.

[48] Fine D, Grattoni A, Hosali S, Ziemys A, De Rosa E, Gill J, Medema R, Hudson L, Kojic M, Milosevic M, Brousseau Iii L, Goodall R, Ferrari M, Liu X. "A Robust Nanofluidic Membrane with Tunable Zero-Order Release for Implantable Dose Specific Drug Delivery," *Lab Chip*. 2010;10:3074-83.

[49] Rajaraman S, Henderson HT. "A Unique Fabrication Approach for Microneedles Using Coherent Porous Silicon Technology," *Sensors and Actuators B: Chemical*. 2005;105:443-8.

[50] Xue M, Zhong X, Shaposhnik Z, Qu Y, Tamanoi F, Duan X, Zink JI. "Ph-Operated Mechanized Porous Silicon Nanoparticles," *Journal of the American Chemical Society*. 2011;133:8798-801.

[51] Tasciotti E, Liu X, Bhavane R, Plant K, Leonard AD, Price BK, Cheng MM, Decuzzi P, Tour JM, Robertson F, Ferrari M. "Mesoporous Silicon Particles as a Multistage Delivery System for Imaging and Therapeutic Applications," *Nature Nanotechnoogyl*. 2008;3:151-7.

[52] Salonen J, Laitinen L, Kaukonen AM, Tuura J, Bjorkqvist M, Heikkila T, Vaha-Heikkila K, Hirvonen J, Lehto VP. "Mesoporous Silicon Microparticles for Oral Drug Delivery: Loading and Release of Five Model Drugs," *Journal of Controlled Release*. 2005;108:362-74.

[53] Liu D, Bimbo LM, Makila E, Villanova F, Kaasalainen M, Herranz-Blanco B, Caramella CM, Lehto VP, Salonen J, Herzig KH, Hirvonen J, Santos HA. "Co-Delivery of a Hydrophobic Small Molecule and a Hydrophilic Peptide by Porous Silicon Nanoparticles," *Journal of Controlled Release*. 2013;170:268-78.

[54] Park JH, Gu L, von Maltzahn G, Ruoslahti E, Bhatia SN, Sailor MJ. "Biodegradable Luminescent Porous Silicon Nanoparticles for in Vivo Applications," *Nature Materials*. 2009;8:331-6.

[55] Santos HA, Makila E, Airaksinen AJ, Bimbo LM, Hirvonen J. "Porous Silicon Nanoparticles for Nanomedicine: Preparation and Biomedical Applications," *Nanomedicine (Lond)*. 2014;9:535-54.

[56] Chiappini C, Tasciotti E, Fakhoury JR, Fine D, Pullan L, Wang YC, Fu L, Liu X, Ferrari M. "Tailored Porous Silicon Microparticles: Fabrication and Properties," *ChemPhysChem*. 2010;11:1029-35.

[57] Godin B, Chiappini C, Srinivasan S, Alexander JF, Yokoi K, Ferrari M, Decuzzi P, Liu X. "Discoidal Porous Silicon Particles: Fabrication and Biodistribution in Breast Cancer Bearing Mice," *Adv Funct Mater*. 2012;22:4225-35.

[58] Barnes TJ, Jarvis KL, Prestidge CA. "Recent Advances in Porous Silicon Technology for Drug Delivery," *Ther Deliv*. 2013;4:811-23.

[59] Serda RE, Mack A, Pulikkathara M, Zaske AM, Chiappini C, Fakhoury JR, Webb D, Godin B, Conyers JL, Liu XW, Bankson JA, Ferrari M. "Cellular Association and Assembly of a Multistage Delivery System," *Small*. 2010;6:1329-40.

[60] Boukherroub R, Wojtyk JTC, Wayner DDM, Lockwood DJ. "Thermal Hydrosilylation of Undecylenic Acid with Porous Silicon," *Journal of The Electrochemical Society*. 2002;149:H59-H63.

[61] Godin B, Gu J, Serda RE, Bhavane R, Tasciotti E, Chiappini C, Liu X, Tanaka T, Decuzzi P, Ferrari M. "Tailoring the Degradation Kinetics of Mesoporous Silicon Structures through Pegylation," *J Biomed Mater Res A*. 2010;94:1236-43.

[62] Mann AP, Tanaka T, Somasunderam A, Liu X, Gorenstein DG, Ferrari M. "E-Selectin-Targeted Porous Silicon Particle for Nanoparticle Delivery to the Bone Marrow," *Adv Mater*. 2011;23:H278-82.

[63] Secret E, Maynadier M, Gallud A, Gary-Bobo M, Chaix A, Belamie E, Maillard P, Sailor MJ, Garcia M, Durand JO, Cunin F. "Anionic Porphyrin-Grafted Porous Silicon Nanoparticles for Photodynamic Therapy," *Chem Commun (Camb)*. 2013;49:4202-4.

[64] Tasciotti E, Godin B, Martinez JO, Chiappini C, Bhavane R, Liu X, Ferrari M. "Near-Infrared Imaging Method for the in Vivo Assessment of the Biodistribution of Nanoporous Silicon Particles," *Mol Imaging*. 2011;10:56-68.

[65] Anglin EJ, Cheng L, Freeman WR, Sailor MJ. "Porous Silicon in Drug Delivery Devices and Materials," *Adv Drug Deliv Rev*. 2008;60:1266-77.

[66] Wu EC, Andrew JS, Buyanin A, Kinsella JM, Sailor MJ. "Suitability of Porous Silicon Microparticles for the Long-Term Delivery of Redox-Active Therapeutics," *Chem Commun (Camb)*. 2011;47:5699-701.

[67] Wu EC, Park JH, Park J, Segal E, Cunin F, Sailor MJ. "Oxidation-Triggered Release of Fluorescent Molecules or Drugs from Mesoporous Si Microparticles," *ACS Nano*. 2008;2:2401-9.

[68] Prestidge CA, Barnes TJ, Mierczynska-Vasilev A, Skinner W, Peddie F, Barnett C. "Loading and Release of a Model Protein from Porous Silicon Powders," *physica status solidi (a)*. 2007;204:3361-6.

[69] Yazdi IK, Murphy MB, Loo C, Liu X, Ferrari M, Weiner BK, Tasciotti E. "Cefazolin-Loaded Mesoporous Silicon Microparticles Show Sustained Bactericidal Effect against Staphylococcus Aureus," *Journal of Tissue Engineering*. 2014;5.

[70] Bimbo LM, Denisova OV, Makila E, Kaasalainen M, De Brabander JK, Hirvonen J, Salonen J, Kakkola L, Kainov D, Santos HA. "Inhibition of Influenza a Virus Infection in Vitro by Saliphenylhalamide-Loaded Porous Silicon Nanoparticles," *ACS Nano*. 2013;7:6884-93.

[71] Shen J, Xu R, Mai J, Kim HC, Guo X, Qin G, Yang Y, Wolfram J, Mu C, Xia X, Gu J, Liu X, Mao ZW, Ferrari M, Shen H. "High Capacity Nanoporous Silicon Carrier for Systemic Delivery of Gene Silencing Therapeutics," *ACS Nano*. 2013;7:9867-80.

[72] Wan Y, Apostolou S, Dronov R, Kuss B, Voelcker NH. "Cancer-Targeting Sirna Delivery from Porous Silicon Nanoparticles," *Nanomedicine (Lond)*. 2014.

[73] Martinez JO, Brown BS, Quattrocchi N, Evangelopoulos M, Ferrari M, Tasciotti E. "Multifunctional to Multistage Delivery Systems: The Evolution of Nanoparticles for Biomedical Applications," *Chin Sci Bull*. 2012;57:3961-71.

[74] Shen H, Rodriguez-Aguayo C, Xu R, Gonzalez-Villasana V, Mai J, Huang Y, Zhang G, Guo X, Bai L, Qin G, Deng X, Li Q, Erm DR, Aslan B, Liu X, Sakamoto J, Chavez-Reyes A, Han HD, Sood AK, Ferrari M, Lopez-Berestein G. "Enhancing Chemotherapy Response with Sustained Epha2 Silencing Using Multistage Vector Delivery," *Clin Cancer Res*. 2013;19:1806-15.

[75] Shen H, You J, Zhang G, Ziemys A, Li Q, Bai L, Deng X, Erm DR, Liu X, Li C, Ferrari M. "Cooperative, Nanoparticle-Enabled Thermal Therapy of Breast Cancer," *Adv Healthc Mater*. 2012;1:84-9.

[76] Tanaka T, Mangala LS, Vivas-Mejia PE, Nieves-Alicea R, Mann AP, Mora E, Han HD, Shahzad MM, Liu X, Bhavane R, Gu J, Fakhoury JR, Chiappini C, Lu C, Matsuo K, Godin B, Stone RL, Nick AM, Lopez-Berestein G, Sood AK, Ferrari M. "Sustained Small Interfering Rna Delivery by Mesoporous Silicon Particles," *Cancer Res*. 2010;70:3687-96.

[77] Jarvis KL, Barnes TJ, Prestidge CA. "Thermal Oxidation for Controlling Protein Interactions with Porous Silicon," *Langmuir*. 2010;26:14316-22.

[78] Wu EC, Andrew JS, Cheng L, Freeman WR, Pearson L, Sailor MJ. "Real-Time Monitoring of Sustained Drug Release Using the Optical Properties of Porous Silicon Photonic Crystal Particles," *Biomaterials*. 2011;32:1957-66.

[79] Dorvee JR, Sailor MJ, Miskelly GM. "Digital Microfluidics and Delivery of Molecular Payloads with Magnetic Porous Silicon Chaperones," *Dalton Trans*. 2008:721-30.

[80] Kinsella JM, Ananda S, Andrew JS, Grondek JF, Chien MP, Scadeng M, Gianneschi NC, Ruoslahti E, Sailor MJ. "Enhanced Magnetic Resonance Contrast of Fe(3)O(4) Nanoparticles Trapped in a Porous Silicon Nanoparticle Host," *Adv Mater*. 2011;23:H248-53.

[81] Park JH, Derfus AM, Segal E, Vecchio KS, Bhatia SN, Sailor MJ. "Local Heating of Discrete Droplets Using Magnetic Porous Silicon-Based Photonic Crystals," *J Am Chem Soc*. 2006;128:7938-46.

[82] Gu L, Park JH, Duong KH, Ruoslahti E, Sailor MJ. "Magnetic Luminescent Porous Silicon Microparticles for Localized Delivery of Molecular Drug Payloads," *Small*. 2010;6:2546-52.

[83] McInnes SJ, Irani Y, Williams KA, Voelcker NH. "Controlled Drug Delivery from Composites of Nanostructured Porous Silicon and Poly(L-Lactide)," *Nanomedicine (Lond)*. 2012;7:995-1016.

[84] Fan D, De Rosa E, Murphy MB, Peng Y, Smid CA, Chiappini C, Liu X, Simmons P, Weiner BK, Ferrari M, Tasciotti E. "Mesoporous Silicon-Plga Composite Microspheres for the Double Controlled Release of Biomolecules for Orthopedic Tissue Engineering," *Adv Funct Mater*. 2012;22:282-93.

[85] De Rosa E, Chiappini C, Fan D, Liu X, Ferrari M, Tasciotti E. "Agarose Surface Coating Influences Intracellular Accumulation and Enhances Payload Stability of a Nano-Delivery System," *Pharm Res*. 2011;28:1520-30.

[86] Parodi A, Quattrocchi N, van de Ven AL, Chiappini C, Evangelopoulos M, Martinez JO, Brown BS, Khaled SZ, Yazdi IK, Enzo MV, Isenhart L, Ferrari M, Tasciotti E. "Synthetic Nanoparticles Functionalized with Biomimetic Leukocyte Membranes Possess Cell-Like Functions," *Nat Nanotechnol*. 2013;8:61-8.

[87] Bonanno LM, Segal E. "Nanostructured Porous Silicon-Polymer-Based Hybrids: From Biosensing to Drug Delivery," *Nanomedicine (Lond)*. 2011;6:1755-70.

[88] Vasani RB, McInnes SJ, Cole MA, Jani AM, Ellis AV, Voelcker NH. "Stimulus-Responsiveness and Drug Release from Porous Silicon Films Atrp-Grafted with Poly(N-Isopropylacrylamide)," *Langmuir*. 2011;27:7843-53.

[89] Segal E, Perelman LA, Cunin F, Di Renzo F, Devoisselle JM, Li YY, Sailor MJ. "Confinement of Thermoresponsive Hydrogels in Nanostructured Porous Silicon Dioxide Templates," *Adv Funct Mater*. 2007;17:1153-62.

[90] Batra I, Coffer JL, Canham LT. "Electronically-Responsive Delivery from a Calcified Mesoporous Silicon Structure," *Biomed Microdevices*. 2006;8:93-7.

[91] Orosco MM, Pacholski C, Miskelly GM, Sailor MJ. "Protein-Coated Porous-Silicon Photonic Crystals for Amplified Optical Detection of Protease Activity," *Adv Mater*. 2006;18:1393-6.

[92] Wu J, Sailor MJ. "Chitosan Hydrogel-Capped Porous Sio2 as a Ph Responsive Nano-Valve for Triggered Release of Insulin," *Adv Funct Mater*. 2009;19:733-41.

[93] Perelman LA, Pacholski C, Li YY, VanNieuwenhze MS, Sailor MJ. "Ph-Triggered Release of Vancomycin from Protein-Capped Porous Silicon Films," *Nanomedicine (Lond)*. 2008;3:31-43.

[94] Jurkic LM, Cepanec I, Pavelic SK, Pavelic K. "Biological and Therapeutic Effects of Ortho-Silicic Acid and Some Ortho-Silicic Acid-Releasing Compounds: New Perspectives for Therapy," *Nutr Metab (Lond)*. 2013;10:2.

[95] Reffitt DM, Ogston N, Jugdaohsingh R, Cheung HF, Evans BA, Thompson RP, Powell JJ, Hampson GN. "Orthosilicic Acid Stimulates Collagen Type 1 Synthesis and Osteoblastic Differentiation in Human Osteoblast-Like Cells in Vitro," *Bone*. 2003;32:127-35.

[96] Anderson SHC, Elliott H, Wallis DJ, Canham LT, Powell JJ. "Dissolution of Different Forms of Partially Porous Silicon Wafers under Simulated Physiological Conditions," *Phys Stat Sol (a)*. 2003;197:331-5.

[97] Martinez JO, Chiappini C, Ziemys A, Faust AM, Kojic M, Liu X, Ferrari M, Tasciotti E. "Engineering Multi-Stage Nanovectors for Controlled Degradation and Tunable Release Kinetics," *Biomaterials*. 2013;34:8469-77.

[98] Hou H, Nieto A, Ma F, Freeman WR, Sailor MJ, Cheng L. "Tunable Sustained Intravitreal Drug Delivery System for Daunorubicin Using Oxidized Porous Silicon," *J Control Release*. 2014;178:46-54.

[99] Anglin EJ, Schwartz MP, Ng VP, Perelman LA, Sailor MJ. "Engineering the Chemistry and Nanostructure of Porous Silicon Fabry-Perot Films for Loading and Release of a Steroid," *Langmuir*. 2004;20:11264-9.

[100] Limnell T, Riikonen J, Salonen J, Kaukonen AM, Laitinen L, Hirvonen J, Lehto VP. "Surface Chemistry and Pore Size Affect Carrier Properties of Mesoporous Silicon Microparticles," *Int J Pharm*. 2007;343:141-7.

[101] Sethi R, Ananta JS, Karmonik C, Zhong M, Fung SH, Liu X, Li K, Ferrari M, Wilson LJ, Decuzzi P. "Enhanced Mri Relaxivity of Gd(3+) -Based Contrast Agents Geometrically Confined within Porous Nanoconstructs," *Contrast Media Mol Imaging*. 2012;7:501-8.

[102] Ananta JS, Godin B, Sethi R, Moriggi L, Liu X, Serda RE, Krishnamurthy R, Muthupillai R, Bolskar RD, Helm L, Ferrari M, Wilson LJ, Decuzzi P. "Geometrical Confinement of Gadolinium-Based Contrast Agents in Nanoporous Particles Enhances T1 Contrast," *Nat Nanotechnol*. 2010;5:815-21.

[103] Xu R, Huang Y, Mai J, Zhang G, Guo X, Xia X, Koay EJ, Qin G, Erm DR, Li Q, Liu X, Ferrari M, Shen H. "Multistage Vectored Sirna Targeting Ataxia-Telangiectasia Mutated for Breast Cancer Therapy," *Small*. 2013;9:1799-808.

[104] Blanco E, Sangai T, Hsiao A, Ferrati S, Bai L, Liu X, Meric-Bernstam F, Ferrari M. "Multistage Delivery of Chemotherapeutic Nanoparticles for Breast Cancer Treatment," *Cancer Lett*. 2013;334:245-52.

[105] Kresge CT, Leonowicz ME, Roth WJ, Vartuli JC, Beck JS. "Ordered Mesoporous Molecular Sieves Synthesized by a Liquid-Crystal Template Mechanism," *Nature*. 1992;359:710-2.

[106] Grün M, Lauer I, Unger KK. "The Synthesis of Micrometer- and Submicrometer-Size Spheres of Ordered Mesoporous Oxide Mcm-41," *Adv Mater*. 1997;9:254-7.

[107] Unger KK, Kumar D, Grün M, Büchel G, Lüdtke S, Adam T, Schumacher K, Renker S. "Synthesis of Spherical Porous Silicas in the Micron and Submicron Size Range: Challenges and

Opportunities for Miniaturized High-Resolution Chromatographic and Electrokinetic Separations," *Journal of Chromatography A*. 2000;892:47-55.

[108] Lundqvist M, Sethson I, Jonsson B-H. "Protein Adsorption onto Silica Nanoparticles: Conformational Changes Depend on the Particles' Curvature and the Protein Stability," *Langmuir*. 2004;20:10639-47.

[109] Vallet-Regi M, Rámila A, del Real RP, Pérez-Pariente J. "A New Property of Mcm-41: Drug Delivery System," *Chemistry of Materials*. 2000;13:308-11.

[110] Gerion D, Herberg J, Bok R, Gjersing E, Ramon E, Maxwell R, Kurhanewicz J, Budinger TF, Gray JW, Shuman MA, Chen FF. "Paramagnetic Silica-Coated Nanocrystals as an Advanced Mri Contrast Agent," *The Journal of Physical Chemistry C*. 2007;111:12542-51.

[111] Chen J-F, Ding H-M, Wang J-X, Shao L. "Preparation and Characterization of Porous Hollow Silica Nanoparticles for Drug Delivery Application," *Biomaterials*. 2004;25:723-7.

[112] Slowing II, Vivero-Escoto JL, Wu C-W, Lin VSY. "Mesoporous Silica Nanoparticles as Controlled Release Drug Delivery and Gene Transfection Carriers," *Adv Drug Deliv Rev*. 2008;60:1278-88.

[113] Descalzo AB, Martínez-Máñez R, Sancenón F, Hoffmann K, Rurack K. "The Supramolecular Chemistry of Organic–Inorganic Hybrid Materials," *Angewandte Chemie International Edition*. 2006;45:5924-48.

[114] Vivero-Escoto JL, Slowing II, Trewyn BG, Lin VSY. "Mesoporous Silica Nanoparticles for Intracellular Controlled Drug Delivery," *Small*. 2010;6:1952-67.

[115] Huo Q, Feng J, Schüth F, Stucky GD. "Preparation of Hard Mesoporous Silica Spheres," *Chemistry of Materials*. 1997;9:14-7.

[116] Qi L, Ma J, Cheng H, Zhao Z. "Micrometer-Sized Mesoporous Silica Spheres Grown under Static Conditions," *Chemistry of Materials*. 1998;10:1623-6.

[117] Kosuge K, Singh PS. "Mesoporous Silica Spheres Via 1-Alkylamine Templating Route," *Microporous and Mesoporous Materials*. 2001;44–45:139-45.

[118] Han Y, Ying JY. "Generalized Fluorocarbon-Surfactant-Mediated Synthesis of Nanoparticles with Various Mesoporous Structures," *Angewandte Chemie International Edition*. 2005;44:288-92.

[119] Huh S, Wiench JW, Yoo J-C, Pruski M, Lin VSY. "Organic Functionalization and Morphology Control of Mesoporous Silicas Via a Co-Condensation Synthesis Method," *Chemistry of Materials*. 2003;15:4247-56.

[120] Slowing II, Trewyn BG, Lin VSY. "Mesoporous Silica Nanoparticles for Intracellular Delivery of Membrane-Impermeable Proteins," *J Am Chem Soc*. 2007;129:8845-9.

[121] Nooney RI, Thirunavukkarasu D, Chen Y, Josephs R, Ostafin AE. "Synthesis of Nanoscale Mesoporous Silica Spheres with Controlled Particle Size," *Chemistry of Materials*. 2002;14:4721-8.

[122] Suzuki K, Ikari K, Imai H. "Synthesis of Silica Nanoparticles Having a Well-Ordered Mesostructure Using a Double Surfactant System," *J Am Chem Soc*. 2003;126:462-3.

[123] Brunner TJ, Wick P, Manser P, Spohn P, Grass RN, Limbach LK, Bruinink A, Stark WJ. "In Vitro Cytotoxicity of Oxide Nanoparticles: Comparison to Asbestos, Silica, and the Effect of Particle Solubility," *Environmental Science & Technology*. 2006;40:4374-81.

[124] Albanese A, Tang PS, Chan WC. "The Effect of Nanoparticle Size, Shape, and Surface Chemistry on Biological Systems," *Annual review of biomedical engineering*. 2012;14:1-16.

[125] Jiang J, Oberdörster G, Biswas P. "Characterization of Size, Surface Charge, and Agglomeration State of Nanoparticle Dispersions for Toxicological Studies," *Journal of Nanoparticle Research*. 2009;11:77-89.

[126] Peters K, Unger R, Kirkpatrick CJ, Gatti A, Monari E. "Effects of Nano-Scaled Particles on Endothelial Cell Function in Vitro: Studies on Viability, Proliferation and Inflammation," *Journal of Materials Science: Materials in Medicine*. 2004;15:321-5.

[127] Teeguarden JG, Hinderliter PM, Orr G, Thrall BD, Pounds JG. "Particokinetics in Vitro: Dosimetry Considerations for in Vitro Nanoparticle Toxicity Assessments," *Toxicological Sciences*. 2007;95:300-12.

[128] Trewyn BG, Whitman CM, Lin VSY. "Morphological Control of Room-Temperature Ionic Liquid Templated Mesoporous Silica Nanoparticles for Controlled Release of Antibacterial Agents," *Nano Letters*. 2004;4:2139-43.

[129] Che S, Liu Z, Ohsuna T, Sakamoto K, Terasaki O, Tatsumi T. "Synthesis and Characterization of Chiral Mesoporous Silica," *Nature*. 2004;429:281-4.

[130] Huh S, Wiench JW, Trewyn BG, Song S, Pruski M, Lin VS-Y. "Tuning of Particle Morphology and Pore Properties in Mesoporous Silicas with Multiple Organic Functional Groups," *Chem Commun*. 2003:2364-5.

[131] Wang S-G, Wu C-W, Chen K, Lin VSY. "Fine-Tuning Mesochannel Orientation of Organically Functionalized Mesoporous Silica Nanoparticles," *Chemistry – An Asian Journal*. 2009;4:658-61.

[132] Vinu A, Hossain KZ, Ariga K. "Recent Advances in Functionalization of Mesoporous Silica," *Journal of nanoscience and nanotechnology*. 2005;5:347-71.

[133] Yang P, Gai S, Lin J. "Functionalized Mesoporous Silica Materials for Controlled Drug Delivery," *Chemical Society Reviews*. 2012;41:3679-98.

[134] Radu DR, Lai C-Y, Huang J, Shu X, Lin VSY. "Fine-Tuning the Degree of Organic Functionalization of Mesoporous Silica Nanosphere Materials Via an Interfacially Designed Co-Condensation Method," *Chem Commun (Camb)*. 2005:1264-6.

[135] Lu J, Liong M, Zink JI, Tamanoi F. "Mesoporous Silica Nanoparticles as a Delivery System for Hydrophobic Anticancer Drugs," *Small*. 2007;3:1341-6.

[136] Joo SH, Park JY, Tsung C-K, Yamada Y, Yang P, Somorjai GA. "Thermally Stable Pt/Mesoporous Silica Core-Shell Nanocatalysts for High-Temperature Reactions," *Nat Mater*. 2009;8:126-31.

[137] Liz-Marzán LM, Giersig M, Mulvaney P. "Synthesis of Nanosized Gold−Silica Core−Shell Particles," *Langmuir*. 1996;12:4329-35.

[138] Yoon T-J, Yu KN, Kim E, Kim JS, Kim BG, Yun S-H, Sohn B-H, Cho M-H, Lee J-K, Park SB. "Specific Targeting, Cell Sorting, and Bioimaging with Smart Magnetic Silica Core–Shell Nanomaterials," *Small*. 2006;2:209-15.

[139] Lee C-H, Lo L-W, Mou C-Y, Yang C-S. "Synthesis and Characterization of Positive-Charge Functionalized Mesoporous Silica Nanoparticles for Oral Drug Delivery of an Anti-Inflammatory Drug," *Adv Funct Mater*. 2008;18:3283-92.

[140] Seleem MN, Munusamy P, Ranjan A, Alqublan H, Pickrell G, Sriranganathan N. "Silica-Antibiotic Hybrid Nanoparticles for Targeting Intracellular Pathogens," *Antimicrobial Agents and Chemotherapy*. 2009;53:4270-4.

[141] Pan L, He Q, Liu J, Chen Y, Ma M, Zhang L, Shi J. "Nuclear-Targeted Drug Delivery of Tat Peptide-Conjugated Monodisperse Mesoporous Silica Nanoparticles," *J Am Chem Soc*. 2012;134:5722-5.

[142] Torney F, Trewyn BG, Lin VSY, Wang K. "Mesoporous Silica Nanoparticles Deliver DNA and Chemicals into Plants," *Nat Nano*. 2007;2:295-300.

[143] Xia T, Kovochich M, Liong M, Meng H, Kabehie S, George S, Zink JI, Nel AE. "Polyethyleneimine Coating Enhances the Cellular Uptake of Mesoporous Silica Nanoparticles and Allows Safe Delivery of Sirna and DNA Constructs," *ACS Nano*. 2009;3:3273-86.

[144] AAOS. Orthopaedic Practice in the U.S. 2012. Secondary "Orthopaedic Practice in the U.S. 2012," 2013.

[145] Hawn MT, Vick CC, Richman J, Holman W, Deierhoi RJ, Graham LA, Henderson WG, Itani KM. "Surgical Site Infection Prevention: Time to Move Beyond the Surgical Care Improvement Program," *Annals of surgery*. 2011;254:494-501.

[146] Cantón R, Morosini MI. "Emergence and Spread of Antibiotic Resistance Following Exposure to Antibiotics," *FEMS microbiology reviews*. 2011;35:977-91.

[147] Greene LR. "Guide to the Elimination of Orthopedic Surgical Site Infections:" APIC; 2010.

[148] Dale WB, Peter MH. "Antimicrobial Prophylaxis for Surgery: An Advisory Statement from the National Surgical Infection Prevention Project," *Clinical Infectious Diseases*. 2004;38:1706-15.

[149] Bratzler DW, Dellinger EP, Olsen KM, Perl TM, Auwaerter PG, Bolon MK, Fish DN, Napolitano LM, Sawyer RG, Slain D. "Clinical Practice Guidelines for Antimicrobial Prophylaxis in Surgery," *American journal of health-system pharmacy*. 2013;70:195-283.

[150] Suzuki Y, Tanihara M, Nishimura Y, Suzuki K, Kakimaru Y, Shimizu Y. "A New Drug Delivery System with Controlled Release of Antibiotic Only in the Presence of Infection," *Journal of biomedical materials research*. 1998;42:112-6.

[151] Lin S-S, Ueng SW, Liu S-J, Chan E-C, Chao E-K, Tsai C-H, Chen K-T, Wei F-C, Shih C-H. "Development of a Biodegradable Antibiotic Delivery System," *Clinical orthopaedics and related research*. 1999;362:240-50.

[152] Nelson CL. "The Current Status of Material Used for Depot Delivery of Drugs," *Clinical orthopaedics and related research*. 2004;427:72-8.

[153] El-Husseiny M, Patel S, MacFarlane R, Haddad F. "Biodegradable Antibiotic Delivery Systems," *Journal of Bone & Joint Surgery, British Volume*. 2011;93:151-7.

[154] Sharma A, Kumar Arya D, Dua M, Chhatwal GS, Johri AK. "Nano-Technology for Targeted Drug Delivery to Combat Antibiotic Resistance," *Expert opinion on drug delivery*. 2012;9:1325-32.

[155] Hetrick EM, Schoenfisch MH. "Reducing Implant-Related Infections: Active Release Strategies," *Chemical Society Reviews*. 2006;35:780-9.

[156] Anderson EM, Noble ML, Garty S, Ma H, Bryers JD, Shen TT, Ratner BD. "Sustained Release of Antibiotic from Poly (2-Hydroxyethyl Methacrylate) to Prevent Blinding Infections after Cataract Surgery," *Biomaterials*. 2009;30:5675-81.

[157] Al-Kassas RS, El-Khatib MM. "Ophthalmic Controlled Release in Situ Gelling Systems for Ciprofloxacin Based on Polymeric Carriers," *Drug delivery*. 2009;16:145-52.

[158] Kong M, Chen XG, Xing K, Park HJ. "Antimicrobial Properties of Chitosan and Mode of Action: A State of the Art Review," *International journal of food microbiology*. 2010;144:51-63.

[159] Hanssen AD. "Local Antibiotic Delivery Vehicles in the Treatment of Musculoskeletal Infection," *Clinical orthopaedics and related research*. 2005;437:91-6.

[160] Brunet L, Lyon DY, Hotze EM, Alvarez PJ, Wiesner MR. "Comparative Photoactivity and Antibacterial Properties of C60 Fullerenes and Titanium Dioxide Nanoparticles," *Environmental science & technology*. 2009;43:4355-60.

[161] Hetrick EM, Shin JH, Stasko NA, Johnson CB, Wespe DA, Holmuhamedov E, Schoenfisch MH. "Bactericidal Efficacy of Nitric Oxide-Releasing Silica Nanoparticles," *ACS nano*. 2008;2:235-46.

[162] Shen S-C, Ng WK, Shi Z, Chia L, Neoh KG, Tan RBH. "Mesoporous Silica Nanoparticle-Functionalized Poly (Methyl Methacrylate)-Based Bone Cement for Effective Antibiotics Delivery," *Journal of Materials Science: Materials in Medicine*. 2011;22:2283-92.

[163] Popat KC, Eltgroth M, LaTempa TJ, Grimes CA, Desai TA. "Decreased *Staphylococcus Epidermis* Adhesion and Increased Osteoblast Functionality on Antibiotic-Loaded Titania Nanotubes," *Biomaterials*. 2007;28:4880-8.

[164] Vale N, Mäkilä E, Salonen J, Gomes P, Hirvonen J, Santos HA. "New Times, New Trends for Ethionamide: *in Vitro* Evaluation of Drug-Loaded Thermally Carbonized Porous Silicon Microparticles," *European Journal of Pharmaceutics and Biopharmaceutics*. 2012;81:314-23.

[165] Perelman LA, Pacholski C, Li YY, VanNieuwenhze MS, Sailor MJ. "Ph-Triggered Release of Vancomycin from Protein-Capped Porous Silicon Films," 2008.

[166] Gao P, Nie X, Zou M, Shi Y, Cheng G. "Recent Advances in Materials for Extended-Release Antibiotic Delivery System," *The Journal of antibiotics*. 2011;64:625-34.

[167] Kaur IP, Singh H. "Nanostructured Drug Delivery for Better Management of Tuberculosis," *Journal of Controlled Release*. 2014.

[168] Yang C, Plackett D, Needham D, Burt HM. "Plga and Phbv Microsphere Formulations and Solid-State Characterization: Possible Implications for Local Delivery of Fusidic Acid for the Treatment and Prevention of Orthopaedic Infections," *Pharmaceutical research*. 2009;26:1644-56.

[169] Sun Jung Yoon SHK, Hyun Jung Ha, Youn Kyung Ko, Jung Won So, Moon Suk Kim, Young Il Yang, Gilson Khang, John M. Rhee and Hai Bang Lee. "Reduction of Inflammatory Reaction of Poly(D,L-Lactic-Co-Glycolic Acid) Using Demineralized Bone Particles," *Tissue Engineering Part A*. 2008;14:539-47.

[170] Savage DJ, Liu X, Curley SA, Ferrari M, Serda RE. "Porous Silicon Advances in Drug Delivery and Immunotherapy," *Current opinion in pharmacology*. 2013;13:834-41.

[171] Fine D, Grattoni A, Goodall R, Bansal SS, Chiappini C, Hosali S, van de Ven AL, Srinivasan S, Liu X, Godin B. "Silicon Micro-and Nanofabrication for Medicine," *Advanced Healthcare materials*. 2013.

[172] Salonen J, Kaukonen AM, Hirvonen J, Lehto VP. "Mesoporous Silicon in Drug Delivery Applications," *Journal of pharmaceutical sciences*. 2008;97:632-53.

[173] Sakamoto JH, van de Ven AL, Godin B, Blanco E, Serda RE, Grattoni A, Ziemys A, Bouamrani A, Hu T, Ranganathan SI. "Enabling Individualized Therapy through Nanotechnology," *Pharmacological Research*. 2010;62:57-89.

[174] Anglin EJ, Cheng L, Freeman WR, Sailor MJ. "Porous Silicon in Drug Delivery Devices and Materials," *Advanced drug delivery reviews*. 2008;60:1266-77.

[175] McInnes SJ, Voelcker NH. "Silicon-Polymer Hybrid Materials for Drug Delivery," *Future medicinal chemistry*. 2009;1:1051-74.

[176] Godin B, Gu J, Serda RE, Bhavane R, Tasciotti E, Chiappini C, Liu X, Tanaka T, Decuzzi P, Ferrari M. "Tailoring the Degradation Kinetics of Mesoporous Silicon Structures through Pegylation," *Journal of Biomedical Materials Research Part A*. 2010;94:1236-43.

[177] Limnell T, Riikonen J, Salonen J, Kaukonen A, Laitinen L, Hirvonen J, Lehto V-P. "Surface Chemistry and Pore Size Affect Carrier Properties of Mesoporous Silicon Microparticles," *International journal of pharmaceutics*. 2007;343:141-7.

[178] Prestidge CA, Barnes TJ, Lau C-H, Barnett C, Loni A, Canham L. "Mesoporous Silicon: A Platform for the Delivery of Therapeutics," 2007.

[179] Chiappini C, Tasciotti E, Fakhoury JR, Fine D, Pullan L, Wang YC, Fu L, Liu X, Ferrari M. "Tailored Porous Silicon Microparticles: Fabrication and Properties," *Chemphyschem*. 2010;11:1029-35.

[180] Murphy MB, Khaled SM, Fan D, Yazdi IK, Sprintz M, Buchanan RM, Smid CA, Weiner BK, Ferrari M, Tasciotti E. "A Multifunctional Nanostructured Platform for Localized Sustained Release of Analgesics and Antibiotics," *European Journal of Pain Supplements*. 2011;5:423-32.

[181] Santos HA, Riikonen J, Salonen J, Mäkilä E, Heikkilä T, Laaksonen T, Peltonen L, Lehto V-P, Hirvonen J. "In Vitro Cytotoxicity of Porous Silicon Microparticles: Effect of the Particle Concentration, Surface Chemistry and Size," *Acta biomaterialia*. 2010;6:2721-31.

[182] Bimbo LM, Sarparanta M, Santos HA, Airaksinen AJ, Makila E, Laaksonen T, Peltonen L, Lehto V-P, Hirvonen J, Salonen J. "Biocompatibility of Thermally Hydrocarbonized Porous Silicon Nanoparticles and Their Biodistribution in Rats," *ACS nano*. 2010;4:3023-32.

[183] Salonen J, Laitinen L, Kaukonen A, Tuura J, Björkqvist M, Heikkilä T, Vähä-Heikkilä K, Hirvonen J, Lehto VP. "Mesoporous Silicon Microparticles for Oral Drug Delivery: Loading and Release of Five Model Drugs," *Journal of Controlled Release*. 2005;108:362-74.

[184] Serda RE, Gu J, Bhavane RC, Liu XW, Chiappini C, Decuzzi P, Ferrari M. "The Association of Silicon Microparticles with Endothelial Cells in Drug Delivery to the Vasculature," *Biomaterials*. 2009;30:2440-8.

[185] Tanaka T, Mangala LS, Vivas-Mejia PE, Nieves-Alicea R, Mann AP, Mora E, Han HD, Shahzad MMK, Liu X, Bhavane R. "Sustained Small Interfering Rna Delivery by Mesoporous Silicon Particles," *Cancer research*. 2010;70:3687-96.

[186] Tasciotti E, Liu X, Bhavane R, Plant K, Leonard AD, Price BK, Cheng MM-C, Decuzzi P, Tour JM, Robertson F, Ferrari M. "Mesoporous Silicon Particles as a Multistage Delivery System for Imaging and Therapeutic Applications," *Nat Nano*. 2008;3:151-7.

[187] Chhablani J, Nieto A, Hou H, Wu EC, Freeman WR, Sailor MJ, Cheng L. "Oxidized Porous Silicon Particles Covalently Grafted with Daunorubicin as a Sustained Intraocular Drug Delivery System," *Investigative ophthalmology & visual science*. 2013;54:1268-79.

[188] Liu D, Bimbo LM, Mäkilä E, Villanova F, Kaasalainen M, Herranz-Blanco B, Caramella CM, Lehto V-P, Salonen J, Herzig K-H. "Co-Delivery of a Hydrophobic Small Molecule and a Hydrophilic Peptide by Porous Silicon Nanoparticles," *Journal of Controlled Release*. 2013;170:268-78.

[189] Wang M, Coffer JL, Dorraj K, Hartman PS, Loni A, Canham LT. "Sustained Antibacterial Activity from Triclosan-Loaded Nanostructured Mesoporous Silicon," *Molecular pharmaceutics*. 2010;7:2232-9.

[190] A Santos H, M Bimbo L, Lehto V-P, J Airaksinen A, Salonen J, Hirvonen J. "Multifunctional Porous Silicon for Therapeutic Drug Delivery and Imaging," *Current drug discovery technologies*. 2011;8:228-49.

[191] Furuya EY, Lowy FD. "Antimicrobial-Resistant Bacteria in the Community Setting," *Nature Reviews Microbiology*. 2006;4:36-45.

[192] Prokuski L. "Prophylactic Antibiotics in Orthopaedic Surgery," *Journal of the American Academy of Orthopaedic Surgeons*. 2008;16:283-93.

[193] Patel R. "Biofilms and Antimicrobial Resistance," *Clinical orthopaedics and related research*. 2005;437:41-7.

[194] Low SP, Williams KA, Canham LT, Voelcker NH. "Generation of Reactive Oxygen Species from Porous Silicon Microparticles in Cell Culture Medium," *Journal of Biomedical Materials Research Part A*. 2010;93:1124-31.

[195] Cohen MH, Melnik K, Boiarski AA, Ferrari M, Martin FJ. "Microfabrication of Silicon-Based Nanoporous Particulates for Medical Applications," *Biomedical Microdevices*. 2003;5:253-9.

[196] Salonen J, Lehto V-P. "Fabrication and Chemical Surface Modification of Mesoporous Silicon for Biomedical Applications," *Chemical Engineering Journal*. 2008;137:162-72.

[197] Serda RE, Ferrati S, Godin B, Tasciotti E, Liu X, Ferrari M. "Mitotic Trafficking of Silicon Microparticles," *Nanoscale*. 2009;1:250-9.

[198] Liang D, Chow D, White C. "High-Performance Liquid Chromatographic Assay of Cefazolin in Rat Tissues," *Journal of Chromatography B: Biomedical Sciences and Applications*. 1994;656:460-5.

[199] Murphy MB, Blashki D, Buchanan RM, Yazdi IK, Ferrari M, Simmons PJ, Tasciotti E. "Adult and Umbilical Cord Blood-Derived Platelet-Rich Plasma for Mesenchymal Stem Cell Proliferation, Chemotaxis, and Cryo-Preservation," *Biomaterials*. 2012;33:5308-16.

[200] Kilpeläinen M, Mönkäre J, Vlasova MA, Riikonen J, Lehto V-P, Salonen J, Järvinen K, Herzig K-H. "Nanostructured Porous Silicon Microparticles Enable Sustained Peptide (Melanotan Ii) Delivery," *European Journal of Pharmaceutics and Biopharmaceutics*. 2011;77:20-5.

[201] Hughes GA. "Nanostructure-Mediated Drug Delivery," *Nanomedicine: Nanotechnology, Biology and Medicine*. 2005;1:22-30.

[202] Olson Michael E, Horswill Alexander R. "Staphylococcus Aureus Osteomyelitis: Bad to the Bone," *Cell host & microbe*. 2013;13:629-31.

[203] Wikler MA. "Performance Standards for Antimicrobial Susceptibility Testing: Sixteenth Informational Supplement," Clinical and Laboratory Standards Institute; 2006.

[204] Martinez JO, Boada C, Yazdi IK, Evangelopoulous M, Brown BS, Liu X, Ferrari M, Tasciotti E. "Short and Long Term, in Vitro and in Vivo Correlations of Cellular and Tissue Responses to Mesoporous Silicon Nanovectors," *Small*. 2012.

[205] Martinez JO, Evangelopoulos M, Chiappini C, Liu X, Ferrari M, Tasciotti E. "Degradation and Biocompatibility of Multistage Nanovectors in Physiological Systems," *Journal of Biomedical Materials Research Part A*. 2013.

[206] Tanaka T, Godin B, Bhavane R, Nieves-Alicea R, Gu J, Liu X, Chiappini C, Fakhoury J, Amra S, Ewing A. "In Vivo Evaluation of Safety of Nanoporous Silicon Carriers Following Single and Multiple Dose Intravenous Administrations in Mice," *International journal of pharmaceutics*. 2010;402:190-7.

[207] Low SP, Voelcker NH, Canham LT, Williams KA. "The Biocompatibility of Porous Silicon in Tissues of the Eye," *Biomaterials*. 2009;30:2873-80.

[208] Balmayor ER, Azevedo HS, Reis RL. "Controlled Delivery Systems: From Pharmaceuticals to Cells and Genes," *Pharmaceutical research*. 2011;28:1241-58.

[209] Huh AJ, Kwon YJ. "“Nanoantibiotics”: A New Paradigm for Treating Infectious Diseases Using Nanomaterials in the Antibiotics Resistant Era," *Journal of Controlled Release*. 2011;156:128-45.

[210] Wu P, Grainger DW. "Drug/Device Combinations for Local Drug Therapies and Infection Prophylaxis," *Biomaterials*. 2006;27:2450-67.

[211] Engler AC, Wiradharma N, Ong ZY, Coady DJ, Hedrick JL, Yang Y-Y. "Emerging Trends in Macromolecular Antimicrobials to Fight Multi-Drug-Resistant Infections," *Nano Today*. 2012;7:201-22.

[212] Pelgrift RY, Friedman AJ. "Nanotechnology as a Therapeutic Tool to Combat Microbial Resistance," *Advanced drug delivery reviews*. 2013;65:1803-15.

[213] Hajipour MJ, Fromm KM, Akbar Ashkarran A, Jimenez de Aberasturi D, Larramendi IRd, Rojo T, Serpooshan V, Parak WJ, Mahmoudi M. "Antibacterial Properties of Nanoparticles," *Trends in biotechnology*. 2012;30:499-511.

[214] De Rosa E, Chiappini C, Fan D, Liu X, Ferrari M, Tasciotti E. "Agarose Surface Coating Influences Intracellular Accumulation and Enhances Payload Stability of a Nano-Delivery System," *Pharmaceutical research*. 2011;28:1520-30.

[215] Murphy MB, Blashki D, Buchanan RM, Fan D, De Rosa E, Shah RN, Stupp SI, Weiner BK, Simmons PJ, Ferrari M. "Multi-Composite Bioactive Osteogenic Sponges Featuring Mesenchymal Stem Cells, Platelet-Rich Plasma, Nanoporous Silicon Enclosures, and Peptide Amphiphiles for Rapid Bone Regeneration," *Journal of Functional Biomaterials*. 2011;2:39-66.

[216] Fan D, De Rosa E, Murphy MB, Peng Y, Smid CA, Chiappini C, Liu X, Simmons P, Weiner BK, Ferrari M. "Mesoporous Silicon-Plga Composite Microspheres for the Double Controlled Release of Biomolecules for Orthopedic Tissue Engineering," *Advanced Functional Materials*. 2012;22:282-93.

[217] Parodi A, Quattrocchi N, van de Ven AL, Chiappini C, Evangelopoulos M, Martinez JO, Brown BS, Khaled SZ, Yazdi IK, Enzo MV. "Synthetic Nanoparticles Functionalized with Biomimetic Leukocyte Membranes Possess Cell-Like Functions," *Nature nanotechnology*. 2012.

[218] Baquero F, Negri MC. "Strategies to Minimize the Development of Antibiotic Resistance," *Journal of chemotherapy (Florence, Italy)*. 1997;9 Suppl 3:29-37.

[219] Gao P, Nie X, Zou M, Shi Y, Cheng G. "Recent Advances in Materials for Extended-Release Antibiotic Delivery System," *J Antibiot*. 2011;64:625-34.

[220] Schweizer W, Striffeler H, Lüdi D, Fröscher R. "["Single Shot" Prevention in Abdominal Surgery. Antibiotics with Long Half-Life (Ceftriaxone, Ornidazole) Vs. Antibiotics with Short Half-Life (Cefazolin, Metronidazole, Clindamycin)]," *Helvetica chirurgica acta*. 1994;60:483-8.

[221] Gallach D, Recio Sánchez G, Muñoz Noval A, Manso Silván M, Ceccone G, Martín Palma RJ, Torres Costa V, Martínez Duart JM. "Functionality of Porous Silicon Particles: Surface Modification for Biomedical Applications," *Materials Science and Engineering: B*. 2010;169:123-7.

[222] Woo BH, Jiang G, Jo YW, DeLuca PP. "Preparation and Characterization of a Composite Plga and Poly(Acryloyl Hydroxyethyl Starch) Microsphere System for Protein Delivery," *Pharm Res*. 2001;18:1600-6.

[223] van de Weert M, Hennink WE, Jiskoot W. "Protein Instability in Poly(Lactic-Co-Glycolic Acid) Microparticles," *Pharm Res*. 2000;17:1159-67.

[224] Chan JM, Zhang L, Yuet KP, Liao G, Rhee J-W, Langer R, Farokhzad OC. "Plga-Lecithin-Peg Core-Shell Nanoparticles for Controlled Drug Delivery," *Biomaterials*. 2009;30:1627-34.

[225] Jensen DMK, Cun D, Maltesen MJ, Frokjaer S, Nielsen HM, Foged C. "Spray Drying of Sirna-Containing Plga Nanoparticles Intended for Inhalation," *Journal of Controlled Release*. 2010;142:138-45.

[226] Tang BC, Dawson M, Lai SK, Wang Y-Y, Suk JS, Yang M, Zeitlin P, Boyle MP, Fu J, Hanes J. "Biodegradable Polymer Nanoparticles That Rapidly Penetrate the Human Mucus Barrier," *Proceedings of the National Academy of Sciences*. 2009;106:19268-73.

[227] Habraken WJEM, Wolke JGC, Mikos AG, Jansen JA. "Plga Microsphere/Calcium Phosphate Cement Composites for Tissue Engineering: In Vitro Release and Degradation Characteristics," *Journal of Biomaterials Science -- Polymer Edition*. 2008;19:1171-88.

[228] Linhart W, Peters F, Lehmann W, Schwarz K, Schilling AF, Amling M, Rueger JM, Epple M. "Biologically and Chemically Optimized Composites of Carbonated Apatite and Polyglycolide as Bone Substitution Materials," *Journal of Biomedical Materials Research*. 2001;54:162-71.

[229] Torchilin VP. "Multifunctional Nanocarriers," *Adv Drug Deliv Rev*. 2006;58:1532-55.

[230] Canham LT. "Bioactive Silicon Structure Fabrication through Nanoetching Techniques," *Adv Mater*. 1995;7:1033-7.

[231] Park J-H, Gu L, von Maltzahn G, Ruoslahti E, Bhatia SN, Sailor MJ. "Biodegradable Luminescent Porous Silicon Nanoparticles for in Vivo Applications," *Nat Mater*. 2009;8:331-6.

[232] Chin V, Collins BE, Sailor MJ, Bhatia SN. "Compatibility of Primary Hepatocytes with Oxidized Nanoporous Silicon," *Adv Mater*. 2001;13:1877-80.

[233] Bayliss SC, Buckberry LD, Harris PJ, Tobin M. "Nature of the Silicon-Animal Cell Interface," *Journal of Porous Materials*. 2000;7:191-5.

[234] Low SP, Williams KA, Canham LT, Voelcker NH. "Evaluation of Mammalian Cell Adhesion on Surface-Modified Porous Silicon," *Biomaterials*. 2006;27:4538-46.

[235] Mayne AH, Bayliss SC, Barr P, Tobin M, Buckberry LD. "Biologically Interfaced Porous Silicon Devices," *physica status solidi (a)*. 2000;182:505-13.

[236] Whitehead MA, Fan D, Mukherjee P, Akkaraju GR, Canham LT, Coffer JL. "High-Porosity Poly(ε-Caprolactone)/Mesoporous Silicon Scaffolds: Calcium Phosphate Deposition and Biological Response to Bone Precursor Cells," *Tissue Engineering Part A*. 2008;14:195-206.

[237] Whitehead MA, Fan D, Akkaraju GR, Canham LT, Coffer JL. "Accelerated Calcification in Electrically Conductive Polymer Composites Comprised of Poly(ε -Caprolactone), Polyaniline, and Bioactive Mesoporous Silicon," *Journal of Biomedical Materials Research Part A*. 2007;83A:225-34.

[238] Canham LT. "Nanoscale Semiconducting Silicon as a Nutritional Food Additive," *Nanotechnology*. 2007;18:185704.

[239] Martin FJ, Melnik K, West T, Shapiro J, Cohen M, Boiarski AA, Ferrari M. "Acute Toxicity of Intravenously Administered Microfabricated Silicon Dioxide Drug Delivery Particles in Mice: Preliminary Findings," *Drugs in R&D*. 2005;6:71-81.

[240] Anthony Soon-Whatt G, Alexander Yaw-Fui C, Richard Houa-Gong L, Te-Neng L, Sidney Wing-Kwong Y, May C, Somanesan S, Susan Li-Er L, David Chee-Eng N, Beng-Choo L, Stephen C, Pierce Kah-Hoe C. "A Novel Approach to Brachytherapy in Hepatocellular Carcinoma Using a Phosphorous32 (32p) Brachytherapy Delivery Device—a First-in-Man Study," *International journal of radiation oncology, biology, physics*. 2007;67:786-92.

[241] Anglin EJ, Schwartz MP, Ng VP, Perelman LA, Sailor MJ. "Engineering the Chemistry and Nanostructure of Porous Silicon Fabry-Pérot Films for Loading and Release of a Steroid," *Langmuir*. 2004;20:11264-9.

[242] Foraker AB, Walczak RJ, Cohen MH, Boiarski TA, Grove CF, Swaan PW. "Microfabricated Porous Silicon Particles Enhance Paracellular Delivery of Insulin across Intestinal Caco-2 Cell Monolayers," *Pharm Res*. 2003;20:110-6.

[243] Vaccari L, Canton D, Zaffaroni N, Villa R, Tormen M, di Fabrizio E. "Porous Silicon as Drug Carrier for Controlled Delivery of Doxorubicin Anticancer Agent," *Microelectronic Engineering*.83:1598-601.

[244] Decuzzi P, Godin B, Tanaka T, Lee SY, Chiappini C, Liu X, Ferrari M. "Size and Shape Effects in the Biodistribution of Intravascularly Injected Particles," *Journal of Controlled Release*. 2010;141:320-7.

[245] Serda RE, Gu J, Bhavane RC, Liu X, Chiappini C, Decuzzi P, Ferrari M. "The Association of Silicon Microparticles with Endothelial Cells in Drug Delivery to the Vasculature," *Biomaterials*. 2009;30:2440-8.

[246] Marks DC, Belov L, Davey MW, Davey RA, Kidman AD. "The Mtt Cell Viability Assay for Cytotoxicity Testing in Multidrug-Resistant Human Leukemic Cells," *Leukemia Research*. 1992;16:1165-73.

[247] Bragdon B, Moseychuk O, Saldanha S, King D, Julian J, Nohe A. "Bone Morphogenetic Proteins: A Critical Review," *Cellular Signalling*. 2011;23:609-20.

[248] Gravel D, Taylor G, Ofner M, Johnston L, Loeb M, Roth VR, Stegenga J, Bryce E, the Canadian Nosocomial Infection Surveillance P, Matlow A. "Point Prevalence Survey for

Healthcare-Associated Infections within Canadian Adult Acute-Care Hospitals," *Journal of Hospital Infection*. 2007;66:243-8.

[249] Pellizzer G, Mantoan P, Timillero L, Allegranzi B, Fedeli U, Schievano E, Benedetti P, Saia M, Sax H, Spolaore P. "Prevalence and Risk Factors for Nosocomial Infections in Hospitals of the Veneto Region, North-Eastern Italy," *Infection*. 2008;36:112-9.

[250] Reilly J, Stewart S, Allardice GA, Noone A, Robertson C, Walker A, Coubrough S. "Results from the Scottish National Hai Prevalence Survey," *Journal of Hospital Infection*. 2008;69:62-8.

[251] Nichols RL. "Postoperative Infections in the Age of Drug-Resistant Gram-Positive Bacteria," *The American Journal of Medicine*. 1998;104:11S-6S.

[252] Graves EJ. "Detailed Diagnoses and Procedures, National Hospital Discharge Survey, 1992. Series 13: Data from the National Health Survey," *Vital and health statistics Series 13, Data from the National Health Survey*. 1994:1-281.

[253] Haley RW, Culver DH, White JW, Morgan WM, Emori TG. "The Nationwide Nosocomial Infection Rate: A New Need for Vital Statistics," *American Journal of Epidemiology*. 1985;121:159-67.

[254] Mangram AJ, Horan TC, Pearson ML, Silver LC, Jarvis WR. "Guideline for Prevention of Surgical Site Infection, 1999." *American journal of infection control*. 1999;27:97-134.

[255] Stratchounski L, Taylor E, Dellinger E, Pechere J. "Antibiotic Policies in Surgery: A Consensus Paper," *International journal of antimicrobial agents*. 2005;26:312-22.

[256] Lallemand S, Thouverez M, Bailly P, Bertrand X, Talon D. "Non-Observance of Guidelines for Surgical Antimicrobial Prophylaxis and Surgical-Site Infections," *Pharmacy World and Science*. 2002;24:95-9.

[257] Bratzler DW, Houck PM, Richards C, Steele L, Dellinger EP, Fry DE, Wright C, Ma A, Carr K, Red L. "Use of Antimicrobial Prophylaxis for Major Surgery: Baseline Results from the National Surgical Infection Prevention Project," *Archives of Surgery*. 2005;140:174-82.

[258] Tourmousoglou CE, Yiannakopoulou EC, Kalapothaki V, Bramis J, Papadopoulos JS. "Adherence to Guidelines for Antibiotic Prophylaxis in General Surgery: A Critical Appraisal," *Journal of Antimicrobial Chemotherapy*. 2008;61:214-8.

[259] White PF, Kehlet H. "Improving Postoperative Pain Management: What Are the Unresolved Issues?," *Anesthesiology*. 2010;112:220-5 10.1097/ALN.0b013e3181c6316e.

[260] Al Malyan M, Becchi C, Nikkola L, Viitanen P, Boncinelli S, Chiellini F, Ashammakhi N. "Polymer-Based Biodegradable Drug Delivery Systems in Pain Management," *Journal of Craniofacial Surgery*. 2006;17:302-13.

[261] Hickey T, Kreutzer D, Burgess DJ, Moussy F. "Dexamethasone/Plga Microspheres for Continuous Delivery of an Anti-Inflammatory Drug for Implantable Medical Devices," *Biomaterials*. 2002;23:1649-56.

[262] Zolnik BS, Burgess DJ. "Evaluation of in Vivo–in Vitro Release of Dexamethasone from Plga Microspheres," *Journal of Controlled Release*. 2008;127:137-45.

[263] Curley J, Castillo J, Hotz J, Uezono M, Hernandez S, Lim J-O, Tigner J, Chasin M, Langer R, Berde C. "Prolonged Regional Nerve Blockade: Injectable Biodegradable Bupivacaine/Polyester Microspheres," *Anesthesiology*. 1996;84:1401-10.

[264] Park E-S, Maniar M, Shah JC. "Biodegradable Polyanhydride Devices of Cefazolin Sodium, Bupivacaine, and Taxol for Local Drug Delivery: Preparation, and Kinetics and Mechanism of in Vitro Release," *Journal of Controlled Release*. 1998;52:179-89.

[265] Le Corre P, Estèbe JP, Clément R, Du Plessis L, Chevanne F, Ecoffey C, Le Verge R. "Spray-Dryed Bupivacaine-Loaded Microspheres: In Vitro Evaluation and Biopharmaceutics of Bupivacaine Following Brachial Plexus Administration in Sheep," *Int J Pharm*. 2002;238:191-203.

[266] Kim D-H, Martin DC. "Sustained Release of Dexamethasone from Hydrophilic Matrices Using Plga Nanoparticles for Neural Drug Delivery," *Biomaterials*. 2006;27:3031-7.

[267] Sampson S, Gerhardt M, Mandelbaum B. "Platelet Rich Plasma Injection Grafts for Musculoskeletal Injuries: A Review," *Current Reviews in Musculoskeletal Medicine*. 2008;1:165-74.

[268] Mooren RECM, Hendriks EJ, van den Beucken JJJP, Merkx MAW, Meijer GJ, Jansen JA, Stoelinga PJW. "The Effect of Platelet-Rich Plasma in Vitro on Primary Cells: Rat Osteoblast-Like Cells and Human Endothelial Cells," *Tissue Engineering Part A*. 2010;16:3159-72.

[269] Murphy M, Blashki D, Buchanan R, Fan D, De Rosa E, Shah R, Stupp S, Weiner B, Simmons P, Ferrari M, Tasciotti E. "Multi-Composite Bioactive Osteogenic Sponges Featuring Mesenchymal Stem Cells, Platelet-Rich Plasma, Nanoporous Silicon Enclosures, and Peptide Amphiphiles for Rapid Bone Regeneration," *Journal of Functional Biomaterials*. 2011;2:39-66.

[270] Mainardes RM, Evangelista RC. "PLGA Nanoparticles Containing Praziquantel: Effect of Formulation Variables on Size Distribution," *Int J Pharm*. 2005;290:137-44.

[271] Brennan TJ, Umali EF, Zahn PK. "Comparison of Pre- Versus Post-Incision Administration of Intrathecal Bupivacaine and Intrathecal Morphine in a Rat Model of Postoperative Pain," *Anesthesiology*. 1997;87:1517-28.

[272] Zahn PK, Brennan TJ. "Primary and Secondary Hyperalgesia in a Rat Model for Human Postoperative Pain," *Anesthesiology*. 1999;90:863-72.

[273] Golomb BA, Dang TT, Criqui MH. "Peripheral Arterial Disease Morbidity and Mortality Implications," *Circulation*. 2006;114:688-99.

[274] Vinik A, Park T, Stansberry K, Pittenger G. "Diabetic Neuropathies," *Diabetologia*. 2000;43:957-73.

[275] Yancey P, Brand P. "The Gift of Pain: Why We Hurt and What We Can Do About It," Zondervan; 1997.

[276] Said G. "Diabetic Neuropathy—a Review," *Nature Clinical Practice Neurology*. 2007;3:331-40.

[277] Noordeen SK. "Epidemiology of Leprosy," Mycobacteria: Springer; 1998. p. 379-97.

[278] Denison E, Asenlof P, Lindberg P. "Self-Efficacy, Fear Avoidance, and Pain Intensity as Predictors of Disability in Subacute and Chronic Musculoskeletal Pain Patients in Primary Health Care," *Pain*. 2004;111:245-52.

[279] Shafer A, Fish MP, Gregg KM, Seavello J, Kosek P. "Preoperative Anxiety and Fear: A Comparison of Assessments by Patients and Anesthesia and Surgery Residents," *Anesthesia & Analgesia*. 1996;83:1285-91.

[280] Shevde K, Panagopoulos G. "A Survey of 800 Patients' Knowledge, Attitudes, and Concerns Regarding Anesthesia," *Anesthesia & Analgesia*. 1991;73:190-8.

[281] Waddell G, Newton M, Henderson I, Somerville D, Main CJ. "A Fear-Avoidance Beliefs Questionnaire (Fabq) and the Role of Fear-Avoidance Beliefs in Chronic Low Back Pain and Disability," *Pain*. 1993;52:157-68.

[282] Warfield CA, Kahn CH. "Acute Pain Management: Programs in Us Hospitals and Experiences and Attitudes among Us Adults," *Anesthesiology*. 1995;83:1090-4.

[283] Rathmell JP, Wu CL, Sinatra RS, Ballantyne JC, Ginsberg B, Gordon DB, Liu SS, Perkins FM, Reuben SS, Rosenquist RW, Viscusi ER. "Acute Post-Surgical Pain Management: A Critical Appraisal of Current Practice, December 2-4, 2005," *Reg Anesth Pain Med*. 2006;31:1-42.

[284] Joshi GP, Ogunnaike BO. "Consequences of Inadequate Postoperative Pain Relief and Chronic Persistent Postoperative Pain," *Anesthesiology Clinics of North America*. 2005;23:21-36.

[285] Macrae W. "Chronic Pain after Surgery," *Br J Anaesth*. 2001;87:88-98.

[286] Macrae W. "Chronic Post-Surgical Pain: 10 Years On," *Br J Anaesth*. 2008;101:77-86.

[287] Macrae W, Davies H. "Chronic Postsurgical Pain," *Epidemiology of pain*. 1999:125-42.

[288] Burckhardt CS, Jones KD. "Effects of Chronic Widespread Pain on the Health Status and Quality of Life of Women after Breast Cancer Surgery," *Health Qual Life Outcomes*. 2005;3:30.

[289] Perkins FM, Kehlet H. "Chronic Pain as an Outcome of Surgery: A Review of Predictive Factors," *Anesthesiology*. 2000;93:1123-33.

[290] Poobalan A, Bruce J, King P, Chambers W, Krukowski Z, Smith W. "Chronic Pain and Quality of Life Following Open Inguinal Hernia Repair," *British journal of surgery*. 2001;88:1122-6.

[291] Kwon JH. "Overcoming Barriers in Cancer Pain Management," *Journal of Clinical Oncology*. 2014:JCO. 2013.52. 4827.

[292] Lander J. "Clinical Judgments in Pain Management," *Pain*. 1990;42:15-22.

[293] McNeill JA, Sherwood GD, Starck PL. "The Hidden Error of Mismanaged Pain: A Systems Approach," *Journal of pain and symptom management*. 2004;28:47-58.

[294] Olmstead DL, Scott SD, Austin WJ. "Unresolved Pain in Children: A Relational Ethics Perspective," *Nursing ethics*. 2010;17:695-704.

[295] Apfelbaum JL, Chen C, Mehta SS, Gan TJ. "Postoperative Pain Experience: Results from a National Survey Suggest Postoperative Pain Continues to Be Undermanaged," *Anesthesia & Analgesia*. 2003;97:534-40.

[296] Mattila K, Toivonen J, Janhunen L, Rosenberg PH, Hynynen M. "Postdischarge Symptoms after Ambulatory Surgery: First-Week Incidence, Intensity, and Risk Factors," *Anesthesia & Analgesia*. 2005;101:1643-50.

[297] Akca O, Melischek M, Scheck T, Hellwagner K, Arkiliç CF, Kurz A, Kapral S, Heinz T, Lackner FX, Sessler DI. "Postoperative Pain and Subcutaneous Oxygen Tension," *The Lancet*. 1999;354:41-2.

[298] Kabon B, Fleischmann E, Treschan T, Taguchi A, Kapral S, Kurz A. "Thoracic Epidural Anesthesia Increases Tissue Oxygenation During Major Abdominal Surgery," *Anesthesia & Analgesia*. 2003;97:1812-7.

[299] Kehlet H. "Surgical Stress: The Role of Pain and Analgesia," *Br J Anaesth*. 1989;63:189-95.

[300] Cuschieri R, Morran C, Howie J, McArdle C. "Postoperative Pain and Pulmonary Complications: Comparison of Three Analgesic Regimens," *British journal of surgery*. 1985;72:495-8.

[301] Kehlet H. "Acute Pain Control and Accelerated Postoperative Surgical Recovery," *Surgical clinics of north America*. 1999;79:431-43.

[302] Kehlet H, Holte K. "Effect of Postoperative Analgesia on Surgical Outcome," *Br J Anaesth*. 2001;87:62-72.

[303] Modig J, Borg T, Karlström G, Maripuu E, Sahlstedt B. "Thromboembolism after Total Hip Replacement: Role of Epidural and General Anesthesia," *Anesthesia & Analgesia*. 1983;62:174-80.

[304] Pearse E, Caldwell B, Lockwood R, Hollard J. "Early Mobilisation after Conventional Knee Replacement May Reduce the Risk of Postoperative Venous Thromboembolism," *Journal of Bone & Joint Surgery, British Volume*. 2007;89:316-22.

[305] Rosenberg J, Kehlet H. "Does Effective Postoperative Pain Management Influence Surgical Morbidity?," *European surgical research*. 1999;31:133-7.

[306] Institute of Medicine . Committee on Advancing Pain Research C, Education. "Relieving Pain in America: A Blueprint for Transforming Prevention, Care, Education, and Research," National Academies Press; 2011.

[307] Cullen KA, Hall MJ, Golosinskiy A, Statistics NCfH. "Ambulatory Surgery in the United States, 2006," US Department of Health and Human Services, Centers for Disease Control and Prevention, National Center for Health Statistics; 2009.

[308] Kamming D, Chung F, Williams D, McGrath BM, Curti B. "Pain Management in Ambulatory Surgery," *Journal of PeriAnesthesia Nursing*. 2004;19:174-82.

[309] Rabbitts JA, Groenewald CB, Moriarty JP, Flick R. "Epidemiology of Ambulatory Anesthesia for Children in the United States: 2006 and 1996," *Anesthesia & Analgesia*. 2010;111:1011-5.

[310] Raval MV, Hamilton BH, Ingraham AM, Ko CY, Hall BL. "The Importance of Assessing Both Inpatient and Outpatient Surgical Quality," *Annals of surgery*. 2011;253:611-8.

[311] Rawal N, Hylander J, NYDAHL RA, Olofsson I, Gupta A. "Survey of Postoperative Analgesia Following Ambulatory Surgery," *Acta Anaesthesiologica Scandinavica*. 1997;41:1017-22.

[312] Kehlet H, Dahl JB. "Anaesthesia, Surgery, and Challenges in Postoperative Recovery," *The Lancet*. 2003;362:1921-8.

[313] Shnaider I, Chung F. "Outcomes in Day Surgery," *Current opinion in Anesthesiology*. 2006;19:622-9.

[314] Coley KC, Williams BA, DaPos SV, Chen C, Smith RB. "Retrospective Evaluation of Unanticipated Admissions and Readmissions after Same Day Surgery and Associated Costs," *Journal of clinical anesthesia*. 2002;14:349-53.

[315] Brownstein MJ. "A Brief History of Opiates, Opioid Peptides, and Opioid Receptors". *Proceedings of the National Academy of Sciences of the United States of America*. 1993;90:5391.

[316] Kritikos PG, Papadaki, SP. "The History of the Poppy and of Opium and Their Expansion in Antiquity in the Eastern Mediterranean Area," *Bulletin of Narcotics*. 1967

19 17-38.

[317] Carr DB, Reines HD, Schaffer J, Polomano RC, Lande S. "The Impact of Technology on the Analgesic Gap and Quality of Acute Pain Management," *Reg Anesth Pain Med*. 2005;30:286-91.

[318] Foley KM. "Pain Relief into Practice: Rhetoric without Reform," *Journal of clinical oncology*. 1995;13:2149-51.

[319] Huang N, Cunningham F, Laurito CE, Chen C. "Can We Do Better with Postoperative Pain Management?," *The American Journal of Surgery*. 2001;182:440-8.

[320] Angst MS, Clark JD. "Opioid-Induced Hyperalgesia: A Qualitative Systematic Review," *Anesthesiology*. 2006;104:570-87.

[321] Philip BK, Reese PR, Burch SP. "The Economic Impact of Opioids on Postoperative Pain Management," *J Clin Anesth*. 2002;14:354-64.

[322] Centers for Disease C, Prevention. "Vital Signs: Overdoses of Prescription Opioid Pain Relievers---United States, 1999--2008," *MMWR Morbidity and mortality weekly report*. 2011;60:1487.

[323] Joranson DE, Ryan KM, Gilson AM, Dahl JL. "Trends in Medical Use and Abuse of Opioid Analgesics," *Jama*. 2000;283:1710-4.

[324] Kehlet H, Holte K. "Review of Postoperative Ileus," *The American journal of surgery*. 2001;182:S3-S10.

[325] Laxmaiah Manchikanti MD, Bert Fellows MA, Hary Ailinani MD. "Therapeutic Use, Abuse, and Nonmedical Use of Opioids: A Ten-Year Perspective," *Pain Physician*. 2010;13:401-35.

[326] Oderda GM, Evans RS, Lloyd J, Lipman A, Chen C, Ashburn M, Burke J, Samore M. "Cost of Opioid-Related Adverse Drug Events in Surgical Patients," *Journal of pain and symptom management*. 2003;25:276-83.

[327] Oderda GM, Said Q, Evans RS, Stoddard GJ, Lloyd J, Jackson K, Rublee D, Samore MH. "Opioid-Related Adverse Drug Events in Surgical Hospitalizations: Impact on Costs and Length of Stay," *Annals of Pharmacotherapy*. 2007;41:400-7.

[328] Volkow ND, McLellan TA. "Curtailing Diversion and Abuse of Opioid Analgesics without Jeopardizing Pain Treatment,"*Jama*. 2011;305:1346-7.

[329] Webster BS, Verma SK, Gatchel RJ. "Relationship between Early Opioid Prescribing for Acute Occupational Low Back Pain and Disability Duration, Medical Costs, Subsequent Surgery and Late Opioid Use," *Spine*. 2007;32:2127-32.

[330] Brown AK, Christo PJ, Wu CL. "Strategies for Postoperative Pain Management," *Best Practice & Research Clinical Anaesthesiology*. 2004;18:703-17.

[331] Buvanendran A, Kroin JS. "Multimodal Analgesia for Controlling Acute Postoperative Pain," *Curr Opin Anaesthesiol*. 2009;22:588-93.

[332] Gan T, Joshi G, Zhao S, Hanna D, Cheung R, Chen C. "Presurgical Intravenous Parecoxib Sodium and Follow-up Oral Valdecoxib for Pain Management after Laparoscopic Cholecystectomy Surgery Reduces Opioid Requirements and Opioid-Related Adverse Effects," *Acta Anaesthesiologica Scandinavica*. 2004;48:1194-207.

[333] Kehlet H. "Multimodal Approach to Control Postoperative Pathophysiology and Rehabilitation," *Br J Anaesth*. 1997;78:606-17.

[334] Kehlet H, Dahl JB. "The Value of" Multimodal" or" Balanced Analgesia" in Postoperative Pain Treatment," *Anesthesia & Analgesia*. 1993;77:1048-56.

[335] Kehlet H, Wilmore DW. "Multimodal Strategies to Improve Surgical Outcome," *Am J Surg*. 2002;183:630-41.

[336] Baig MK, Zmora O, Derdemezi J, Weiss EG, Nogueras JJ, Wexner SD. "Use of the on-Q Pain Management System Is Associated with Decreased Postoperative Analgesic Requirement: Double Blind Randomized Placebo Pilot Study," *J Am Coll Surg*. 2006;202:297-305.

[337] Capdevila X, Bringuier S, Borgeat A. "Infectious Risk of Continuous Peripheral Nerve Blocks," *Anesthesiology*. 2009;110:182-8.

[338] Capdevila X, Pirat P, Bringuier S, Gaertner E, Singelyn F, Bernard N, Choquet O, Bouaziz H, Bonnet F, French Study Group on Continuous Peripheral Nerve B. "Continuous Peripheral Nerve Blocks in Hospital Wards after Orthopedic Surgery: A Multicenter Prospective Analysis of the Quality of Postoperative Analgesia and Complications in 1,416 Patients," *Anesthesiology*. 2005;103:1035-45.

[339] Dowling R, Thielmeier K, Ghaly A, Barber D, Boice T, Dine A. "Improved Pain Control after Cardiac Surgery: Results of a Randomized, Double-Blind, Clinical Trial," *J Thorac Cardiovasc Surg*. 2003;126:1271-8.

[340] Forastiere E, Sofra M, Giannarelli D, Fabrizi L, Simone G. "Effectiveness of Continuous Wound Infusion of 0.5% Ropivacaine by on-Q Pain Relief System for Postoperative Pain Management after Open Nephrectomy," *Br J Anaesth*. 2008;101:841-7.

[341] Chahar P, Cummings KC, 3rd. "Liposomal Bupivacaine: A Review of a New Bupivacaine Formulation," *J Pain Res*. 2012;5:257-64.

[342] Golf M, Daniels SE, Onel E. "A Phase 3, Randomized, Placebo-Controlled Trial of Depofoam(R) Bupivacaine (Extended-Release Bupivacaine Local Analgesic) in Bunionectomy," *Adv Ther*. 2011;28:776-88.

[343] Gorfine SR, Onel E, Patou G, Krivokapic ZV. "Bupivacaine Extended-Release Liposome Injection for Prolonged Postsurgical Analgesia in Patients Undergoing Hemorrhoidectomy: A Multicenter, Randomized, Double-Blind, Placebo-Controlled Trial," *Dis Colon Rectum*. 2011;54:1552-9.

[344] de Melo NF, Grillo R, Guilherme VA, de Araujo DR, de Paula E, Rosa AH, Fraceto LF. "Poly(Lactide-Co-Glycolide) Nanocapsules Containing Benzocaine: Influence of the Composition of the Oily Nucleus on Physico-Chemical Properties and Anesthetic Activity," *Pharm Res*. 2011;28:1984-94.

[345] Garcia X, Escribano E, Domenech J, Queralt J, Freixes J. "In Vitro Characterization and in Vivo Analgesic and Anti-Allodynic Activity of Plga-Bupivacaine Nanoparticles," *Journal of Nanoparticle Research*. 2010;13:2213-23.

[346] Gou M, Wu L, Yin Q, Guo Q, Guo G, Liu J, Zhao X, Wei Y, Qian Z. "Transdermal Anaesthesia with Lidocaine Nano-Formulation Pretreated with Low-Frequency Ultrasound in Rats Model," *Journal of Nanoscience and Nanotechnology*. 2009;9:6360-5.

[347] Sandkuhler J. "Models and Mechanisms of Hyperalgesia and Allodynia," *Physiol Rev*. 2009;89:707-58.

[348] Zahn PK, Pogatzki EM, Brennan TJ. "Mechanisms for Pain Caused by Incisions," *Reg Anesth Pain Med*. 2002;27:514-6.

[349] Coley KC, Williams BA, DaPos SV, Chen C, Smith RB. "Retrospective Evaluation of Unanticipated Admissions and Readmissions after Same Day Surgery and Associated Costs," *J Clin Anesth*. 2002;14:349-53.

[350] Wu CL, Berenholtz SM, Pronovost PJ, Fleisher LA. "Systematic Review and Analysis of Postdischarge Symptoms after Outpatient Surgery," *Anesthesiology*. 2002;96:994-1003.

[351] Parodi A, Haddix SG, Taghipour N, Scaria S, Taraballi F, Cevenini A, Yazdi IK, Corbo C, Palomba R, Khaled SZ, Martinez JO, Brown BS, Isenhart L, Tasciotti E. "Bromelain Surface Modification Increases the Diffusion of Silica Nanoparticles in the Tumor Extracellular Matrix," *ACS Nano*. 2014;8:9874-83.

[352] Ricci EJ, Lunardi LO, Nanclares DMA, Marchetti JM. "Sustained Release of Lidocaine from Poloxamer 407 Gels," *Int J Pharm*. 2005;288:235-44.

[353] Brennan TJ. "Postoperative Models of Nociception," *ILAR journal / National Research Council, Institute of Laboratory Animal Resources*. 1999;40:129-36.

[354] Brennan TJ, Vandermeulen EP, Gebhart GF. "Characterization of a Rat Model of Incisional Pain," *Pain*. 1996;64:493-502.

[355] Lai J, Porreca F, Hunter JC, Gold MS. "Voltage-Gated Sodium Channels and Hyperalgesia," *Annu Rev Pharmacol Toxicol*. 2004;44:371-97.

[356] Wang Y, Wu J, Guo R, Zhao Y, Wang Y, Zhang M, Chen Z, Wu A, Yue Y. "Surgical Incision Induces Phosphorylation of Ampa Receptor Glur1 Subunits at Serine-831 Sites and Glur1 Trafficking in Spinal Cord Dorsal Horn Via a Protein Kinase Cγ-Dependent Mechanism," *Neuroscience*. 2013;240:361-70.

[357] Wu C, Xu J, Kang S, Spofford CM, Brennan TJ. "Animal Models of Postoperative Pain," Animal Models of Pain: Springer; 2011. p. 181-200.

[358] Cui W, Li Y, Li S, Yang W, Jiang J, Han S, Li J. "Systemic Lidocaine Inhibits Remifentanil-Induced Hyperalgesia Via the Inhibition of Cpkcgamma Membrane Translocation in Spinal Dorsal Horn of Rats," *Journal of neurosurgical anesthesiology*. 2009;21:318-25.

[359] Jones TL, Lustig AC, Sorkin LS. "Secondary Hyperalgesia in the Postoperative Pain Model Is Dependent on Spinal Calcium/Calmodulin-Dependent Protein Kinase Ii Alpha Activation," *Anesth Analg*. 2007;105:1650-6, table of contents.

[360] Xu J, Brennan TJ. "Guarding Pain and Spontaneous Activity of Nociceptors after Skin Versus Skin Plus Deep Tissue Incision," *Anesthesiology*. 2010;112:153.

[361] Hampshire V. "Handheld Digital Equipment for Weight Composite Distress Paradigms: New Considerations and for Rapid Documentation and Intervention of Rodent Populations," *Journal of the American Association for Laboratory Animal Science*. 2001;40:11-7.

[362] Hampshire V, Davis J, McNickle C. "Red-Carpet Rodent Care: Making the Most of Dollars and Sense in the Animal Facility," *Lab animal*. 2000;29:40-6.

[363] Hampshire V, Davis J, McNickle C, Williams L, Eskildson H. "Retrospective Comparison of Rat Recovery Weights Using Inhalation and Injectable Anaesthetics, Nutritional and Fluid Supplementation for Right Unilateral Neurosurgical Lesioning," *Laboratory Animals*. 2001;35:223-9.

[364] Sharp J, Azar T, Lawson D. "Selective Adaptation of Male Rats to Repeated Social Encounters and Experimental Manipulations," *Journal of the American Association for Laboratory Animal Science*. 2005;44:28-31.

[365] Sharp J, Zammit T, Azar T, Lawson D. "Recovery of Male Rats from Major Abdominal Surgery after Treatment with Various Analgesics," *Journal of the American Association for Laboratory Animal Science*. 2003;42:22-7.

[366] Taylor DK. "Study of Two Devices Used to Maintain Normothermia in Rats and Mice During General Anesthesia," *Journal of the American Association for Laboratory Animal Science*. 2007;46:37-41.

[367] Turner PV, Smiler KL, Hargaden M, Koch MA. "Refinements in the Care and Use of Animals in Toxicology Studiesregulation, Validation, and Progress," *Journal of the American Association for Laboratory Animal Science*. 2003;42:8-15.

[368] Harkness JE, Ridgway MD. "Chromodacryorrhea in Laboratory Rats (Rattus Norvegicus): Etiologic Considerations," *Laboratory animal science*. 1980;30:841-4.

[369] Hipolide DC, Tufik S. "Paradoxical Sleep Deprivation in Female Rats Alters Drug-Induced Behaviors," *Physiol Behav*. 1995;57:1139-43.

[370] Kerins C, Carlson D, McIntosh J, Bellinger L. "Meal Pattern Changes Associated with Temporomandibular Joint Inflammation/Pain in Rats; Analgesic Effects," *Pharmacology Biochemistry and Behavior*. 2003;75:181-9.

[371] Rivers WHR, Head H. "A Human Experiment in Nerve Division," *Brain*. 1908;31:323-450.

[372] von FREY M. "The Distribution of Afferent Nerves in the Skin," *Journal of the American Medical Association*. 1906;47:645-8.

[373] Yu T, Malugin A, Ghandehari H. "Impact of Silica Nanoparticle Design on Cellular Toxicity and Hemolytic Activity," *ACS nano*. 2011;5:5717-28.

[374] Tanaka T, Godin B, Bhavane R, Nieves-Alicea R, Gu J, Liu X, Chiappini C, Fakhoury JR, Amra S, Ewing A, Li Q, Fidler IJ, Ferrari M. "In Vivo Evaluation of Safety of Nanoporous Silicon Carriers Following Single and Multiple Dose Intravenous Administrations in Mice," *Int J Pharm*. 2010;402:190-7.

[375] Lu J, Liong M, Li Z, Zink JI, Tamanoi F. "Biocompatibility, Biodistribution, and Drug-Delivery Efficiency of Mesoporous Silica Nanoparticles for Cancer Therapy in Animals," *Small*. 2010;6:1794-805.

[376] Lee CH, Cheng SH, Wang YJ, Chen YC, Chen NT, Souris J, Chen CT, Mou CY, Yang CS, Lo LW. "Near-Infrared Mesoporous Silica Nanoparticles for Optical Imaging: Characterization and in Vivo Biodistribution," *Advanced Functional Materials*. 2009;19:215-22.

[377] Tang F, Li L, Chen D. "Mesoporous Silica Nanoparticles: Synthesis, Biocompatibility and Drug Delivery," *Advanced materials*. 2012;24:1504-34.

[378] Suwalski A, Dabboue H, Delalande A, Bensamoun SF, Canon F, Midoux P, Saillant G, Klatzmann D, Salvetat J-P, Pichon C. "Accelerated Achilles Tendon Healing by Pdgf Gene Delivery with Mesoporous Silica Nanoparticles," *Biomaterials*. 2010;31:5237-45.

[379] Huang X, Li L, Liu T, Hao N, Liu H, Chen D, Tang F. "The Shape Effect of Mesoporous Silica Nanoparticles on Biodistribution, Clearance, and Biocompatibility in Vivo," *ACS Nano*. 2011;5:5390-9.

[380] Farokhzad OC, Langer R. "Impact of Nanotechnology on Drug Delivery," *ACS Nano*. 2009;3:16-20.

[381] Serda RE, Godin B, Blanco E, Chiappini C, Ferrari M. "Multi-Stage Delivery Nano-Particle Systems for Therapeutic Applications," *Biochimica et Biophysica Acta (BBA) - General Subjects*. 2011;1810:317-29.

[382] Kostarelos K. "Rational Design and Engineering of Delivery Systems for Therapeutics: Biomedical Exercises in Colloid and Surface Science," *Adv Colloid Interface Sci*. 2003;106:147-68.

[383] Malmsten M, Bysell H, Hansson P. "Biomacromolecules in Microgels — Opportunities and Challenges for Drug Delivery," *Current Opinion in Colloid & Interface Science*. 2010;15:435-44.

[384] Vizirianakis IS. "Nanomedicine and Personalized Medicine toward the Application of Pharmacotyping in Clinical Practice to Improve Drug-Delivery Outcomes," *Nanomedicine: Nanotechnology, Biology and Medicine*. 2011;7:11-7.

[385] Yih TC, Al-Fandi M. "Engineered Nanoparticles as Precise Drug Delivery Systems," *Journal of Cellular Biochemistry*. 2006;97:1184-90.